

**FINAL TECHNICAL REPORT
GTRI PROJECT A-5676**

***Additional Development of Pneumatic Technology
for High Speed Civil Transport Aircraft***

SUMMARY OF RESEARCH, FINAL REPORT



**Submitted to:
NASA Langley Research Center
Grants Officer, MS 126
Hampton, VA 23681-2199**

Grant Number: NAG-1-2051

**by
Robert J. Englar, Principal Research Engineer & Principal Investigator
F. Scott Willie and Warren J. Lee, Cooperative Education Students**

**Georgia Tech Research Institute
Acoustics and Aerodynamics Research Branch
Aerospace, Transportation & Advanced Systems Laboratory
Georgia Institute of Technology
Atlanta GA 30332-0844**

Period Covered: April 6, 1998 to July 5, 1999

October 3, 1999

**FINAL TECHNICAL REPORT
GTRI PROJECT A-5676**

***Additional Development of Pneumatic Technology
for High Speed Civil Transport Aircraft***

SUMMARY OF RESEARCH, FINAL REPORT

**Submitted to:
NASA Langley Research Center
Grants Officer, MS 126
Hampton, VA 23681-2199**

Grant Number: NAG-1-2051

**by
Robert J. Englar, Principal Research Engineer & Principal Investigator
F. Scott Willie and Warren J. Lee, Cooperative Education Students**

**Georgia Tech Research Institute
Acoustics and Aerodynamics Research Branch
Aerospace, Transportation & Advanced Systems Laboratory
Georgia Institute of Technology
Atlanta GA 30332-0844**

Period Covered: April 6, 1998 to July 5, 1999

October 3, 1999

FOREWORD

The research effort described in this Summary of Research and Final Report was sponsored by NASA Langley Research Center under Grant Number NAG-1-2051. This Grant is entitled "Additional Development and System Analyses of Pneumatic Technology for High Speed Civil Transport Aircraft", and this report covers that portion of the Grant identified as Task 1, "Additional Development of Pneumatic Technology for High Speed Civil Transport Aircraft". A second portion of the Grant, Task 2, "System Analyses of Pneumatic Technology for High Speed Civil Transport Aircraft", is covered in a supplemental Summary of Research prepared by the Aerospace Systems Design Lab of the GT School of Aerospace Engineering. The Grant was originally a twelve-month project beginning April 6, 1998 and ending April 5, 1999, but the period of performance was extended three months to July 5, 1999. The NASA LaRC Technical Monitor was Ms Linda S. Bangert, MS 286.

The GTRI program manager is Mr. Robert J. Englar, Principal Research Engineer in the Aerospace, Transportation & Advanced Systems Lab's Acoustics and Aerodynamics Branch. Mr. Englar was assisted by Drs. Dimitri Mavris and Jimmy Tai of the GT School of Aerospace Engineering's Aerospace Systems Design Lab, which conducted the research in Task 2.

The authors are grateful to NASA LaRC personnel Ms Linda S. Bangert, Mr. Edgar G. Waggoner and Mr. Guy Kemmerly, all of MS 286, for technical direction and guidance, plus their continued support and encouragement in preparation for and conduct of this grant.

Additional Development of Pneumatic Technology for High Speed Civil Transport Aircraft

SUMMARY

In the Task 1 portion of this NASA research grant, configuration development and experimental investigations have been conducted on a series of pneumatic high-lift and control surface devices applied to a generic HSCT model configuration to determine their potential for improved aerodynamic performance, plus stability and control of higher performance aircraft. These investigations were intended to optimize pneumatic lift and drag performance; provide adequate control and longitudinal stability; reduce separation flowfields at high angle of attack; increase takeoff/climbout lift-to-drag ratios; and reduce system complexity and weight. Experimental aerodynamic evaluations were performed on a semi-span HSCT generic model with improved fuselage fineness ratio and with interchangeable plain flaps, blown flaps, pneumatic CCW high-lift configurations, plain and blown canards, a novel CC cylinder blown canard, and a clean cruise wing for reference. Conventional tail power was also investigated for longitudinal trim capability.

Also evaluated was unsteady pulsed blowing of the wing high-lift system to determine if reduced pulsed mass flow rates and blowing requirements could be made to yield the same lift as that resulting from steady-state blowing. Depending on the pulsing frequency applied, reduced mass flow rates were indeed found able to provide lift augmentation at lesser blowing values than for the steady conditions.

Significant improvements in the aerodynamic characteristics leading to improved performance and stability/control were identified, and the various components were compared to evaluate the pneumatic potential of each. Aerodynamic results were provided to the Georgia Tech Aerospace System Design Lab to conduct the companion system analyses and feasibility study (Task 2) of these concepts applied to an operational advanced HSCT aircraft.

Results and conclusions from these experimental evaluations are presented herein, as are recommendations for further development and follow-on investigations. Also provided as an Appendix for reference are the basic results from the previous pneumatic HSCT investigations.

TABLE OF CONTENTS

<u>Section</u>	<u>Page</u>
FOREWORD.....	i
SUMMARY.....	ii
BACKGROUND and INTRODUCTION.....	1
OBJECTIVES AND APPROACH.....	5
Task 1 - Experimental Development.....	5
Task 2 - Systems Analyses.....	6
TEST CONFIGURATION SELECTION; MODEL DESIGN and FABRICATION.....	6
SUBSONIC WIND TUNNEL TESTS and EVALUATIONS.....	9
EXPERIMENTAL DATA ANALYSES and COMPARISONS.....	20
Reynolds Number Variation.....	20
Flap Configuration Variation, Comparison of Blown High-Lift Configurations.....	20
Configurations for Pitch Trim., Blown Canard Development.....	22
Pulsed Blowing Investigations.....	23
CONCLUSIONS.....	63
RECOMMENDATIONS.....	64
REFERENCES.....	65
APPENDIX A Baseline Data from Previous Pneumatic HSCT Investigations.....	67

BACKGROUND AND INTRODUCTION

Pneumatic (blown) high-lift airfoils and control surfaces have recently been developed by Georgia Tech Research Institute (GTRI) under NASA Langley Research Center sponsorship (NASA Grant NAG-1-1517, Reference 1). This work has built on previous advanced blown airfoil and wing development for NASA (References 2 and 3). Results from these projects have shown great potential for application to advanced subsonic commercial transport aircraft (Reference 4).

The advantages of pneumatic technology are not limited to lower-speed advanced subsonic transport aircraft. Recent designs for proposed High Speed Civil Transport (HSCT) configurations employ highly-swept wings and achieve lift augmentation by leading-edge vortex generation. This, however, usually requires approach and takeoff at very high angles of attack, additional tail power for trim, and such unusual features as fuselage nose droop or synthetic vision on some designs. Vortex flows can also result in flow separations, higher drag, increased power requirements and reduced lift/drag ratios. These high angles of attack and high power settings for terminal area operation can also result in higher noise levels perceived near the airport, as well as reduced climbout performance. Recently, GTRI personnel have investigated for NASA the application of simplified pneumatic technology to HSCT-type configurations to provide alternative means of lift increase, angle of attack reduction and improved aerodynamic control (References 1 and 5). The generic HSCT model of Figure 1 was tested subsonically at GTRI over a large range of angle of attack for several vortex-flap leading-edge configurations, and employed pneumatic Circulation Control Wing (CCW) trailing-edge devices for high lift. Also evaluated here were conventional-type horizontal tail surfaces for longitudinal trim/control in the high-lift modes. To provide additional pitch trim and to enhance wing lift by reducing wing upwash and the resulting vortex burst, two canards (both blown and unblown) were installed and evaluated. Figure 2 shows blowing on an AR= 2.58 canard, and Figure 3 shows blowing over a pneumatic wing trailing edge. Additionally, blown and vortex-flap leading-edge (LE) devices were evaluated on the highly-swept wing leading edges.

Results from these subsonic evaluations of this generic HSCT configuration showed some very dramatic lift and drag improvements. Quoting our Reference 5 (which is also provided herein for reference as Appendix A):

“Relative to the cruise baseline HSCT configuration, these blown devices have shown significant improvements, including the following:

- Lift augmentation values ($\Delta C_L/C_{\mu}$) measured on these highly swept wings show a 1200% return on the blowing momentum input.*
- C_{Lmax} increases of more than 100% and stall angle increases of greater than 45% resulted from a combination of blown canard and blown wing trailing edge ability to augment circulation lift while delaying stall due to vortex burst.*
- Drag reductions greater than 100%, partly due to jet thrust recovery and partly due to operation at much lower body and wing incidence to achieve a desired lift.*
- Lift generation at much lower angle of attack, reducing the need for such typical HSCT characteristics as a drooped nose and aft fuselage upsweep.*

- *Blown canards (or even unblown canards) appear able to trim the nose-down pitch of these configurations, as well as to limit the circulation-induced upwash at the wing and thus delay stall due to vortex bursting .*

Additional trends observed were:

- *Neither the conventional nor the enlarged all-flying horizontal tails were alone able to trim this generic HSCT configuration in the high-lift modes tested. The canards alone provided the necessary trim capability, but were longitudinally unstable.*
- *Without canards, aerodynamic lift for the wing/tail combination appeared to reach a vortex-burst-induced limiting value for this aircraft, independent of how the wing circulation lift was achieved (incidence, blowing, flaps, etc.). Canards can help the configuration to exceed this limit by reducing upwash onto the wing and delaying vortex burst."*

Figures 4 and 5 (from Reference 5) confirm the effectiveness of blown canards and pneumatic wing trailing edges in increasing C_{Lmax} , α_{stall} , and pneumatic lift at $\alpha=0^\circ$. Combined with reduced drag due to blowing or lower α , this can increase vehicle L/D ratios.

This data confirmed the aerodynamic performance potential of pneumatic lift and control surfaces on HSCT-type transports. Interest in the mid-1990s in HSCT terminal area performance placed new emphasis on additional factors including: generation of high lift/drag ratios during aircraft takeoff and climbout; minimization of blowing levels for pneumatic configurations; and use of canards to trim/control the aircraft at reduced drag while increasing L/D. Figure 6 shows a stowable canard employed on the TU 144 supersonic transport, but reveals/implies increased mechanical complexity, size and weight. It is suggested, based on the performance benefits shown by the blown canards of Reference 5, that evaluation of pneumatic canards in place of mechanical canards/flaps could provide significant advantages in performance, simplicity, and weight savings for HSCT configurations.

Thus, additional research was initiated under the present Grant to investigate a number of issues relating to: optimizing pneumatic performance and providing longitudinal trim and control; increasing L/D by reducing drag during augmented lift; preventing separated and vortex flows; minimizing blowing rates; and reducing system complexity. Goals of these research efforts included:

- Optimize high-lift and L/D capability with **minimum blowing requirements and/ or pulsed blowing** to reduce the impact on the propulsion or air-supply systems.
- Develop longitudinal trim/control capability and lift augmentation by using **improved and simplified pneumatic canards**, small enough to be retractable or stored.
- Reduce separated flowfields by eliminating the need for high-angle-of-attack operation and the resulting vortex flows. This will also reduce corresponding drag and associated power requirements, and **increase vehicle lift/drag ratios** on takeoff and climbout.
- Reduce mechanical or internal **complexity and weight** of the high-lift and trim/control systems (such as canards).
- **Eliminate aircraft rotational requirements on takeoff** or landing by flying at low α , and thus reduce landing gear length and aft body upsweep requirements.

- Use **advanced lift system and pneumatic canard capabilities** to provide additional design options, such as elimination of nose droop or synthetic vision, as well as downsizing of the wing planform if it was previously sized primarily to meet takeoff and landing requirements.
- **Reduce terminal area noise levels** for HSCT aircraft by allowing much steeper approach and climbout flight path angles (and associated smaller noise footprints); reduced flight speeds; reduced operational angle of attack; and reduced power levels.

Under the present research program, a number of the above goals were accomplished in Task 1, a series of experimental investigations conducted by and at GTRI. However, the true value of these technical advances cannot be ascertained until these concepts are evaluated at a system integration level. Thus pneumatic technology was evaluated in a synthesis model to quantify both the gains that may be possible and any associated disadvantages. Using the experimental data from Task 1, systems analyses were conducted as Task 2 by the Georgia Tech Aerospace Systems Design Laboratory (ASDL). Similar previous studies by ASDL (References 6 and 7) indicated that technologies that improve the low-speed aerodynamics of the vehicle can have the greatest potential benefit because they improve the poor subsonic performance of the HSCT, eliminate the need for synthetic vision, and lower airport noise by allowing steeper take-off and approach trajectories, thus implicitly reducing the need for heavy and expensive noise suppression devices.

As a follow-on to the 1996-1997 research effort for NASA LaRC under Reference 1, this current effort addresses the above issues in order to advance this pneumatic technology (including new blown canards, advanced CCW and unsteady pulsed blowing) and to confirm its usefulness to the commercial transport industry. This current work further develops the aerodynamic configuration of a simplified blown HSCT aircraft. It also identifies the relative performance gains and associated benefits/disadvantages (Reference 8), as well as the economic viability of such a configuration employed as an efficient HSCT-type transport.

This final technical report summarizes the Task 1 research effort. It describes the design and fabrication of a new generic HSCT configuration plus advanced pneumatic lift and control surface devices, and includes details of the experimental setup and test techniques employed. Experimental results are presented which reveal the aerodynamic and control characteristics off these pneumatic devices on HSCT configurations, and resulting conclusions are provided as are recommended follow-on activities. The results of Task 2 are summarized in Reference 8.

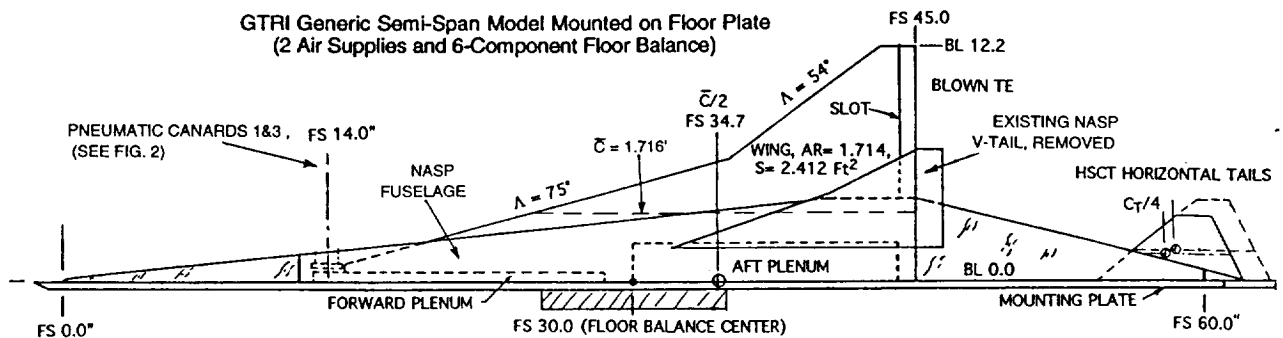


Figure 1 - Planform of the GTRI semi-span NASP/HSCT model configuration, from Reference 5 programs

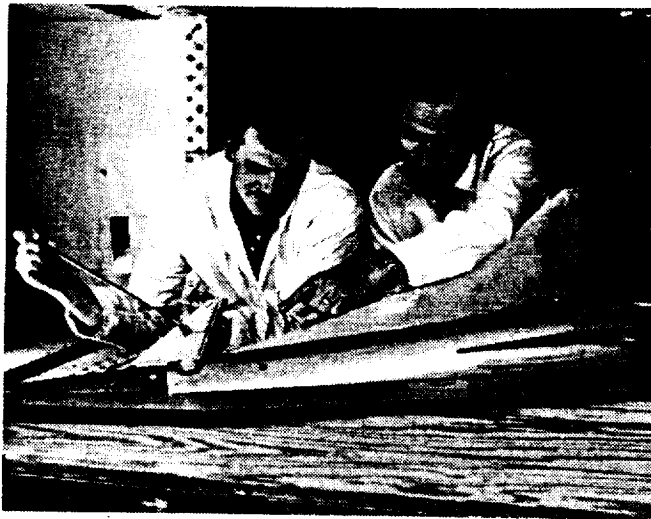


Figure 2 - Static flow visualization of blowing over Canard 3 aft-swept CCW trailing edge

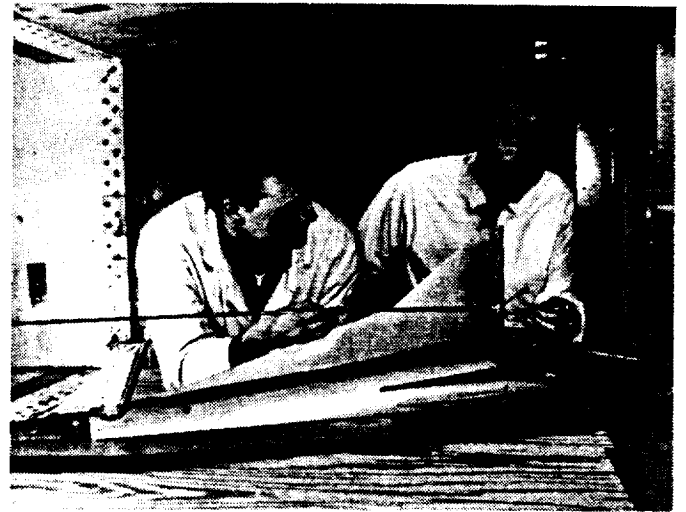


Figure 3 - Static flow visualization of blowing over 20° pneumatic flap

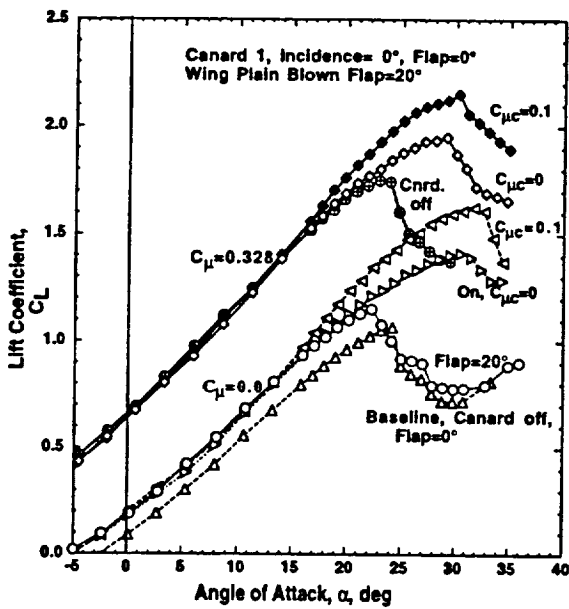


Figure 4 - Effectiveness of wing blowing & Canard 1 (AR=1.29) blowing, tail off

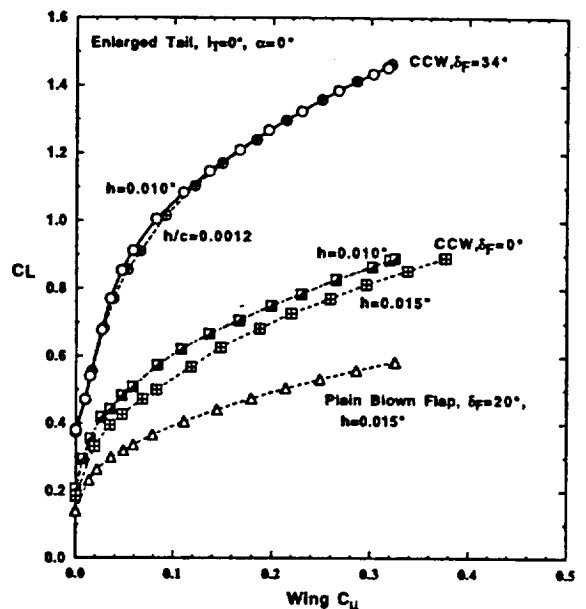


Figure 5 - Lift augmentation due to various blown trailing-edge flaps, $\alpha=0^\circ$

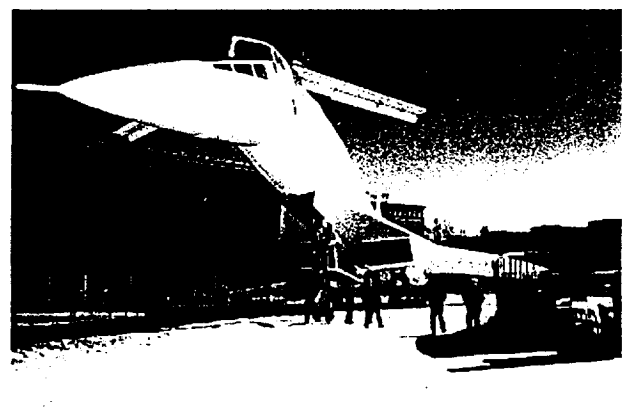
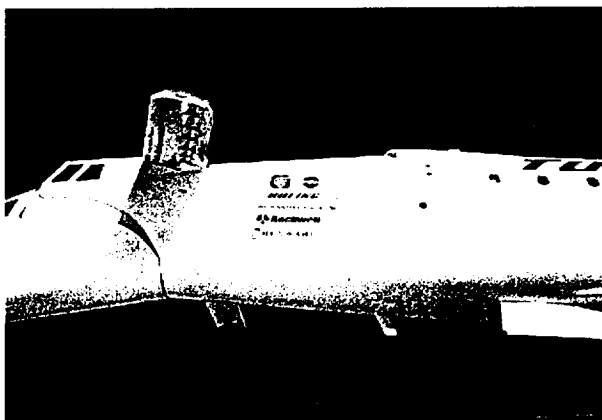


Figure 6 - TU 144 stowable canards with multi-element mechanical high-lift devices

OBJECTIVES AND APPROACH

The primary objectives of this research grant were twofold. First was the experimental development of advanced pneumatic HSCT generic configurations employing pneumatic CCW flaps and blown canard surfaces, and a slimmer fuselage more representative of a generic HSCT. Special emphasis was placed on development of blown wings and canards as means to increase L/D ratios, which will allow accomplishing most of the research goals listed above.

These results then served as a foundation from which to pursue the second objective, which was to evaluate pneumatic technology from overall systems-analysis and technology-integration points of view for an HSCT-type aircraft. Specific emphasis will be placed on feasibility and economic assessment of this new technology.

The following statements summarize these two tasks:

Task 1 - Development and Aerodynamic Evaluation of Advanced Pneumatic HSCT Configurations

During Phases III and IV of the existing NASA-sponsored program (Reference 1), blown lift and canard surfaces installed on a generic HSCT model were shown to dramatically increase aircraft lift and stall angle while yielding large thrust recovery and associated drag reduction (Reference 5). However, in that proof-of-concept evaluation, the aircraft employed a broad-diameter generic fuselage from a previous NASP configuration. Furthermore, longitudinal trim of the vehicle was not successfully demonstrated using horizontal tails. To further increase lift achieved at low aircraft angle of attack while reducing blowing requirements, a thin dual-radius Circulation Control Wing (CCW) blown flap will be operated in an unsteady pulsed-blowing mode. The baseline NASP fuselage shown in Figure 1 will be replaced with that of a thinner generic HSCT fuselage configuration. Subsonic wind-tunnel evaluations will be conducted in the same GTRI facility as previously used, the Model Test Facility (MTF) research tunnel. The unsteady wing blowing should further increase the aerodynamic performance measured during the previous test while requiring much lower blowing rates, and yielding a simple but even more effective pneumatic HSCT aircraft. A new small circular-cylinder pneumatic canard plus the previous blown canards will be evaluated in conjunction with the CCW blown flap installed on the wing.

Specific Task 1 elements are:

- **Design and fabrication of a new model fuselage** to represent a generic HSCT configuration, rather than the current NASP body (data to define the fuselage contour will be supplied by NASA); fuselage will include separate air plenums for canard and wing blowing
- Fabrication and installation of a smaller **circular-cross-section pneumatic canard**, and modification of the **mount for the existing pneumatic canards** to allow their installation within the new slimmer HSCT fuselage
- Modification of **horizontal tail and mounting support** to allow tail installation on the new HSCT fuselage

- **Installation of the pneumatic test setup** and the blown HSCT semi-span model in the MTF subsonic research wind tunnel
- **Experimental subsonic evaluations**, including variation in vehicle angle of attack, wing CCW flap and canard blowing rates, and longitudinal trim capability of the tail and of the canards, both conventional and pneumatic
- **Evaluation** of the effectiveness and simplicity of the **new blown circular-cylinder canard**, and parametric tradeoffs of slot height, slot location, blowing pressure and mass flows to reduce vehicle required blowing rates
- **Evaluation of drag reduction and overall increase in vehicle L/D** due to the streamlined fuselage and to pneumatic canards and wing blowing
- Design and fabrication of an **unsteady pulsed-blowing system** and recording instrumentation, plus system calibration
- **Evaluation of pulsed blowing** on the wing CCW flap to minimize required blowing rate and to optimize the blowing performance due to increased flowfield entrainment
- Evaluation of **suppression of wing flowfield separation and vortex flow elimination** by existing and new pneumatic canards
- Force, moment and blowing parameter measurement with tunnel corrections, and **data reduction** to aerodynamic coefficients
- **Data conversion and input** to Georgia Tech ASDL systems analyses and technology integration studies to allow conduct of Task 2

Task 2 - Systems Analysis and Viability Study for Pneumatic HSCT-Type Configurations

These resulting data, including demonstrated aerodynamic characteristics, will be supplied to Georgia Tech's Aerospace Systems Design Lab in the School of Aerospace Engineering to evaluate economic and performance payoffs in Task 2. The results of that effort are provided as Reference 8.

TEST CONFIGURATION SELECTION; MODEL DESIGN AND FABRICATION

To accomplish the above experimental evaluations, certain modifications were necessary to the existing half-span HSCT wind-tunnel model used in Reference 5. (Because it will be used herein for reference to the previous test configurations and results, Reference 5 has been included as Appendix A). Of primary importance, the NASP-based fuselage of Figure 1 was replaced with a much more relevant generic HSCT fuselage; the geometry of this configuration was provided by NASA LaRC and is shown in Figure 7, the design layout for the model. The obvious advantages of this new configuration are much thinner fuselage radii at all longitudinal stations, and the resulting increase in exposed wing area plus reduced cross-section body area, leading to increased lift, reduced drag and increased lift-to-drag ratio. Furthermore, the wing blowing slot could now be extended further inboard (from 9.0 to 11.25 inches), giving an increased slot length and much larger effective blown wing area. The semi-span wing employed is the same as that from Reference 5 and Figure 1 herein, namely a flat plate with bevelled leading edge (LE) to produce high-alpha vortex flow, but now with a greater exposed area and

chord. The wing plain flaps and CCW flaps (shown in Figure 8) are also the same as for the previous tests, except that a new 10° CCW flap (with 59° of blowing jet turning has now been fabricated for testing as an intermediate takeoff flap configuration.

The blown canards, Figure 9, to be evaluated under these investigations include: Canard 1 (AR=1.29 with a CCW-type trailing edge), Canard 3 (AR=2.58, aft sweep and with a similar CCW TE) and a Circulation Control circular cylinder cross-section canard. This latter configuration, the CC cylinder canard, represents an attempt to dramatically increase the blown lift and pitching moment available from the canard, or conversely, to reduce the canard blowing required to provide pitch stability and further lift augmentation. Previous subsonic investigations of 2-dimensional tangentially-blown cylinders similar to this have shown C_l values approaching 12-14 (Reference 9). The obvious benefit is a much smaller canard to provide pitch trim (unlike the mechanical devices on the SST of Figure 6), resulting in a much smaller storage area required, or even the possibility of a telescoping circular-cross-section canard that could be retracted into the fuselage for high speed. Furthermore, the unblown CC circular canard is insensitive to angle of attack change, so that it does not experience the pitch instability normally associated with canards at increasing α . A special canard mount was designed to allow both an air supply and the ability to rotate the canard in order to vary the blowing slot location θ_{slot} . To mount the two horizontal tails of Figure 1, a new horizontal tail mounting device was necessary due to the thinner aft fuselage characteristics. The tail area was increased inboard to retain the same tail span as in Figure 1. To record unsteady pressure in the wing plenum during the pulsed blowing evaluations, two new Kulite 25 psid differential transducers were purchased and installed at the inboard and outboard ends of the wing blowing plenum. The above components were designed and fabricated for GTRI under subcontract by prototype and fabrication shop Novatek, Inc. of Smyrna, GA.

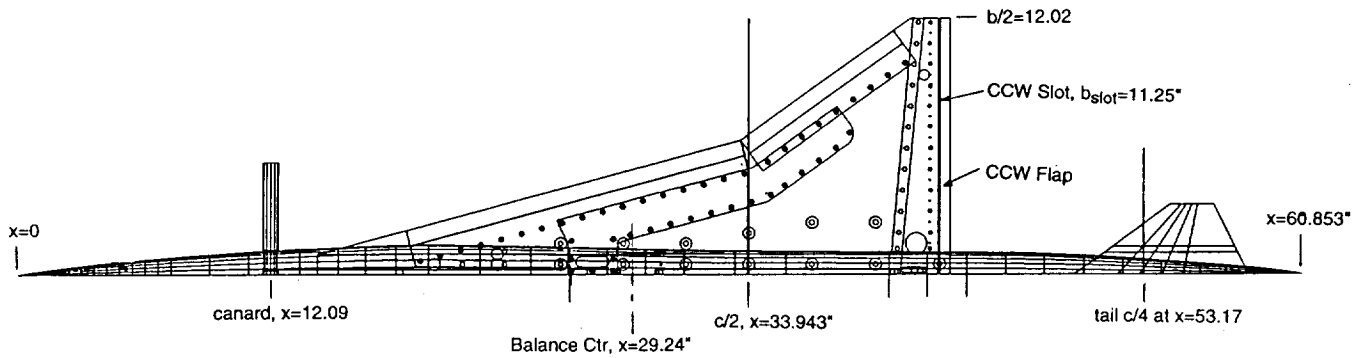


Figure 7 - Revised geometry of current pneumatic HSCT half-span wind-tunnel model

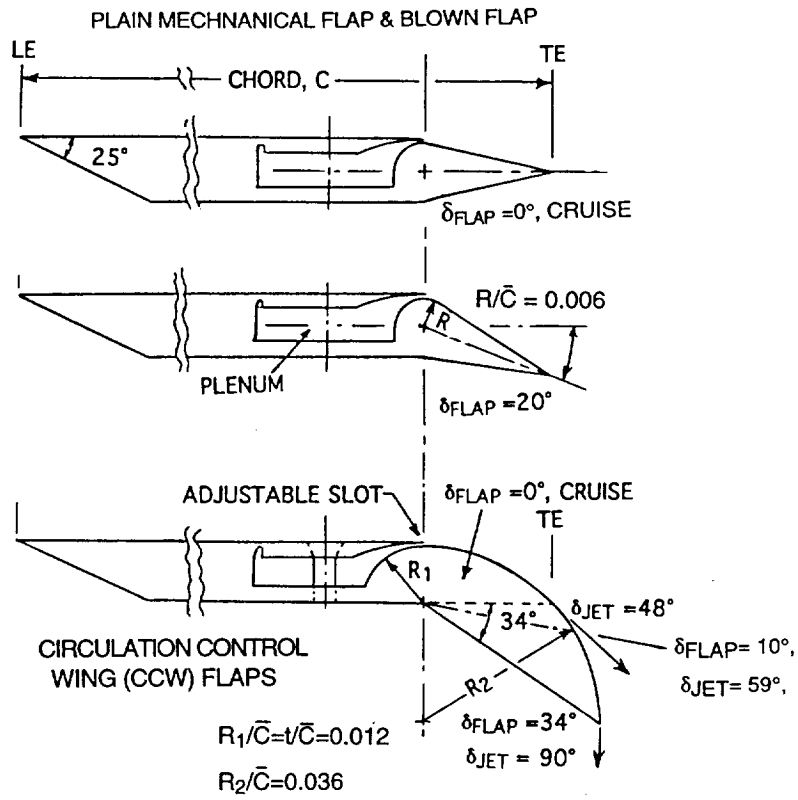


Figure 8 - Blown conventional and CCW trailing-edge configurations

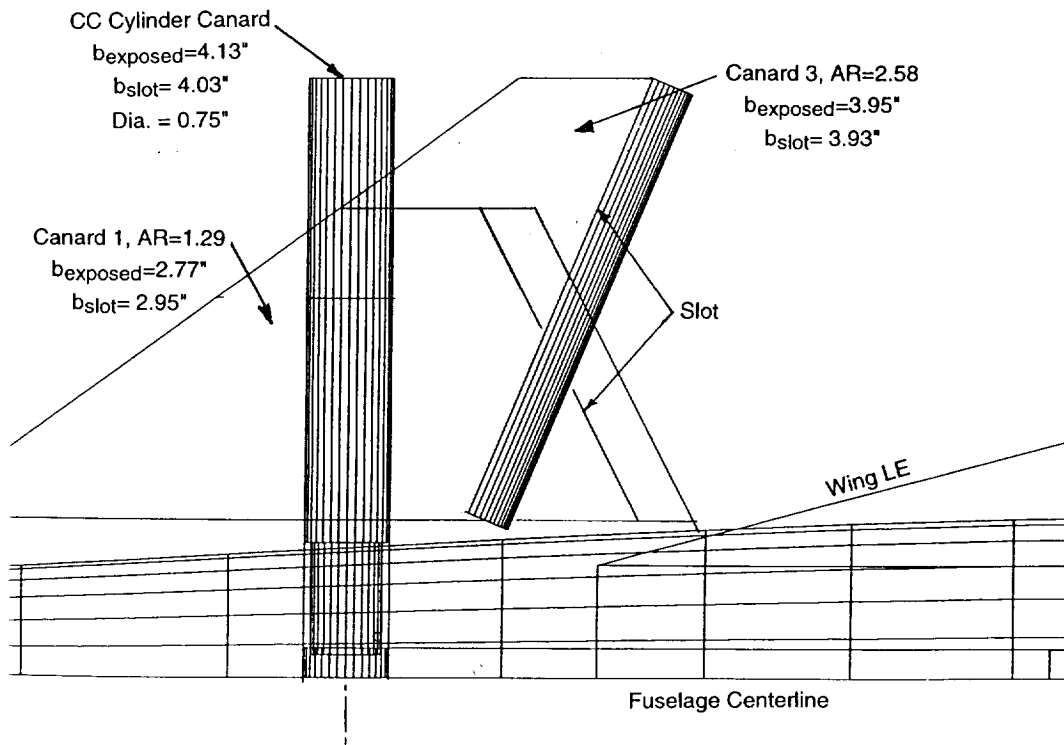


Figure 9 - Pneumatic canards developed and evaluated

GTRI MODEL TEST FACILITY

TEST SECTION

90"H X 43"W X 90"L
 $V_{max} = 200$ ft/sec
 $q_{max} = 50$ psf
Nominal Turbulence 0.4%
Blown Walls for BL control

INSTRUMENTATION

Automatic Pressure SV
6 Component Balances
Hydraulic Mount for IGE Tests
Variable Pitch/Yaw during run
3-D Traverse Mechanism
2-D Laser Velocimeter
On-Line Data Acquisition
On-Line Color Data Display/Plot
Hot Wire/Hot Film Anemometers

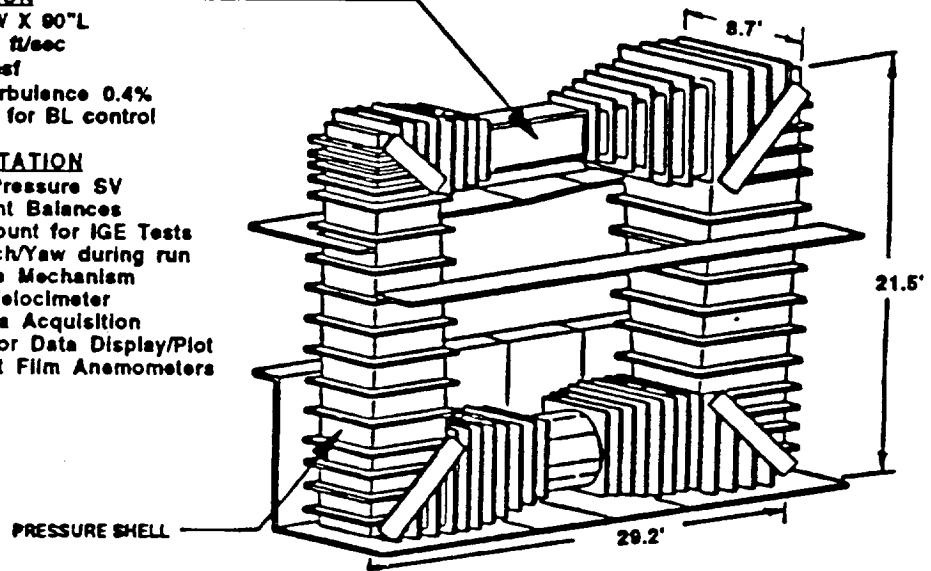


Figure 10 - GTRI Model Test Facility Research Wind Tunnel

SUBSONIC WIND TUNNEL TESTS AND EVALUATIONS

The new semi-span pneumatic HSCT body-wing model (right side) was mounted in the GTRI Model Test Facility (MTF) research tunnel, Figure 10, on a six-component floor balance. Figure 11 shows the model at $\alpha=0^\circ$ angle of attack with the enlarged horizontal tail and the CC cylinder canard installed. Figure 12 shows the model at positive angle of attack with the blown Canard 1 (AR=1.29) installed. The top of the model is towards the camera, making the photo appear inverted. The model centerline was approximately 1 inch off the tunnel floor when mounted on a 3/8-inch splitter plate, which was bolted to a circular disk mounting plate attached to the balance frame. Tares on the mounting plate and disk assembly alone were run and these values were subtracted from all test data as functions of freestream dynamic pressure and angle of attack. This model mounting plate and disk were attached to an automated rotating pitch table which was computer controlled to allow variation in angle of attack, α .

Two flexible air supply lines (Figure 13) were attached to feed into the model mounting fixture and then were wrapped around the pitch mechanism to eliminate hose pressure effects in lift, pitch and drag. In the model fuselage, these two air supply lines were kept separate, with one feeding the aft CCW wing plenum and the other leading to the forward canard plenum. Interchangeable flow meters (critical flow nozzles) measured mass flow into the model plenum. Located between the model and the flow meters, the supply lines were fed through trapeze systems to eliminate hose pressure forces. Model internal total pressure pickups measured plenum total pressure, allowing calculation of isentropic jet velocity, V_j . Then the blowing

momentum coefficient, non-dimensionalized by dynamic pressure and model wing area, was calculated as:

$$C_{\mu} = \dot{m}V_j / (qS/2)$$

Reference area and lengths used in the data reduction for this 0.015555-scale model are:

Wing area, semi-span: $S/2 = 1.2061 \text{ ft}^2$
Wing semi-span: $b/2 = 12.02" = 1.00167 \text{ ft}$
Mean Aero Chord: $\bar{c} = 1.7165 \text{ ft}$
Moment Center: x at $\bar{c}/2$: $= 33.943" \text{ aft of fuselage nose (FS 0.00)}$
 $= 4.701" \text{ aft of balance center}$
 $= 0.5578 \text{ fuselage length}$
 z at moment center $= -1.0" \text{, below fuselage centerline}$
Aspect ratio, $AR = 1.714$

Also, see Figure 7 for other dimensions. Note that force and pitching moment coefficients on this half-wing model are based on half-wing area. Thus all coefficients are relevant to the entire aircraft. For example;

$$C_L = L / (q S/2)$$

$$C_M = M / (q \bar{c} S/2)$$

where L and M are experimentally-measured values for only the half-wing. Note that pitching moment is referenced to 50% mean aerodynamic chord ($0.50 \bar{c}$), which has come to be consistent with high-speed aircraft moment center locations.

Test procedures employed in this pneumatic test program generally followed those described in Reference 10. The subsonic evaluations of these pneumatic and conventional flap and canard configurations were conducted at GTRI in the time frame from February 9 to March 23, 1999, and included 249 recorded runs, as shown in Table I, the test run log. After tare and preliminary Reynolds number runs, each new configuration was evaluated through a similar process. Angle of attack sweeps were conducted at several speeds (dynamic pressures, q , and Reynolds numbers), followed by momentum coefficient (C_{μ}) sweeps at $\alpha = 0^\circ$ at several speeds. These were then supplemented by α sweeps at constant C_{μ} values. Frequently, additional parameters were added, such as variation in blowing slot height, slot location on the CC cylinder canard, etc. Following the steady-state evaluations, canard and tail were removed and an investigation of unsteady pulsed blowing on the CCW 34° flap configuration was conducted between June 10 and June 22, 1999, and included 28 additional runs after much setup time with these pulsing devices and actuating valve devices.

The following sections describe trends determined in the data relative to these parameters.

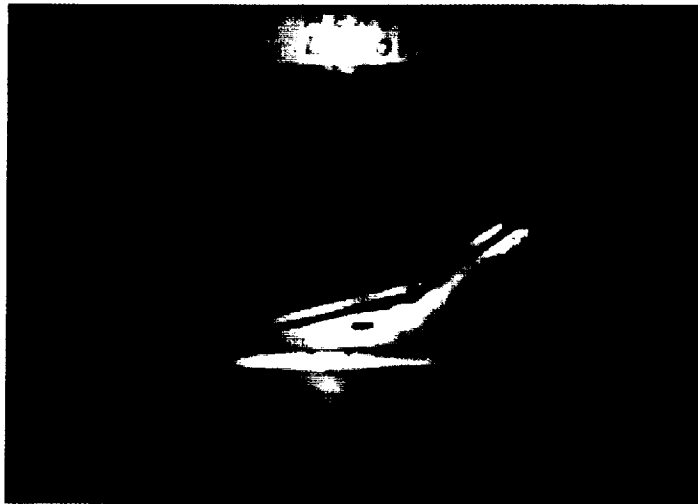


Figure 11 -Wing/Body/Tail model with CC cylinder Canard installed in the MTF tunnel at $\alpha=0^\circ$

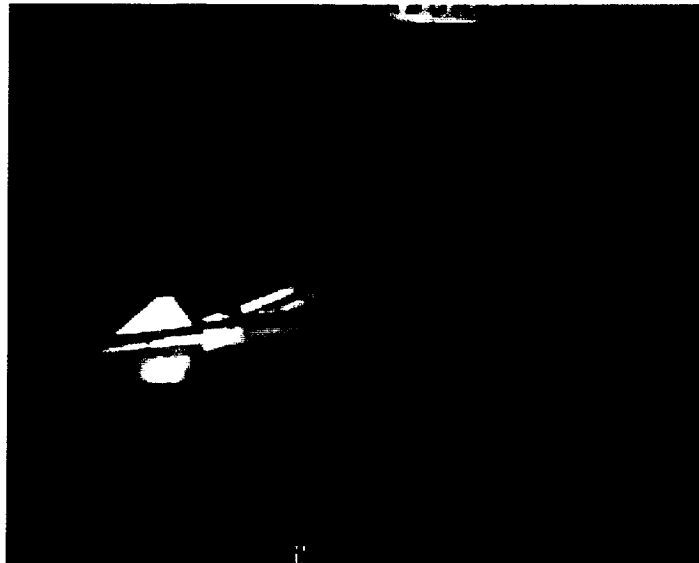


Figure 12 - Wing/Body/Tail model with blown Canard I installed in the MTF tunnel at $\alpha=25^\circ$

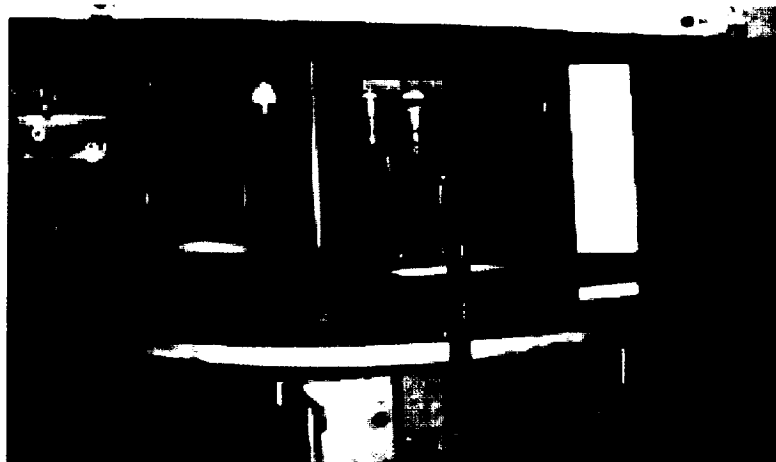


Figure 13 - Air supply lines wrapped around balance mounting structure below tunnel floor; aft line (left connection) attaches to CCW and front line to blown canard

MODEL TEST FACILITY										MODEL:		TEST MTF044		
GEORGIA TECH RESEARCH INSTITUTE										HSCT/CCW Phase III		PAGE 1		
DATE 1999	RUN NO.	CONST FILE	TYPE RUN	Configuration					Angles		Blowing		Q _o psf	COMMENTS
				δ_{lap}	i_{tail}	Canard	h_{ccw}	h_{canard}	α	θ_{slot}	$C_{\mu can}$	$C_{\mu ccw}$		
2/19	507	R507	α sweep	Plain 0	Off	Off	0.015"	Off	-5->30	-			10	Baseline Body, Wing; Plain Flap, 0°
2/22	510	R510							-5->32				10	Alpha Range Variation
	512								-1->32				20	
	513	R513							-2->32				10	Repeat R510
2/23	517	R514							-5->32				20	
	518												30	Production Data Runs; q effects
	519												10	
	520												20	
	521												40	
	522				0°								20	Add Conventional Horizontal Tail, tail=0°
	523													tail = -10°
	524				+10°									tail = +10°
	525				0°									Add Large Horizontal Tail, tail = 0°
	526				-10°									tail = -10°
	527				+10°									tail = +10°
	528		C_{μ} sweep		Off				0			0->0.24		tail off
2/24	529		α sweep						-5->32			0.05		
	530											0.10		
	531											0.20		
	532		C_{μ} sweep						0			0->0.31	15	
	533		α sweep						-5->32			0		
	534											0.20		
	535											0.315		
	536				-10°							0.10	20	Tail Trim Capabilities; tail = -10°
	537											0.315	15	
	538				0°							0.10	20	tail = 0°
	539											0.315	15	
	540				+10°							0	20	tail = +10°
	541	R514		Plain 0	+10°								15	

12

Table I
Wind Tunnel Test Log, GTRI Test MTF 044

MODEL TEST FACILITY
GEORGIA TECH RESEARCH INSTITUTE

MODEL:
 HSCT/CCW PHASE III

TEST MTF044
PAGE 2

DATE 1999	RUN NO.	CONST FILE	TYPE RUN	Configuration					Angles		Blowing		Q ₀ psf	COMMENTS
				δ_{flap}	i_{tail}	Canard	h_{cow}	h_{canard}	α	θ_{slot}	$C_{\mu can}$	$C_{\mu ccw}$		
2/25	542		α sweep	Plain 20	Off	Off	0.015"	Off	-5->32	-		0	10	Switch to Plain flap at 20 degrees
	543												15	
	544												20	
	545				-10°									
	546				0°									
	547				+10°									
	548		C_{μ} sweep		Off				0			0->0.23		
	549											0->0.30	15	
	550		α sweep						-5->32			0.10	20	
	551											0.308	15	
	552				0°							0.10	20	
	553											0.308	15	
	554				-10°							0.10	20	
	555											0.308	15	
	556				+10°							0.10	20	
	557											0.308	15	
2/26	558			CCW 0	Off							0	10	Switch to CCW T.E. with no deflection
	559												15	
	560												20	
	561		C_{μ} sweep						0			0->0.328	15	
	562											0->0.24	20	
	563		α sweep						-5->32			0.082		
	564											0.10		
	565											0.164		
	566											0.20		
	567											0.328	15	
	568				0°							0	20	
2/26	569	R514										0.10	20	
	570											0.20		

MODEL TEST FACILITY
GEORGIA TECH RESEARCH INSTITUTE

MODEL:
 HSCT/CCW PHASE III

TEST MTF044
PAGE 3

DATE 1999	RUN NO.	CONST FILE	TYPE RUN	Configuration					Angles		Blowing		Q _o psf	COMMENTS
				δ_{flap}	i_{tail}	Canard	h_{cow}	h_{canard}	α	θ_{slot}	$C_{\mu can}$	$C_{\mu ccw}$		
2/26	571	R514	α sweep	CCW 0	0°	Off	0.015"	Off	-5->32	-		0.328	15	
	572				-10°							0	20	
	573											0.082		
	574											0.20		
	575											0.327	15	
	576				+10°							0	20	
	577											0.082		
	578											0.20		
	579											0.327	15	
3/1	580											0.20	20	Found missing screw, re-run 578
	581											0.327	15	Re-run 579
	582			CCW 10	Off							0	10	Switch to 10 degree deflection on CCW
	583												15	
	584												20	
	585		C_{μ} sweep						0			0->0.328	15	
	586											0->0.246	20	
	587		α sweep						-5->32			0.082		
	588											0.328	15	
	589				0°							0	20	
	590											0.082		
	591											0.328	15	
	592				-10°							0	20	
	593											0.082		
	594											0.328	15	
	595				+10°							0	20	
	596											0.082		
	597											0.328	15	
3/2	598			CCW 34	Off							0	15	$\delta_{flap} = CCW 34^\circ$
	599												20	
	600				0°									

MODEL TEST FACILITY
GEORGIA TECH RESEARCH INSTITUTE

MODEL:
 HSCT/CCW PHASE III

TEST MTF044
PAGE 4

DATE 1999	RUN NO.	CONST FILE	TYPE RUN	Configuration					Angles		Blowing		Q _o psf	COMMENTS
				δ_{tap}	i_{tail}	Canard	h_{ccw}	h_{canard}	α	θ_{slot}	$C_{\mu can}$	$C_{\mu ccw}$		
3/2	601	R514	α sweep	CCW 34	-10°	Off	0.015"	Off	-5->32	-		0	20	
	602				+10°									
	603		C_{μ} sweep		Off				0			0->0.33	15	
	604											0->0.248	20	
	605		α sweep						-5->32			0.082		
	606											0.328	15	
	607											0.041	20	
	608											0.164		
3/3	609				0°							0.328	15	
	610											0.082	20	
	611				-10°							0.082		
	612											0.328	15	
	613				+10°							0.328		
	614											0.082	20	
	615		C_{μ} sweep		0°				10			0->MAX	10	
	616												15	
	617												20	
	618												15	
	619												30	
	620												35	
3/4	621				Off		0.010"		0			0->0.336	15	Change CCW slot height to 0.010"
	622											0->0.253	20	
	623											0->0.200	25	
	624											0->0.168	30	
	625		α sweep						-5->32			0	20	
3/4	626	R514										0.041	20	
	627											0.082		
	628											0.164		
	629											0.328	15	

MODEL TEST FACILITY
GEORGIA TECH RESEARCH INSTITUTE

MODEL:
 HSCT/CCW PHASE III

TEST MTF044
PAGE 5

DATE 1999	RUN NO.	CONST FILE	TYPE RUN	Configuration					Angles		Blowing		Q _o psf	COMMENTS
				δ_{flap}	i_{tail}	Canard	h_{ccw}	h_{canard}	α	θ_{slot}	$C_{\mu can}$	$C_{\mu ccw}$		
3/4	630	R514	α sweep	CCW 34	Off	Off	0.010"	Off	-5->32	-		0.010	20	
	631											0.020		
	632											0.030		
	633											0.005		
	634											0.015		
	635				0°							0		
	636											0.082		
	637	R637							-5->26			0.328	15	
	638	R514			-10°				-5->32			0	20	
	639											0.082		
3/8	640	R637							-5->26			0.328	15	
	641	R514			+10°				-5->32			0	20	
	642											0.082		
	643	R637							-5->26			0.328	15	
	644	R514		CCW 0	Off				-5->32			0		$\delta_{flap} = CCW 0^\circ$
	645												20	
	646		C_{μ} sweep						0			0->0.257		
	647		α sweep						-5->32			0.082		
	648											0.328	15	
	649				0°							0	20	
	650											0.082		
	651											0.328	15	
	652				-10°							0	20	
	653											0.082		
	654											0.328	15	
3/8	655				+10°							0	20	
	656											0.082		
3/9	657											0.328	15	
	658			CCW 10	Off							0	20	$\delta_{flap} = CCW 10^\circ$

MODEL TEST FACILITY
GEORGIA TECH RESEARCH INSTITUTE

MODEL:

HSCT/CCW PHASE III

TEST MTF044

PAGE 6

DATE	RUN NO.	CONST FILE	TYPE RUN	Configuration					Angles		Blowing		Q _o psf	COMMENTS	
				δ_{flap}	i_{tail}	Canard	h_{ccw}	h_{canard}	α	θ_{slot}	$C_{\mu can}$	$C_{\mu ccw}$			
3/9	659	R514	α sweep	CCW 10	Off	Off	0.010"	Off	-5->32	-		0.082	20		
	660											0.328	15		
	661		C_{μ} sweep						0			0->0.26	20		
	662		α sweep		0°				-5->32			0			
	663											0.082			
	664											0.328	15		
	665				-10°							0	20		
	666											0.082			
	667											0.328	15		
	668				+10°							0	20		
	669											0.082	20		
	670											0.328	15		
3/10	671			CCW 0	0°	Can. 1		0.010"				0	0	20	Add Canard 1
	672	R672							-5->38						Increase α range
	673	R673	C_{μ} sweep						0			0->.021			critical flow meter d= .0894" for canard
	674											0->.03	15		
	675	R672										0->.06	20	flow meter d = 0.1757" for canard	
	676		α sweep						-5->38			0.035		d = 0.2496" for CCW	
	677		C_{μ} sweep					0.015"	0			0->.058			
3/12	678	R678										0->.08			
	679		α sweep						-5->38			0.04			
3/15	680				Off							0.08			
	681				0°										
	682											0.1	15		
3/15	683											0	20	Repeat Run 672	
	684			CCW 34					-5->35			0.164	18	$\delta_{flap} = CCW 34^\circ$	
	685											0.04		x - Bad Run	
	686											0	0.082	20	
	687											0.04			

MODEL TEST FACILITY
GEORGIA TECH RESEARCH INSTITUTE

MODEL:
 HSCT/CCW PHASE III

TEST MTF044
PAGE 7

DATE	RUN NO.	CONST FILE	TYPE RUN	Configuration					Angles		Blowing		Q ₀ psf	COMMENTS
				δ_{flap}	i_{tail}	Canard	h_{ccw}	h_{canard}	α	θ slot	$C_{\mu can}$	$C_{\mu ccw}$		
3/16	688	R678	α sweep	CCW 34	0°	Can. 1	0.010"	0.015"	-5->35	-	0.08	0.082	20	
	689		C_{μ} sweep			Can. 3		0.010"	0		0->0.10	0		Add Canard 3; AR = 2.58
	690		α sweep						-5->35		0	0		
	691										0.04			
	692										0.08			
	693										0	0.082		
	694										0.04			
	695										0.08			
	696			CCW 0							0	0		$\delta_{flap} = CCW 0^\circ$
	697										0.04			
	698										0.08			
3/17	699		C_{μ} sweep			CCcyl			0	0°	0->.085			Add Cylinder Canard
	700		α sweep						-5->35		0.08			
	701										0.04			
	702										0			
	703											0.082		
	704										0.04			
	705										0.08			
3/18	706		C_{μ} sweep						0	-20°	0->.084	0		rotated cylinder $\theta_{slot} = -20^\circ$
	707		α sweep						-5->35		0.04			
	708										0.08			
	709										0			
	710										0.04	0.082		
	711										0.08			
	712									+20°	0.04			rotated cylinder $\theta_{slot} = +20^\circ$
	713										0.08			
	714		C_{μ} sweep						0		0->.085	0		
	715		α sweep						-5->35		0			
	716										0.04			
	717										0.08			

MODEL TEST FACILITY
GEORGIA TECH RESEARCH INSTITUTE

MODEL:
 HSCT/CCW PHASE III

TEST MTF044

PAGE 8

DATE 1999	RUN NO.	CONST FILE	TYPE RUN	Configuration					Angles		Blowing		Q _o psf	COMMENTS
				δ_{flap}	i_{tail}	Canard	h_{ccw}	h_{canard}	α	θ slot	$C_{\mu can}$	$C_{\mu CCW}$		
3/18	718	R678	α sweep	CCW 0	0°	CCcyl	0.010"	0.010"	-5->35	+40°	0	0	20	rotated cylinder $\theta_{slot} = +40^\circ$
3/19	719		C_{μ} sweep						0		0->.08			
	720		α sweep						-5->35		0.04			
	721										0.08			
	722									+10°	0			rotated cylinder $\theta_{slot} = +10^\circ$
	723										0.04			
	724										0.08			
	725		C_{μ} sweep						0		0->.087			
	726		α sweep								0	0.082		
	727										0.04			
	728										0.08			
	729			CCW 10							0	0		$\delta_{flap} = CCW 10^\circ$
	730										0.04			
3/23	731										0.08			
	732		C_{μ} sweep						33		0->.08			
	733		α sweep								0	0.082		
	734										0.04			
	735										0.08			
	736		C_{μ} sweep						32		0->.08			
	737		α sweep	CCW 34					-5->35		0	0		$\delta_{flap} = CCW 34^\circ$
	738	R738									0.04			
	739										0.08			
	740		C_{μ} sweep						33		0->.08			
	741		α sweep						-5->35		0	0.082		
	742										0.04			
	743										0.08			
	744		C_{μ} sweep						31		0->.08			
	745		α sweep		-10°				-5->35		0.08			$i_{tail} = -10^\circ$; LE down

EXPERIMENTAL DATA ANALYSES AND COMPARISONS, STEADY-STATE

These steady-state runs (in contrast to the later pulsed-blowing dynamic investigations) were run primarily to examine the effects on overall performance of the new slimmer-fuselage HSCT aircraft with variations in conventional and blown high lift devices, as well as unblown and blown canards of various types. Effects of both the canards and the horizontal tail were also studied, as were: Reynolds number effects; effect of blowing at constant angle of attack; effect of α at constant blowing C_{μ} ; effect of configuration-dependent variables such as blowing slot height and/or slot location; and effect of all the above on overall aircraft lift/drag ratio, including any penalty for blowing. These test results and comparisons to the original HSCT/CCW configuration of Reference 5 and Appendix A are included in the following section. Plotted data will appear at the end of this main section.

Reynolds Number Variation

Angle of attack sweeps were run at different freestream dynamic pressures from 10 to 40 psf, with and without blowing, to determine Reynolds number effects on the aerodynamic characteristics. A typical example is the α sweeps of Figure 14, where for the clean wing with undeflected (0°) and 20° plain flaps, dynamic pressure variations were run. The following dynamic pressure/Reynolds number relations apply, based on a mean aerodynamic chord (MAC) of 1.7165 ft:

<u>Dynamic Pressure, q, psf</u>	<u>Velocity, fps</u>	<u>Re x 10⁻⁶</u>
10	95.5	0.94
15	116.8	1.13
20	134.3	1.34
30	164.0	1.64
40	190.4	1.87

Figure 14 shows that for dynamic pressures of 15 psf and above, both lift and drag coefficients are relatively free of Reynolds number effect. Thus, in the following data, most runs are at a dynamic pressure of 20 psf ($Re = 1.34 \times 10^6$), except for those cases where higher blowing values are obtained by reducing q to 15 psf and Reynolds number to 1.13×10^6 , which produces no low Reynolds number effects but increases the C_{μ} available from the test air supply.

Flap Configuration Variation, Comparison of Blown Configurations

Previous tests of these pneumatic concepts applied to HSCT-like configurations (Reference 5 and Appendix A) employed the flaps shown in Figure 8 for lift augmentation and for thrust recovery (see Figures 15 and 16 of Appendix A). However, the very wide afterbody of that configuration covered much of the inboard wing. It was thus desired to investigate conventional and blown flap performance on the current slender body of Figure 7, as well as to

investigate slot height effects on the blown wings. The following high-lift configurations (Figure 8) were tested (with and without tails, but without canards at this point):

<u>Flap Type</u>	<u>Flap Deflection</u>	<u>Conventional</u>	<u>Blown</u>	<u>Slot Ht., in.</u>	<u>Runs</u>
Conv. Plain	0°	X	X	0.015	510-541
"	20°	X	X	"	542-557
CCW	0		X	"	558-58"
"	10°		X	"	582-597
"	34°		X	"	598-620
"	34°		X	0.010	621-643
"	0°		X	"	644-657
"	10°		X	"	658-670

The unblown ($C_{\mu} = 0$) plain flap at 0° (Figure 15) represents the basic clean cruise configuration, and these plots also show the effect of tail deflection on pitching moment. Also shown are small increases in lift due to tangential blowing at the flap knee, as well as drag reductions due to thrust recovery. While the conventional tail can trim the clean cruise aircraft, it is not able to trim the nose-down pitching moments added by increased blowing on the 0° plain flap. Similar trends for the blown and unblown conventional plain flap at 20° deflection are shown in Figure 16.

Figures 17, 18, and 19 show similar data for the CCW flap of Figure 8. The significant gains in C_L are due to the much greater jet turning and force augmentation due to the curved CCW surface downstream of the blowing slot. Whereas the flap deflection listed for the CCW devices is the lower surface deflection (Figure 8), the actual jet deflection can reach the following values as C_{μ} is increased:

<u>CCW Flap Deflection, degrees</u>	<u>Jet Turning Angle, degrees</u>
0	48
10	59
34	90

Comparisons of these curves to the baseline aircraft with 0° flap deflection (Figure 15, Run 522, tail = 0°) show significant increases in C_{Lmax} due to flap deflection, blowing, and the CCW configuration. The 34° CCW with blowing can increase C_{Lmax} from 1.39 of the baseline to 2.48 with blowing, an increase of 78%. Notice that the blown CCW has reached an earlier stall as C_{μ} increases due to the increased circulation around the sharp wing leading edge. Prevention of this leading edge stall will yield greater increases.

However, further blown lift improvement results from a decrease in slot height. Figure 20 presents flow visualization showing jet turning at the 34° CCW flap for two slot heights. As

the slot height is reduced by 33% from $h=0.015$ “ to $h=0.010$ ”, the jet attachment and turning increase, and the flow becomes more aligned with the wing chord. Figure 21 shows measured forces and moments for the 34° CCW, and C_{Lmax} (at tail= 0°) now increases to 2.62, or 88% higher than the conventional.

An important improvement in lift generation has occurred for this new blown HSCT model. In Appendix A data, the previous model's C_{Lmax} appeared to be limited to around 1.9 or so, independent of whether achieved by α or by blowing. As Figure 21 shows, the new configuration, even without a trimming canard adding additional lift, is generating C_{Lmax} greater than 2.7, probably due to the increased inboard blowing slot and uncovered blown wing area. Whereas C_{Lmax} is not the only factor governing actual aircraft terminal area flight conditions, it does determine V_{stall} , upon which takeoff and landing speed criteria are based.

Because C_{Lmax} is heavily influenced by strong leading edge vortex flows on these highly swept wings, a fairer comparison of flap type and blowing levels is at $\alpha=0^\circ$, Figure 22, which has the tail removed and shows both slot heights. This data is measured for an increase in C_μ at fixed $\alpha=0^\circ$. As blowing increases for all configurations, lift increases also, but the CCW flap shows far greater augmentation ($\Delta C_L/C_\mu$ of up to 12 at lower C_μ) than the plain blown flap. Drag reduction due to blowing (thrust recovery) occurs for both plain flaps and for the 0° CCW, so these would be acceptable takeoff configurations. The 34° CCW produces increased drag with blowing due to the high induced drag at the greater lift, and thus would be an excellent landing configuration. The intermediate 10° CCW produces higher lift than the other flaps (except CCW 34°), but shows drag decreasing at greater C_μ , so is a possible compromise configuration. The C_L vs C_D blown drag polars show an interesting capability, when for a desired higher C_L at $\alpha=0^\circ$, say above 0.5, either negative or positive drag can be produced by varying the CCW flap configuration.

Note also the equivalent lift/drag values ($C_{Deq}=C_D + C_\mu$), which reduce with both lift and blowing. However, at higher desired C_L values, say above $C_L=0.3$, greater L/D_{eq} occurs for the CCW with increased flap deflection. For example, at $C_L = 0.5$, both the CCW 10° and the CCW 34° flaps yield L/D_{eq} of 6.5 to 7, compared to about 4.3 for the conventional 20° plain blown flap. For $C_L = 1.0$, L/D_{eq} values of 3.5 to 4.0 for the CCW flaps are seen, but that C_L is not achieved at all by the plain blown flaps. Thus, even with the blowing penalty included, the CCW flaps offer a favorable L/D_{eq} improvement over the conventional plain or blown flaps.

Configurations for Pitch Trim

For the blown configurations above, most of the data show increasing nose-down pitch as lift is increased due to blowing. While this does provide excellent longitudinal stability, it frequently poses a problem with longitudinal trim. Notice that in most of the blown cases, even the 10° deflection of the enlarged horizontal tail does not provide trim over the entire α range. In Reference 5 and Appendix A, two blown canards with CCW trailing edges were found to produce pitch trim as well as increased stall angle because of their favorable effects on the upwash flowfield over the wing leading edge. However, a three-surface HSCT may not be the most desirable and unblown canards produce both pitch instability and drag. So, a circular cylinder CC canard was prepared because past data (Reference 9) showed section C_l of near 14 for 2-D cylinders. Also, that much canard lift could yield a greatly reduced canard surface area (or the canard could be telescoping for retraction). Lastly, an unblown cylinder is not angle-of-attack sensitive, and thus is not destabilizing. Figure 23 shows the CC cylinder canard model to

be evaluated, in comparison to the AR=1.29 blown Canard 1. As Figure 9 shows, Canard 1 has less span than the CC cylinder, but the AR=2.58 aft-swept Canard 3 has virtually the same span; all three canards were evaluated. The circular cylinder canard could be rotated within its mount so that its blowing slot location θ_{slot} could also be varied.

Flow visualization on the canards showed interesting trends. In Figure 24, the jet flow stays attached to the CCW aft-swept Canard 3, which results in a maximum jet turning angle of 30°-40°. In all these figures, the picture is taken from the top of the model; the slot is on the upper surface, not on the lower surface of the canard as it appears. When the slot is rotated to vertically over the center of the cylinder, then the slot angle $\theta_{slot} = 0^\circ$. In Figure 25a, even at the most forward canard slot location (-20°) the jet turning appears much greater than for Canard 3, somewhere between 50° - 70° for the cylinder. As the slot is rotated aft to + 40° (Figure 25b&c), jet turning is considerably more than 90°, turning forward to as much as 135° or more.

Figures 26 and 27 compare blown Canard 1 and blown Canard 3 when applied with a wing using a CCW flap configuration of either 0° or 34° deflection. There is relatively little difference between the two. In pitch, they can trim the aircraft at $C_{\mu CCW} = 0.0$, but trim is only possible at higher α when $C_{\mu CCW} = 0.082$. In all cases, they are longitudinally unstable in pitch because of their forward location. Figures 28, 29 and 30 compare three different slot locations for the CC cylinder canard with the wing CCW flap at 0° deflection and at two wing blowing values. As the slot location rotates aft, the cylinder canards are able to trim the $C_{\mu CCW} = 0.082$ case at lesser values of canard blowing, reaching trimmed values at $C_{\mu canard}$ values less than 0.025 to 0.03 at the aft slot locations. Also of importance, as the slot locations rotate aft, the C_L - C_M curves become less unstable until for $\theta_{slot} = +20^\circ$, they are nearing neutral stability. Figures 31 and 32 compare the CC circular cylinder and blown canards for the wing CCW with 34° deflection. The circular cylinder canard provides greater nose up pitch for trim and a more neutral C_L - C_M curve than the conventional canards, probably because of greater lift augmentation with less surface area to destabilize. Figure 33 summarizes the effect of the CC cylinder slot location on lift and pitching moment, again confirming improvement as θ_{slot} rotates aft, until a value of +40° is reached, which is apparently too extreme.

An effect of blown canards discovered in the Reference 5 test was the increase in stall angle with canard blowing because canard downwash offsets the upwash at the wing leading edge. Figure 34 shows a similar effect for the CC cylinder canard applied with both the 10° and 34° CCW wing flaps. In both cases, the model was set at an angle of attack just beyond stall at the wing C_{μ} value shown. Then canard blowing was initiated and increased, as the horizontal axis shows. In all cases a very small value of canard C_{μ} was required to “unstall” the wing. Significant increase in C_L and C_M then resulted as the stall angle was extended.

PULSED BLOWING INVESTIGATIONS

Since any type of blown surface must be supplied with pressurized airflow from the aircraft, it is obviously desirable to reduce required mass flow for a given application. Certain research (References 11, 12 and 13) conducted on 2-D blown airfoils have suggested that proper pulsing of the boundary layer control or circulation control jet flow could decrease by as much as 50% the C_{μ} and mass flows required to achieve the same lift with steady blowing. This was attributed to pulsed blowing producing better mixing and flow entrainment with lower boundary layer losses, leading to higher circulation and increased lift. However, the shape of the pulsed blowing wave (pressure versus time) and the blowing duty cycle (time on versus time off) greatly affect these results. Typically, the referenced experimental results showed that pulsing

frequencies of 40 - 50 cps associated with near-square wave shapes and 50% duty cycle were most successful in producing the reductions in required mass flow . It was desired to determine if this same type of performance from 2-D airfoils could be reached on a highly-swept wing with a CCW trailing edge. The CCW 34° configuration with 0.010" slot height was chosen for this test, and both tail and canard were removed. Model incidence was set at $\alpha = 0^\circ$ and Runs 746-773 were conducted. The two 25 psid Kulite dynamic transducers installed in the CCW wing plenum, one inboard and one outboard, were employed as unsteady pressure instrumentation. These were used to record the plenum pressure traces as the time average value between inboard and outboard plenum pickups. A Moog valve arrangement (borrowed from NASA Glenn Research Center) was inserted into the wing plenum air supply line downstream of the existing critical flow nozzle. Cycling rates from 10 - 80 cps were then available and a near-square pressure wave was recorded; however, this wave did not have a zero reading as the minimum value, but rather produced a positive pressure offset as a minimum. It was thus deemed not acceptable for this test. As an alternative, a solenoid pulsing valve was installed in place of this Moog valve. It generated a near-square wave at the lower frequencies, but that was degraded to a sine wave at frequencies above 25 cps or so. Since the back pressures downstream of the critical flow nozzle but upstream of the solenoid were now high enough to invalidate this flow meter's acceptable pressure ratio range, a venturimeter was substituted as the flow meter.

The pulsed blowing tests were run at $q=20$ psf and a CCW slot height of 0.010". Time averaged jet velocities (taken at a rate of 300 samples per second) are shown in Figure 35 for various pulsing frequencies; these were later evaluated using a hot wire installed near the mid-span slot location. The time-averaged venturimeter weight flow rates are shown versus lift in Figure 36, where it is seen that as the frequency increases and the square wave begins to deteriorate, a crossover in weight flow versus C_L occurs. Below that value, higher frequency requires less weight flow to achieve the same C_L . When time-averaged weight flow and velocity are combined to produce time-averaged C_μ , the resulting Figure 37 shows required blowing requirements: at the best case, relatively low C_μ , the same lift coefficient is recorded for C_μ about 45 - 50% less than the steady-state case. At higher blowing values above this crossover, lower frequencies produce less C_L than the steady-state case, but as frequency increases the steady-state case is approached. One is led to expect that if the equipment could be made to produce quality square-wave pressure traces at higher frequencies greater than 25 cps, the crossover point would move to a higher C_μ and the augmentation effect would be much greater. Reference 13 reported a similar trend, but that the point where pulsed lift reduced to steady-state values at the same mass flows was around 50 cps. One also wonders if perhaps the test should be extended to higher angle of attack to note the entrainment effect on the leading edge vortex flow from this highly swept wing.

MTF044 HSCT, Reynolds No. Effects, C_L v. α , C_L v. C_D

Plain Flap, $\delta_{Flap} = 0^\circ, 20^\circ$, $h = 0.015''$

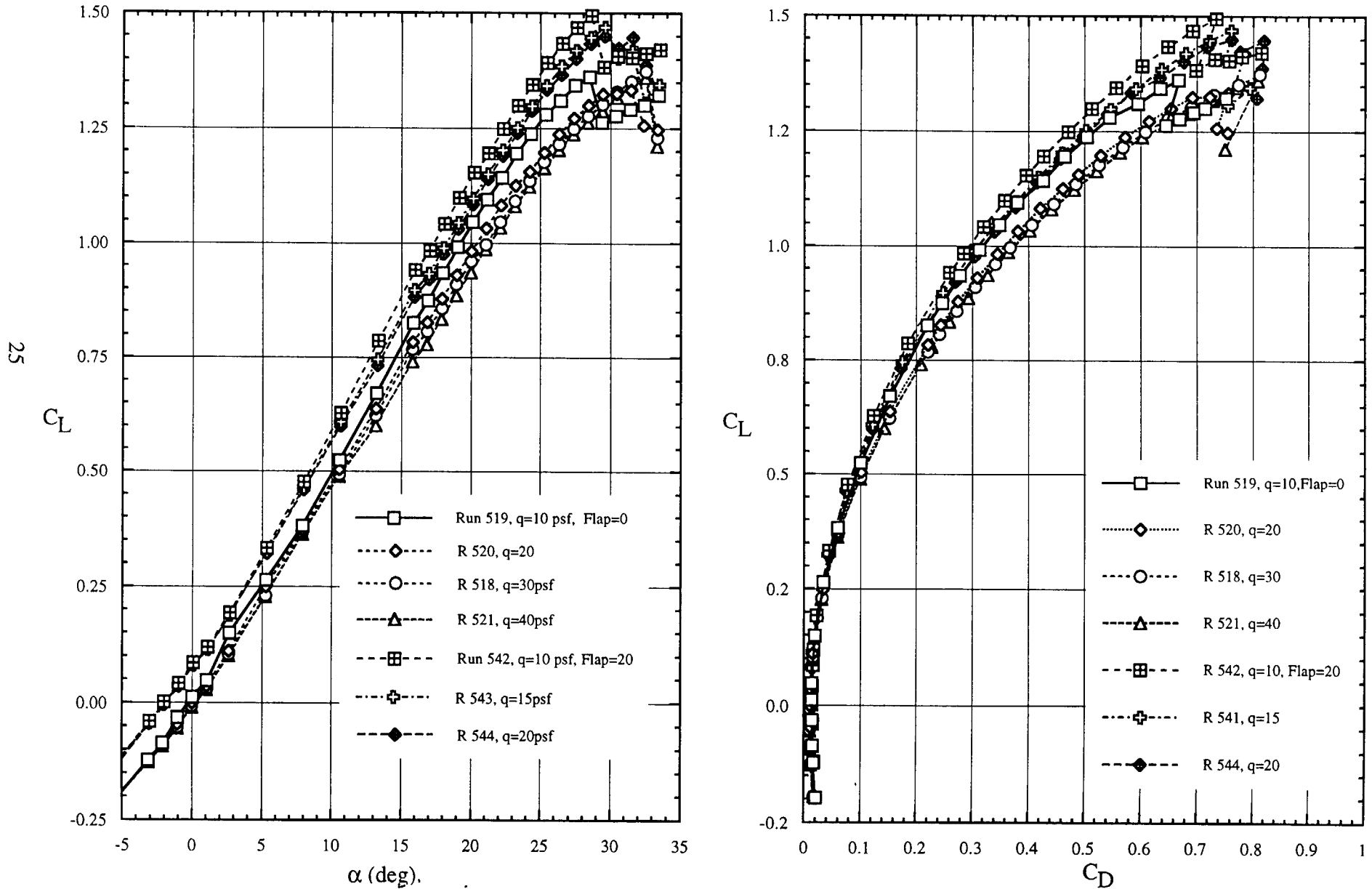


Figure 14- Reynolds number effects for unblown baseline clean wing and for 20° conventional flap

MTF044 HSCT, C_{μ} Effects, C_L v. α , C_L v. C_D

$\delta_{\text{Flap}} = 0^\circ$, $h = 0.015''$

26

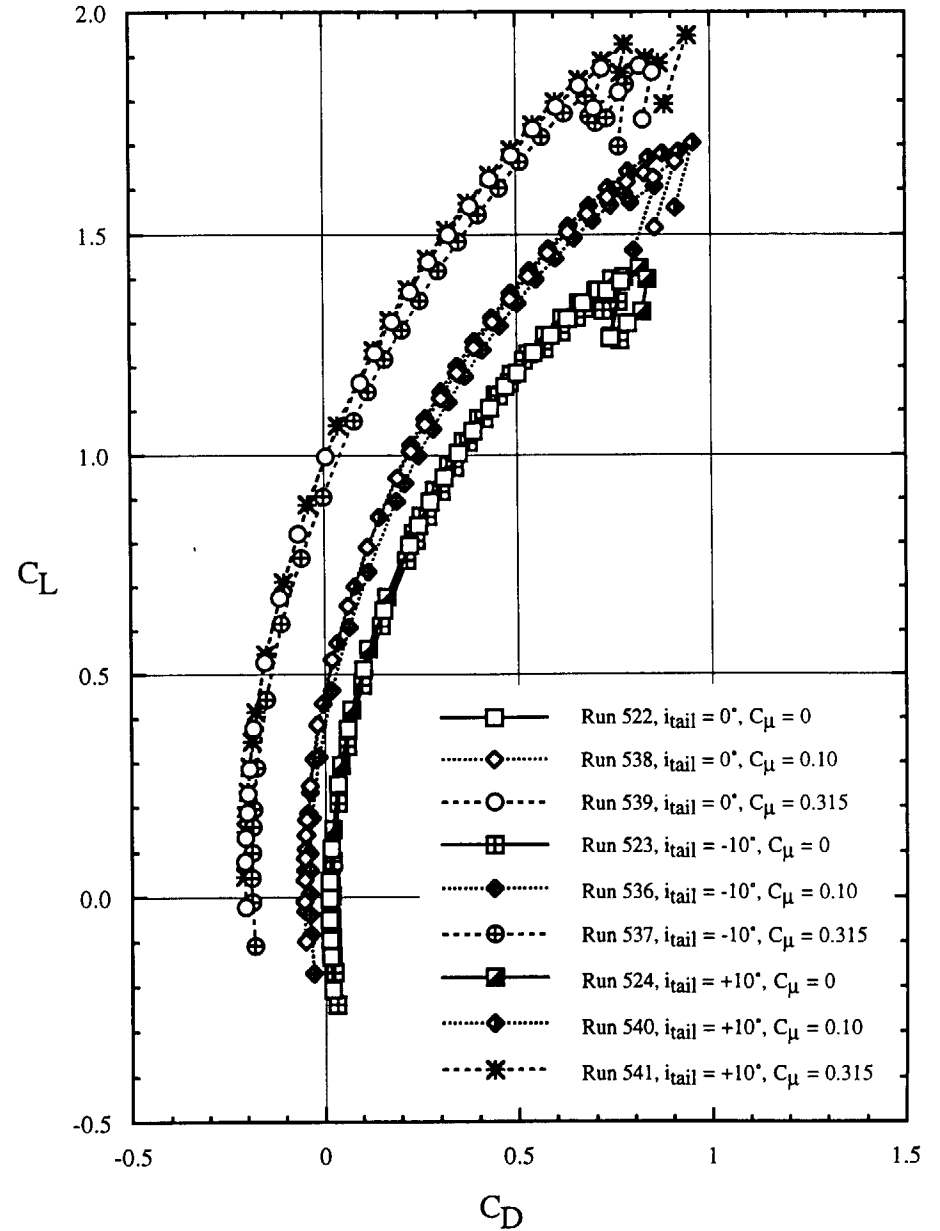
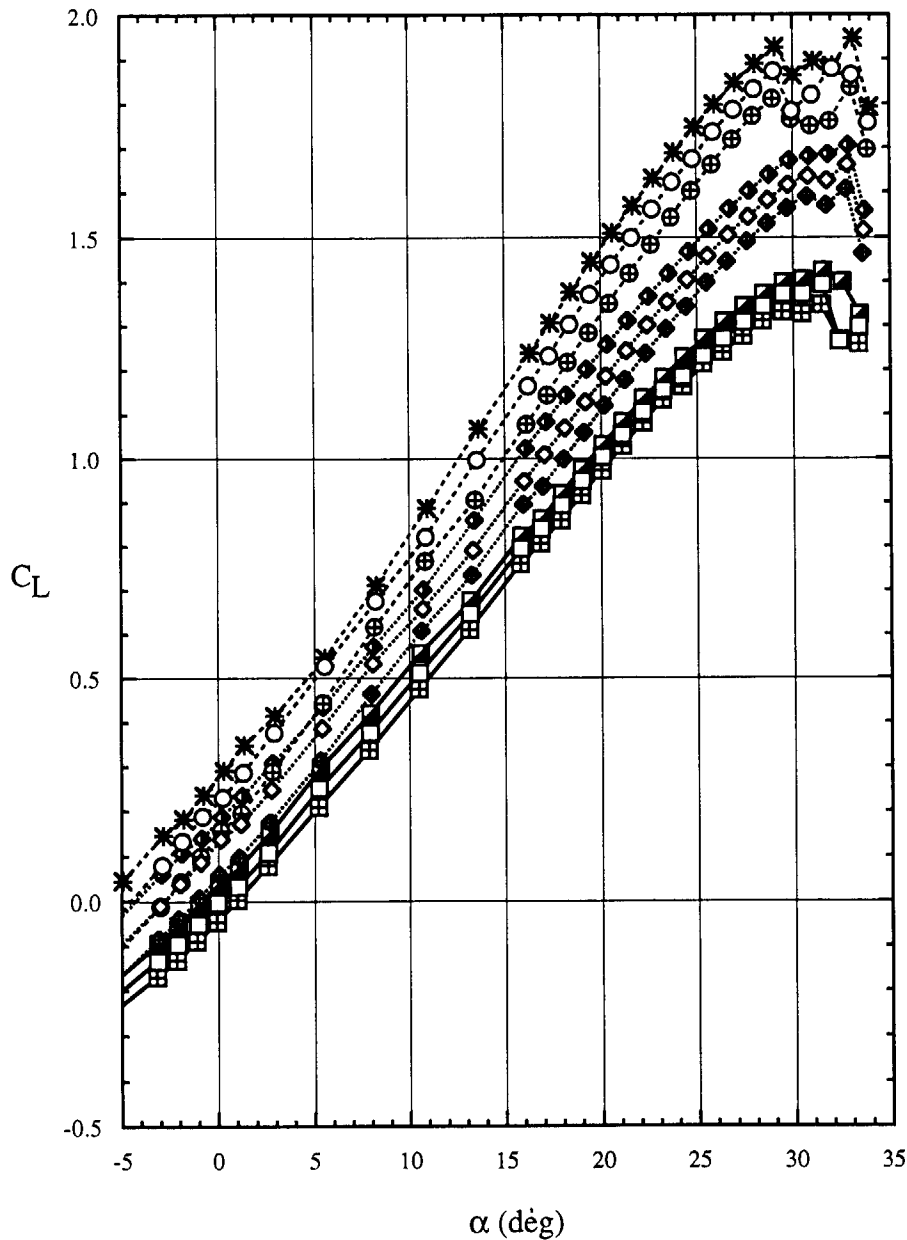


Figure 15 - Effects of blowing on Conventional Plain Flap, 0° deflection
a. Lift and Drag

MTF044 HSCT, C_{μ} Effects, C_L v. C_{M50} , C_L v. L/D_{eq}
 $\delta_{Flap} = 0^\circ$, $h = 0.015''$

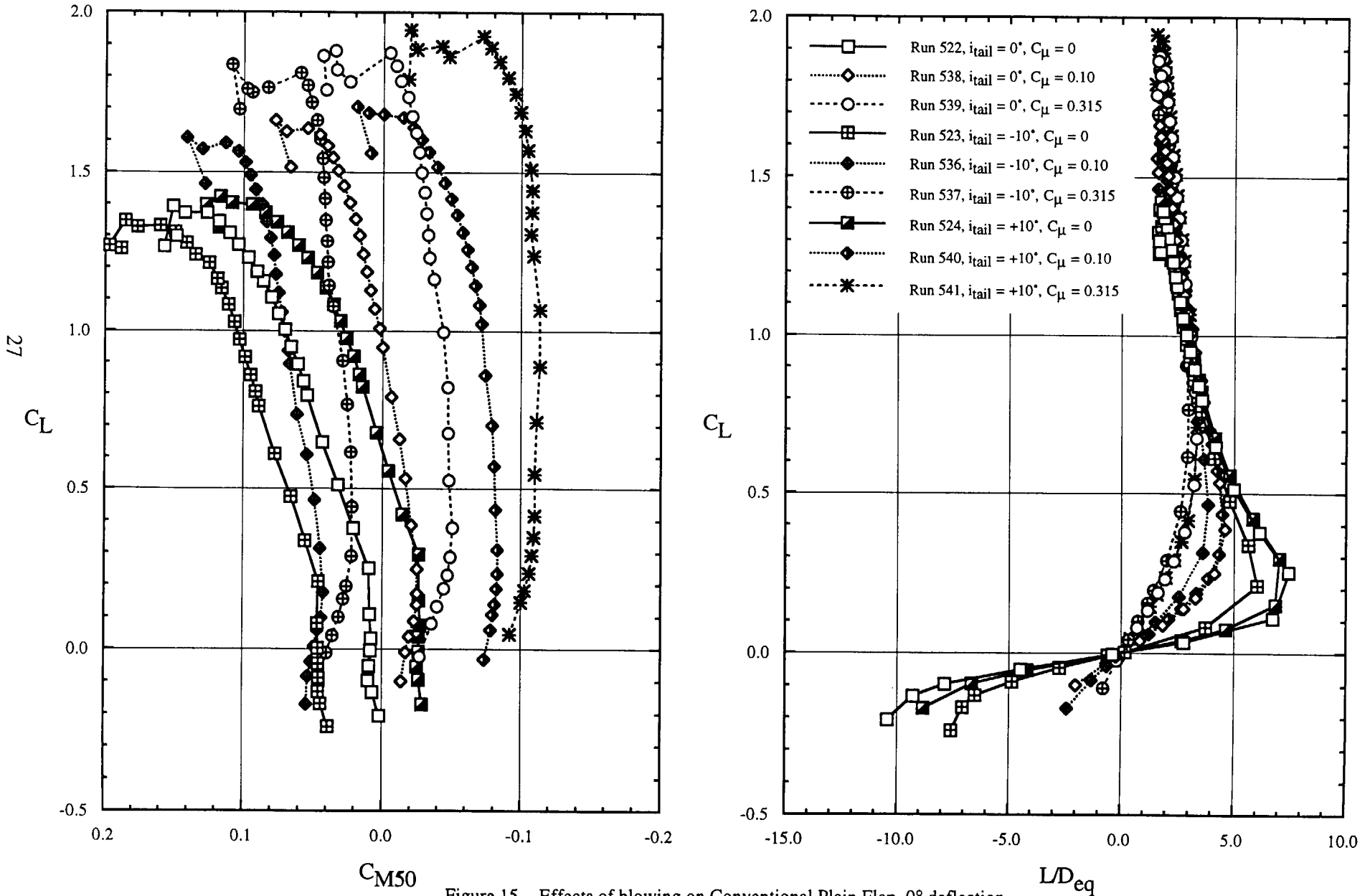
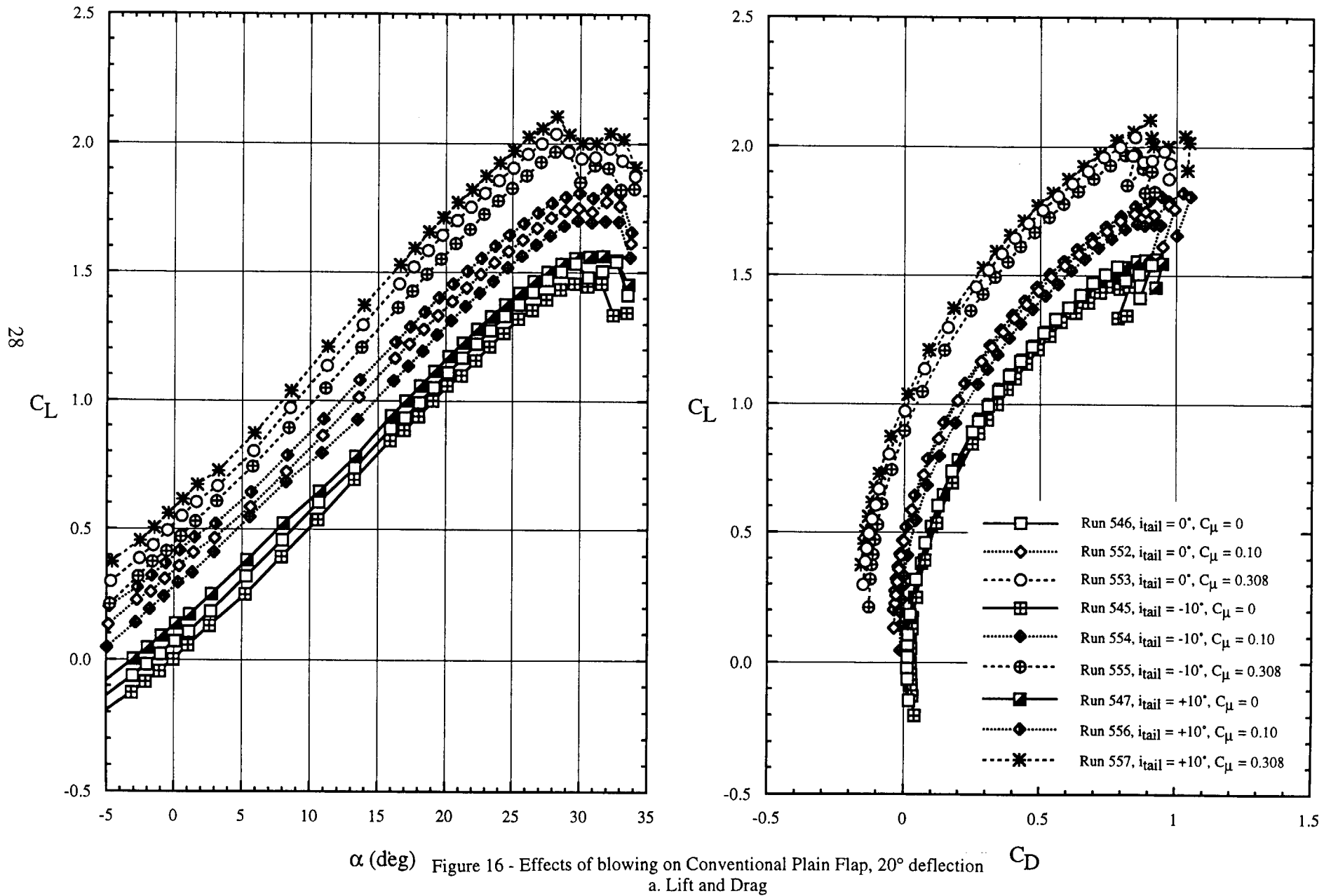


Figure 15 - Effects of blowing on Conventional Plain Flap, 0° deflection,
 b. Pitching Moment and Lift/Drag Ratio

MTF044 HSCT, C_{μ} Effects, C_L v. α , C_L v. C_D

$\delta_{Flap} = 20^\circ, h = 0.015''$



MTF044 HSCT, C_{μ} Effects, C_L v. C_{M50} , C_L v. L/D_{eq}
 $\delta_{Flap} = 20^\circ$, $h = 0.015''$

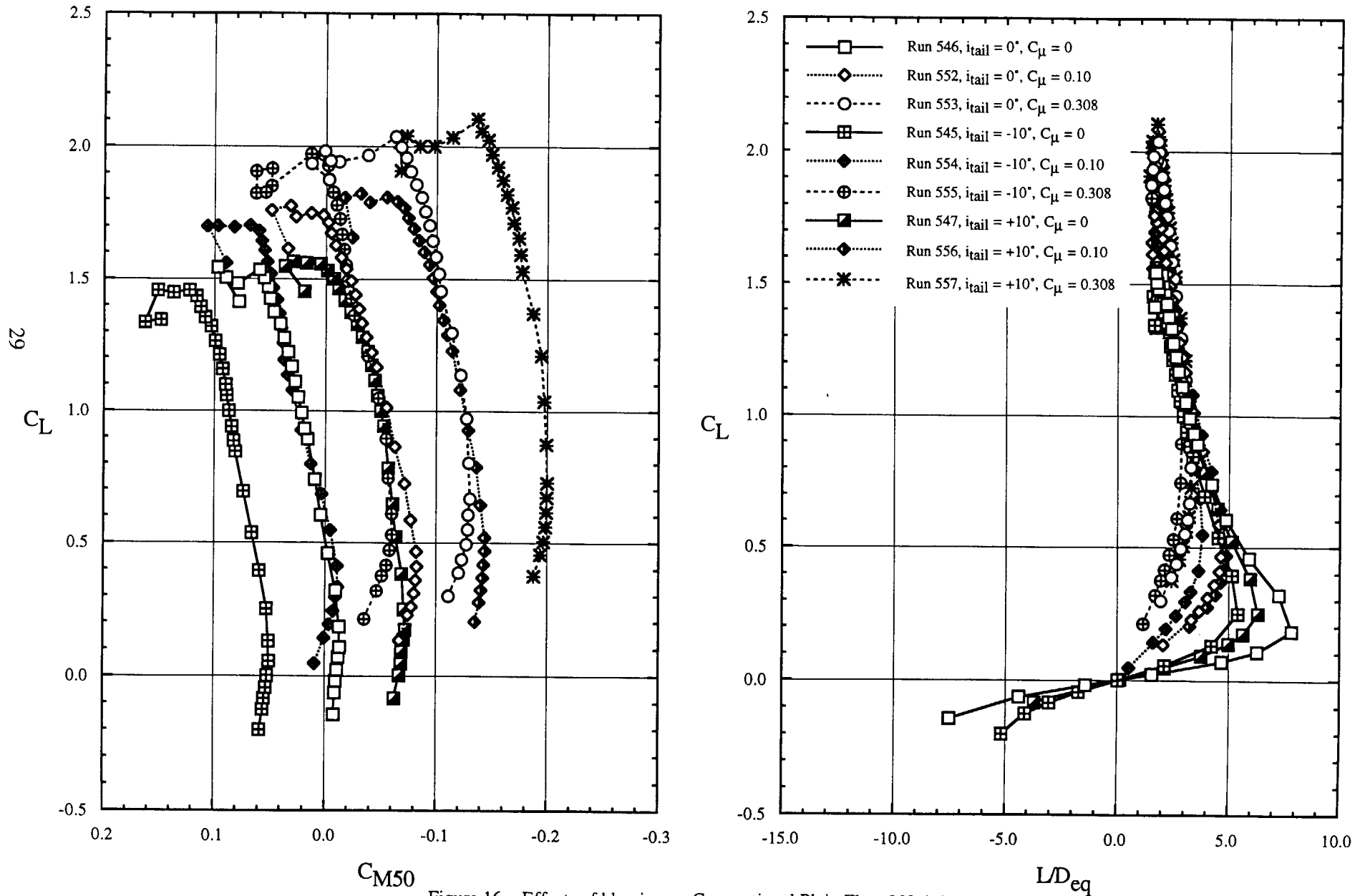


Figure 16 - Effects of blowing on Conventional Plain Flap, 20° deflection,
 b. Pitching Moment and Lift/Drag Ratio

MTF044 HSCT, C_{μ} Effects, C_L v. α , C_L v. C_D

$\delta_{Flap} = \text{CCW } 0^\circ, h = 0.015''$

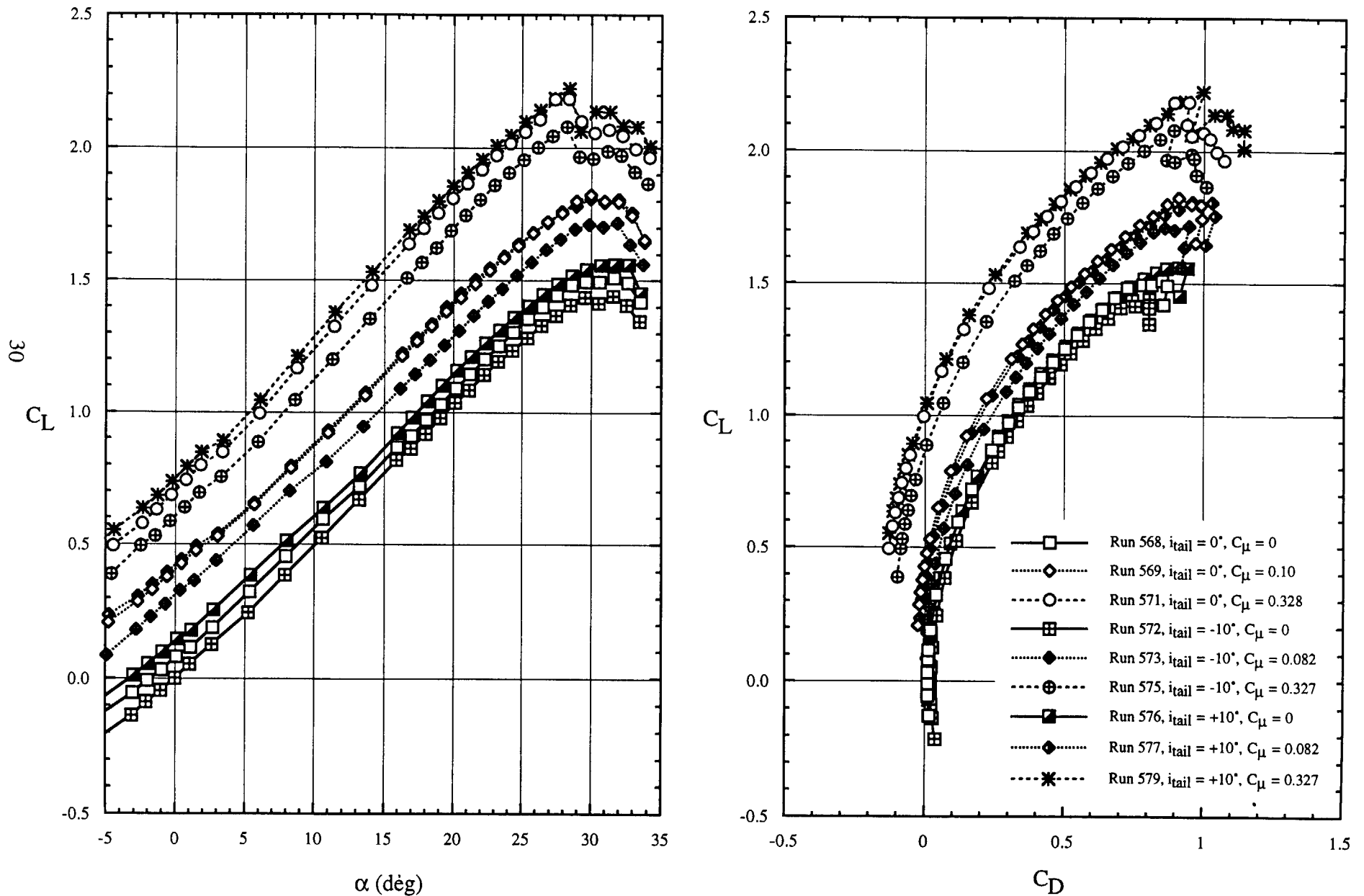


Figure 17 - Effects of blowing on CCW Flap, 0° deflection
a Lift and Drag

MTF044 HSCT, C_μ Effects, C_L v. C_{M50} , C_L v. L/D_{eq}

$\delta_{Flap} = \text{CCW } 0^\circ, h = 0.015''$

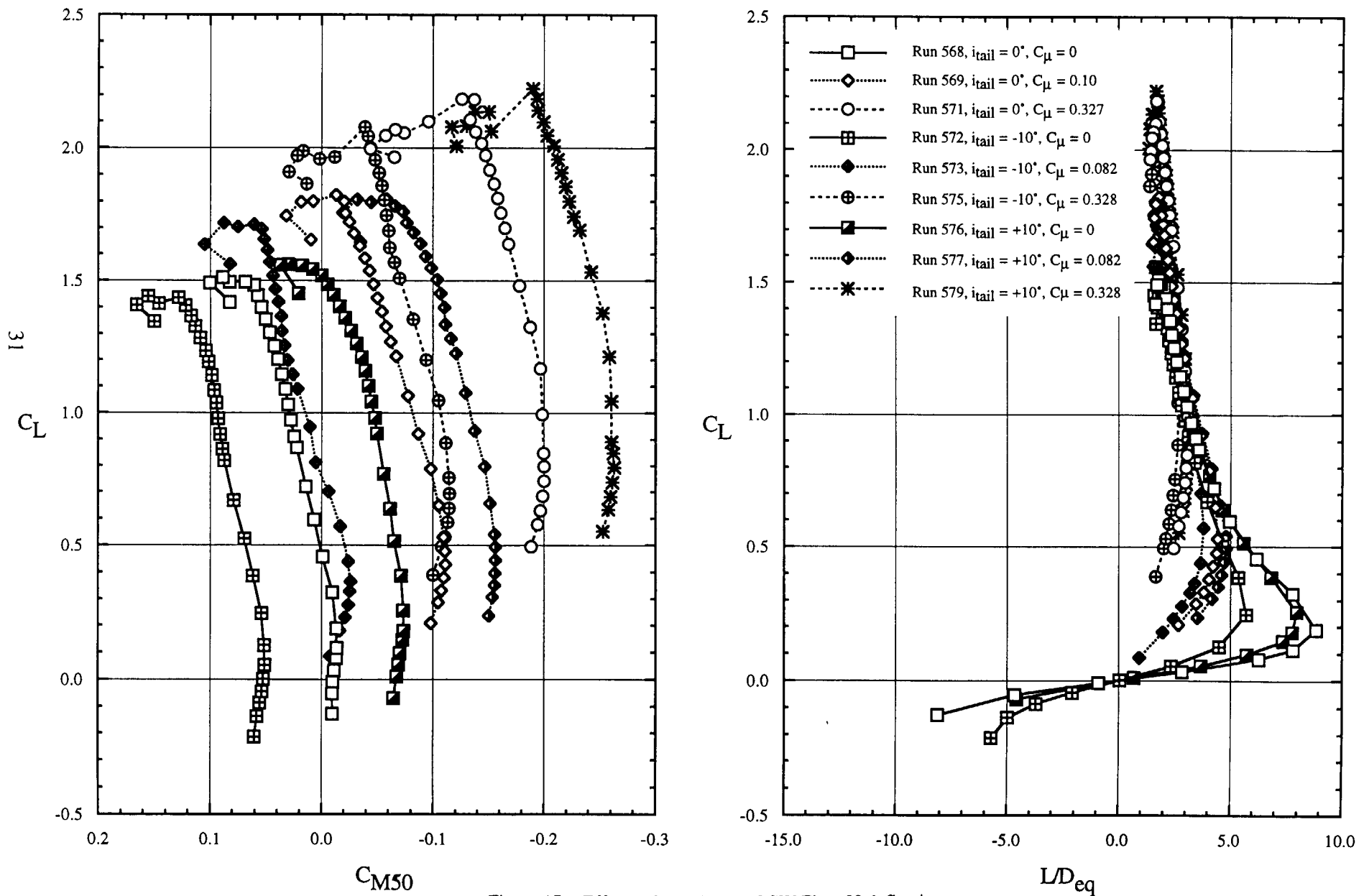


Figure 17 - Effects of blowing on CCW Flap, 0° deflection,
b. Pitching Moment and Lift/Drag Ratio

MTF044 HSCT, C_μ Effects, C_L v. α , C_L v. C_D

$\delta_{\text{Flap}} = \text{CCW } 10^\circ, h = 0.015''$

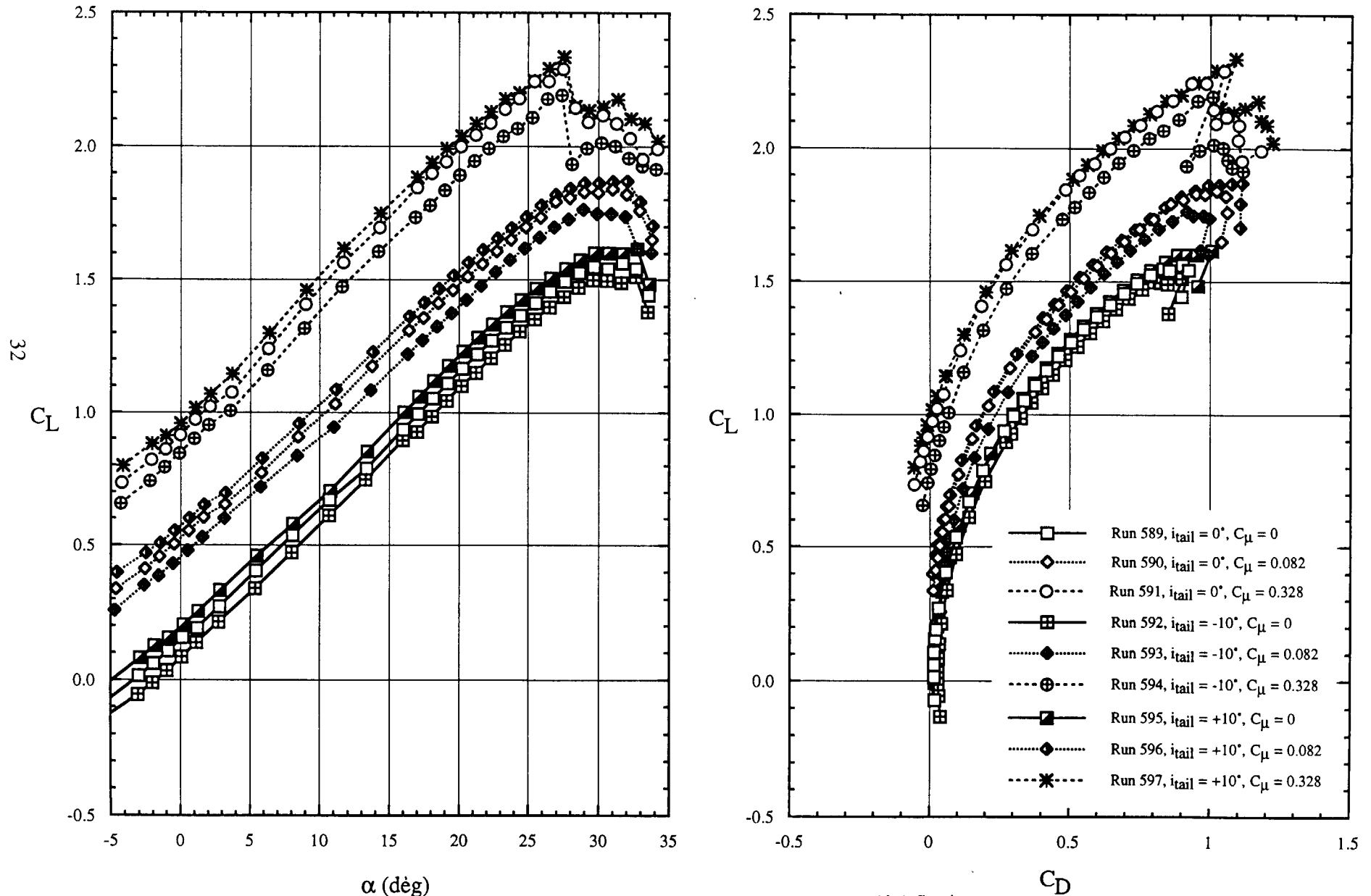


Figure 18 - Effects of blowing on CCW Flap, 10° deflection
a. Lift and Drag

MTF044 HSCT, C_μ Effects, C_L v. C_{M50} , C_L v. L/D_{eq}

$\delta_{Flap} = \text{CCW } 10^\circ, h = 0.015''$

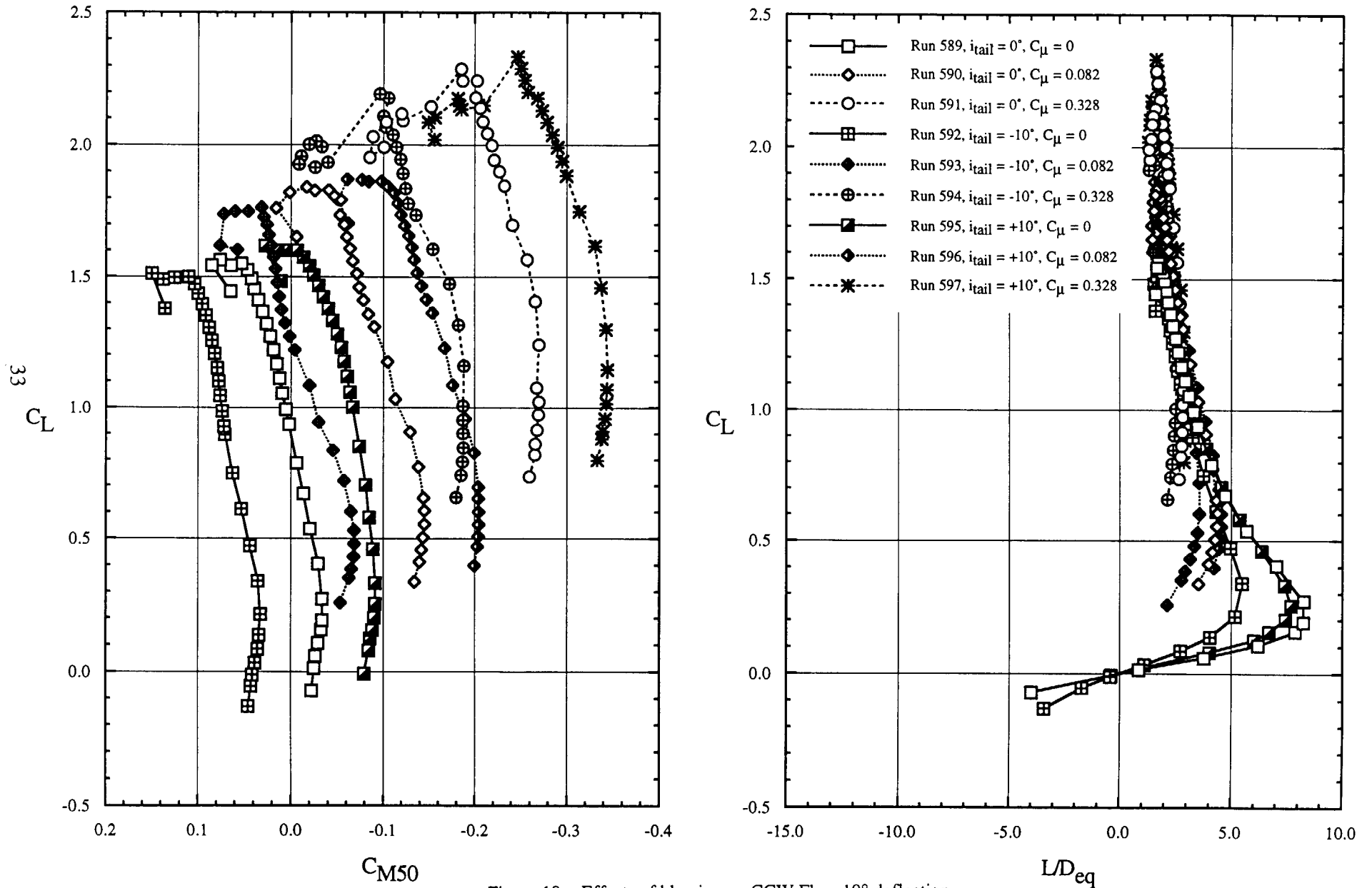


Figure 18 - Effects of blowing on CCW Flap, 10° deflection,
b. Pitching Moment and Lift/Drag Ratio

MTF044 HSCT, C_{μ} Effects, C_L v. α , C_L v. C_D

$\delta_{Flap} = \text{CCW } 34^\circ, h = 0.015''$

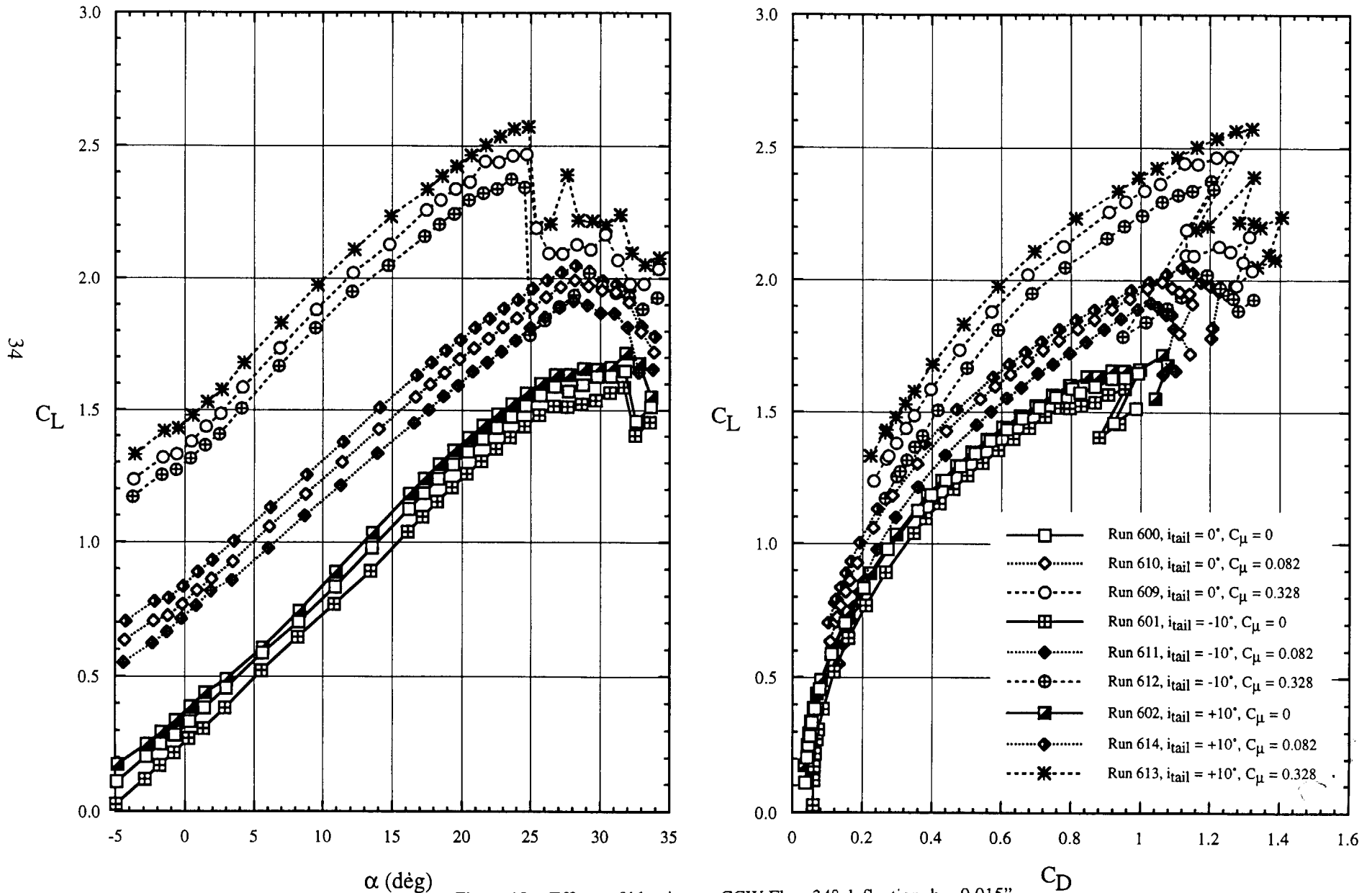


Figure 19 - Effects of blowing on CCW Flap, 34° deflection, $h = 0.015''$
 a. Lift and Drag

MTF044 HSCT, C_{μ} Effects, C_L v. C_{M50} , C_L v. L/D_{eq}

$\delta_{Flap} = \text{CCW } 34^\circ, h = 0.015''$

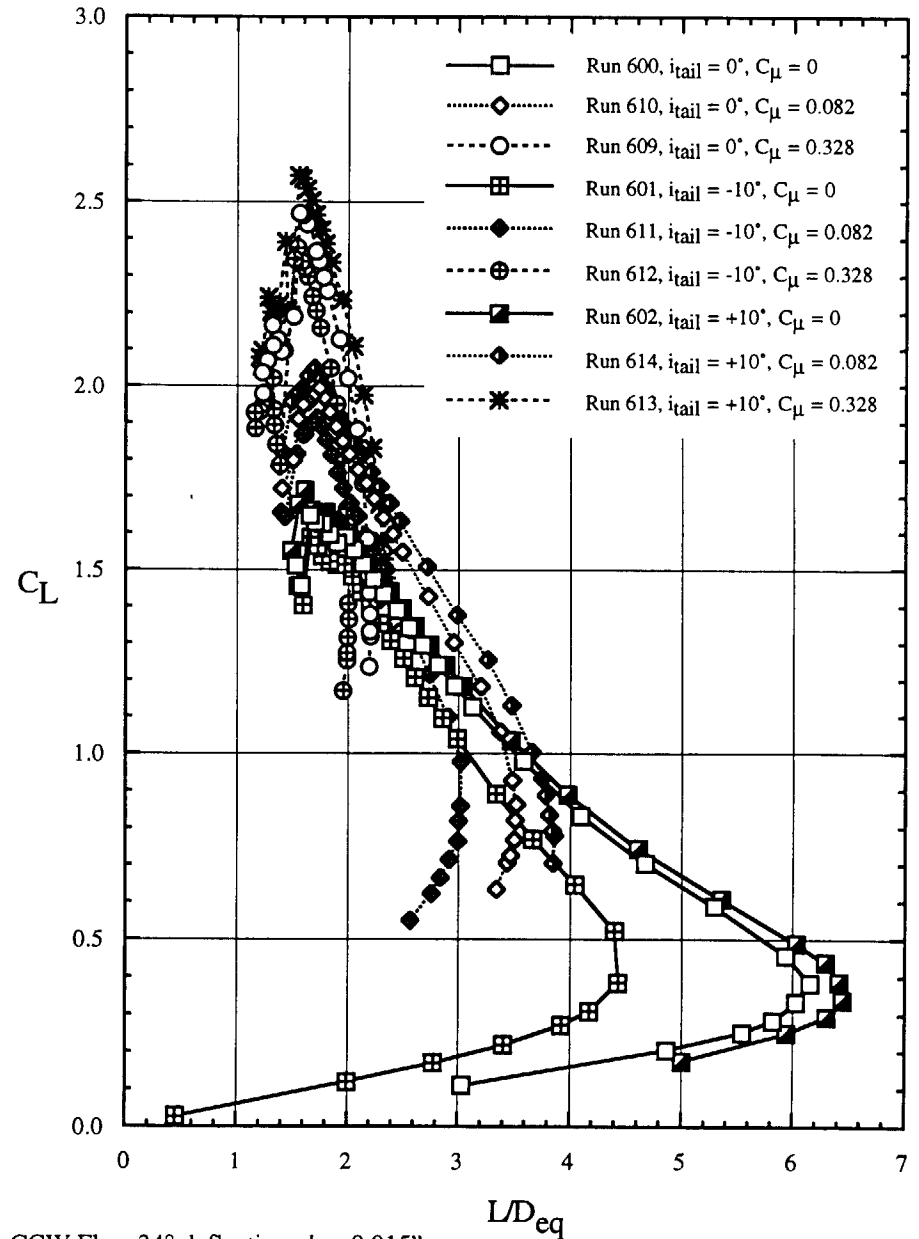
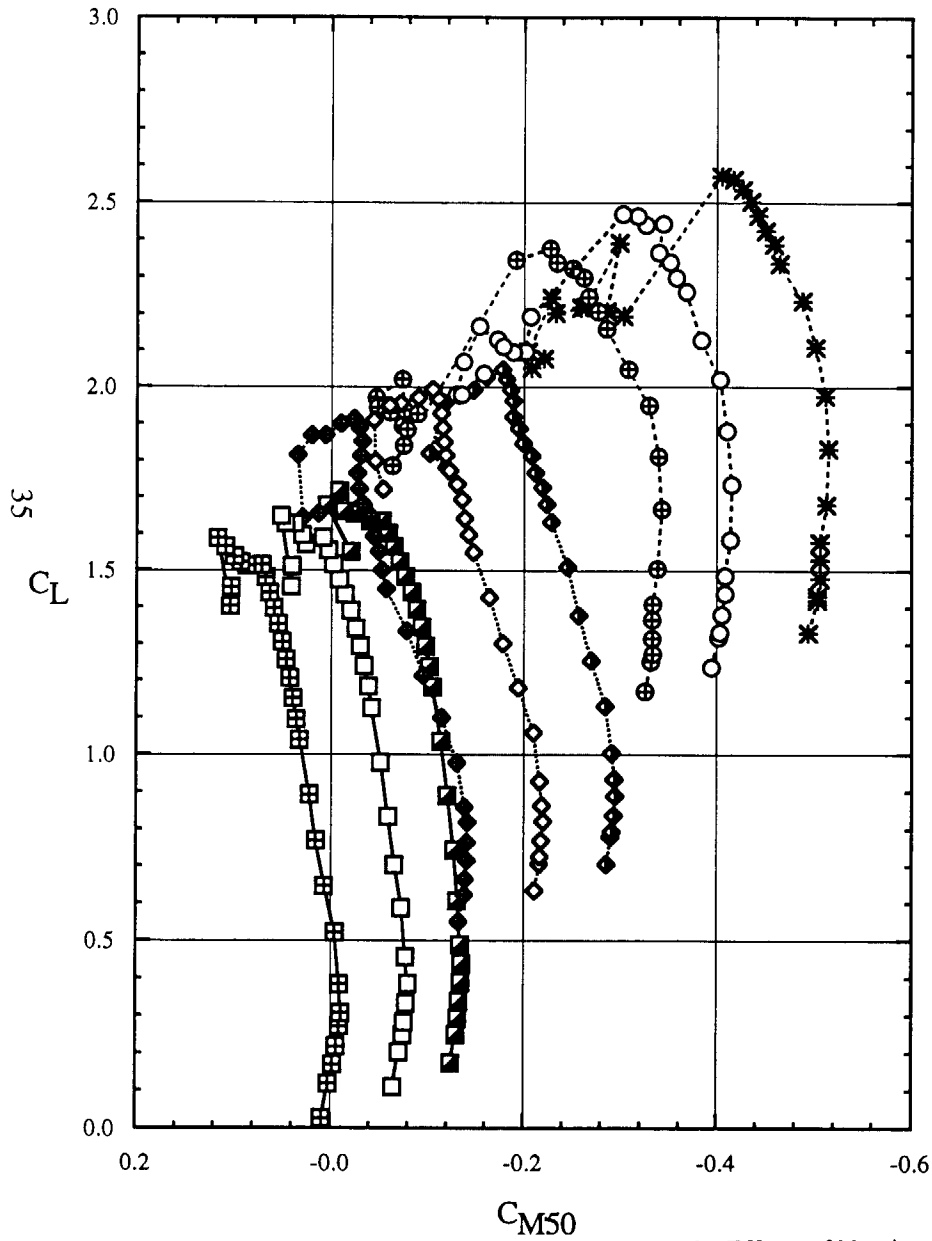


Figure 19- Effects of blowing on CCW Flap, 34° deflection, $h = 0.015''$
 b. Pitching Moment and Lift/Drag Ratio



Figure 20 - Flow visualization showing jet turning on CCW 34° Flap with two slot heights
 a. Slot height, $h = 0.015''$

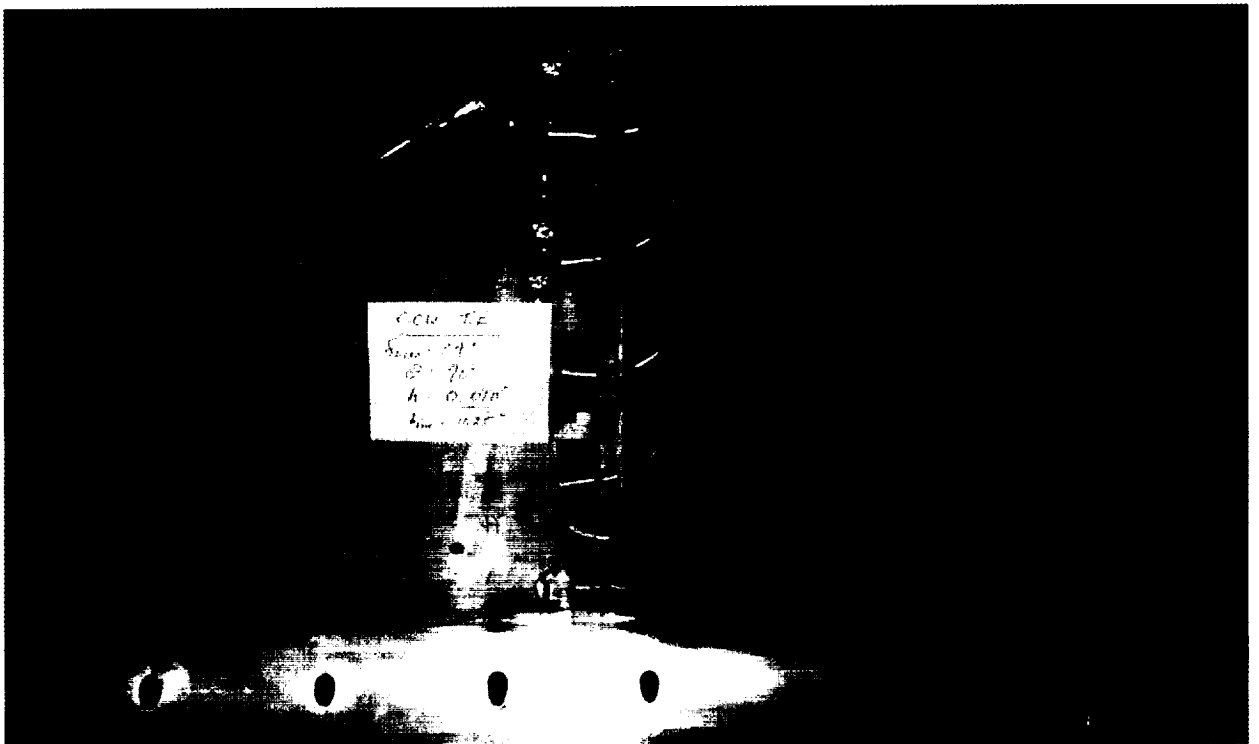


Figure 20 - Flow visualization showing jet turning on CCW 34° Flap with two slot heights
 b. Slot height, $h = 0.010''$

MTF044 HSCT, C_{μ} Effects, C_L v. α , C_L v. C_D

$\delta_{Flap} = \text{CCW } 34^\circ, h = 0.010''$

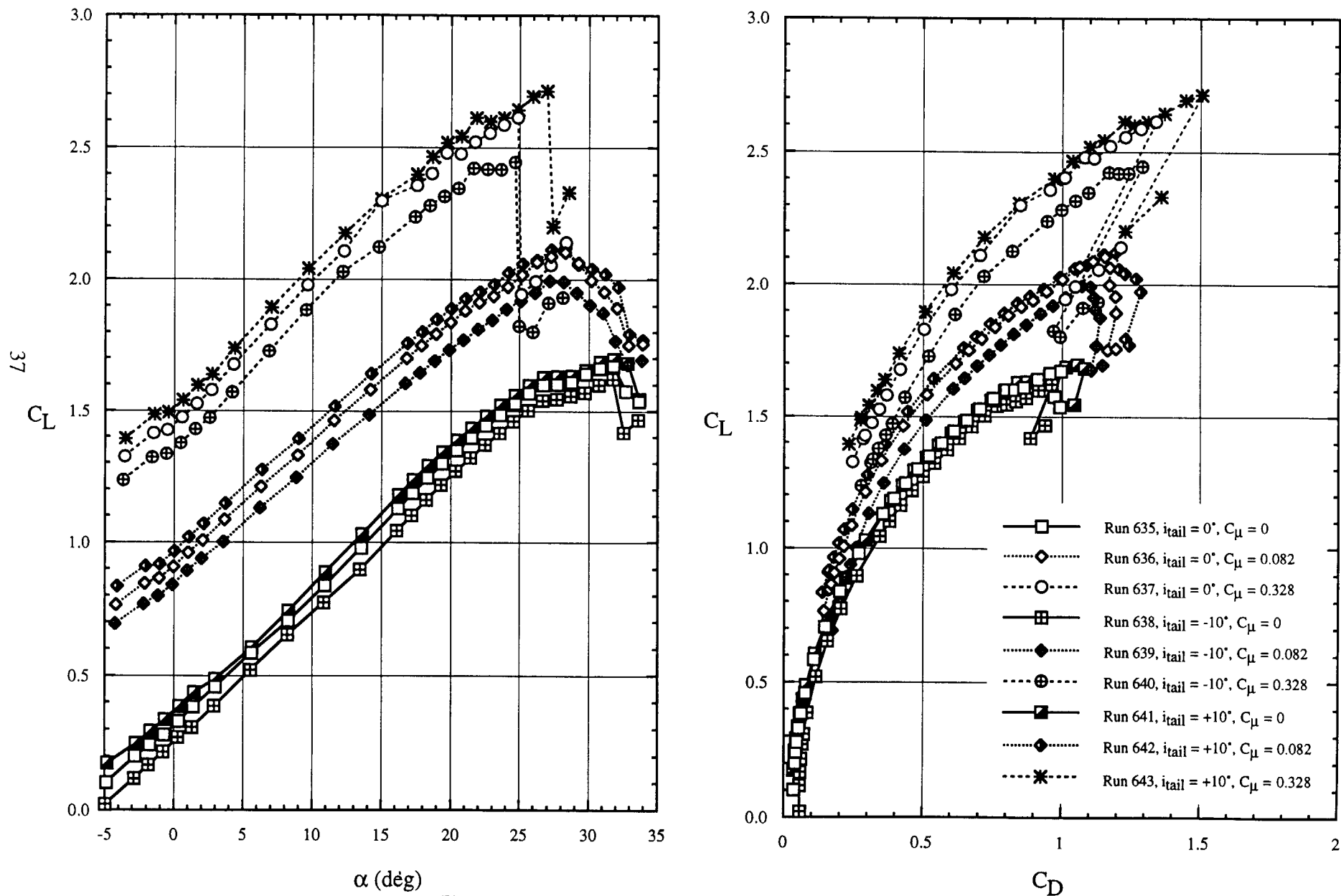


Figure 21 - Effects of blowing on CCW Flap, 34° deflection, $h = 0.010''$
 a. Lift and Drag

MTF044 HSCT, C_{μ} Effects, C_L v. C_{M50} , C_L v. L/D_{eq}

$\delta_{Flap} = \text{CCW } 34^\circ, h = 0.010''$

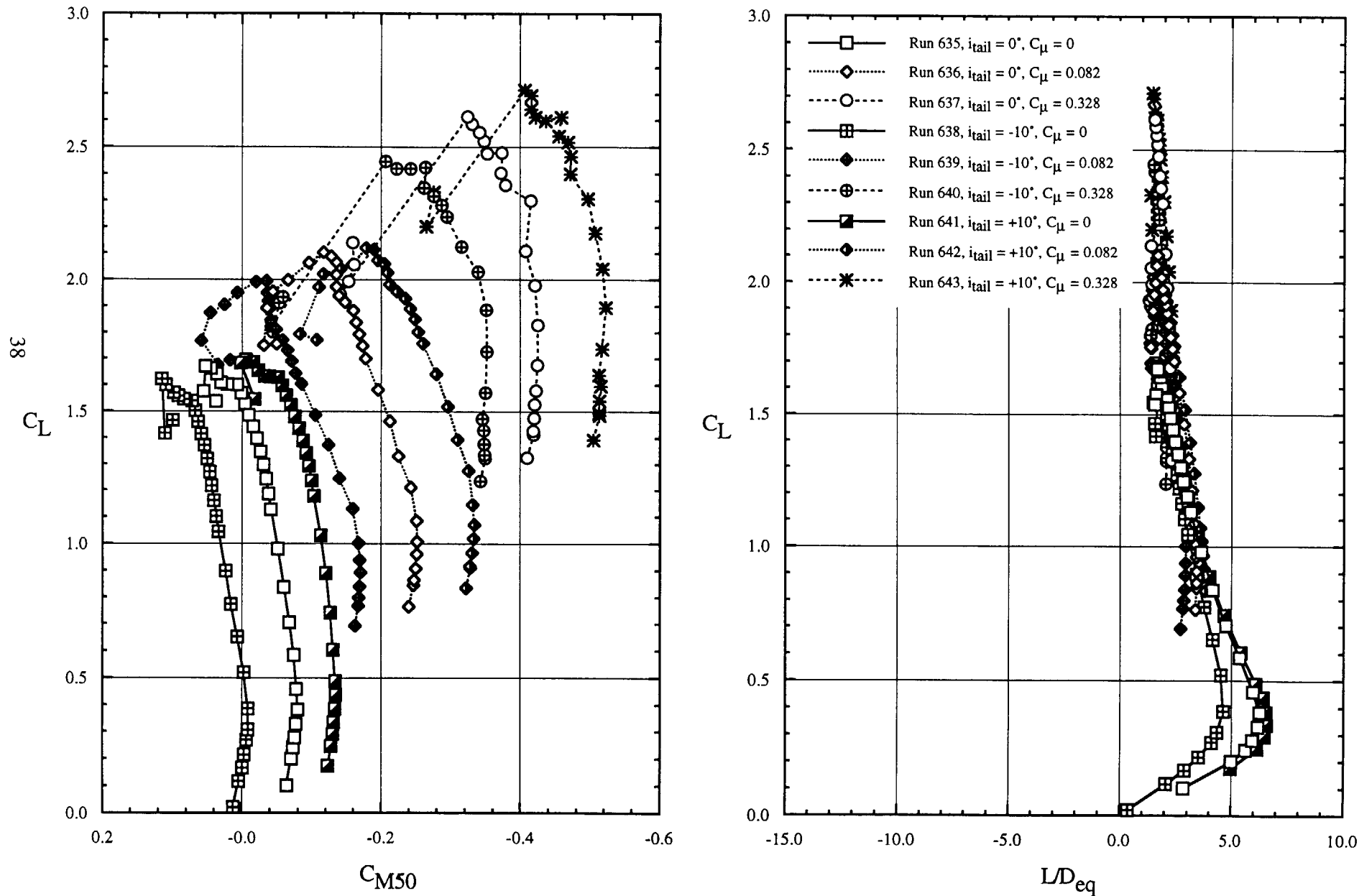


Figure 21- Effects of blowing on CCW Flap, 34° deflection, $h = 0.010''$
 b. Pitching Moment and Lift/Drag Ratio

MTF044 HSCT, Flap Effects, C_L v. C_μ , C_D v. C_μ

Tail Off, $\alpha = 0$

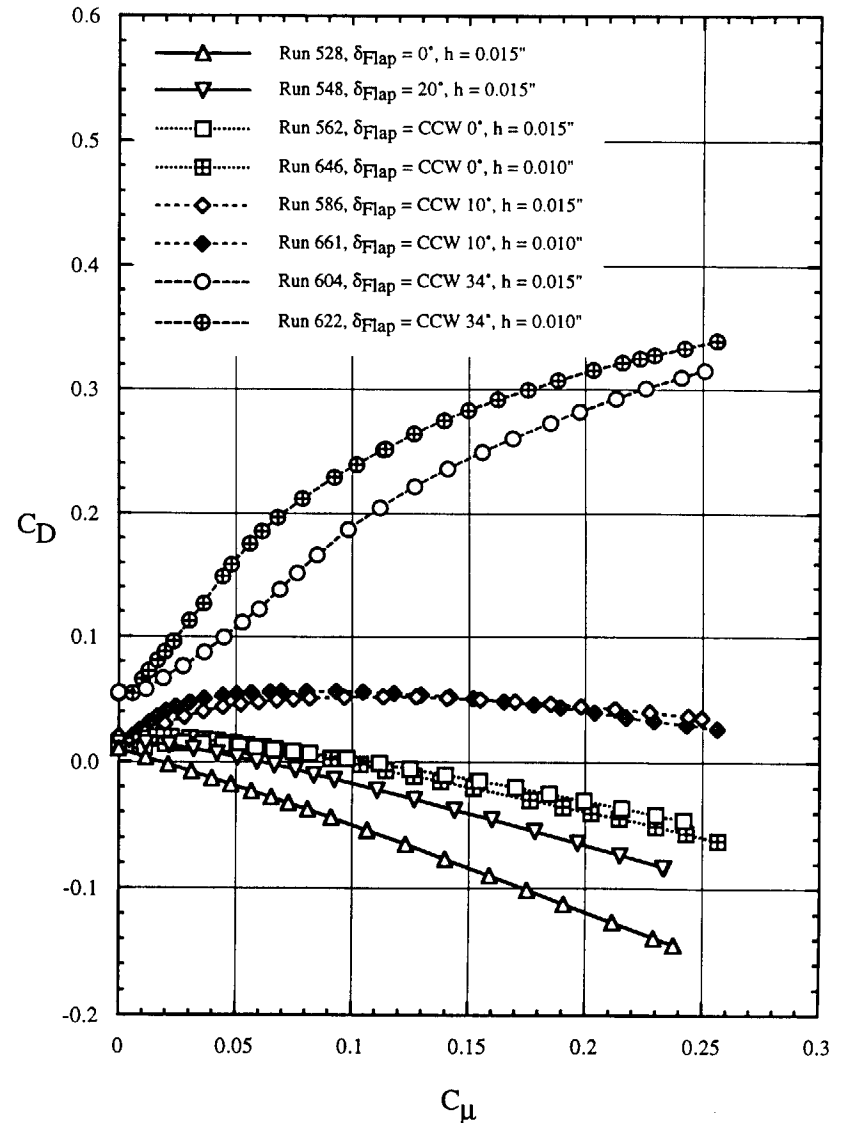
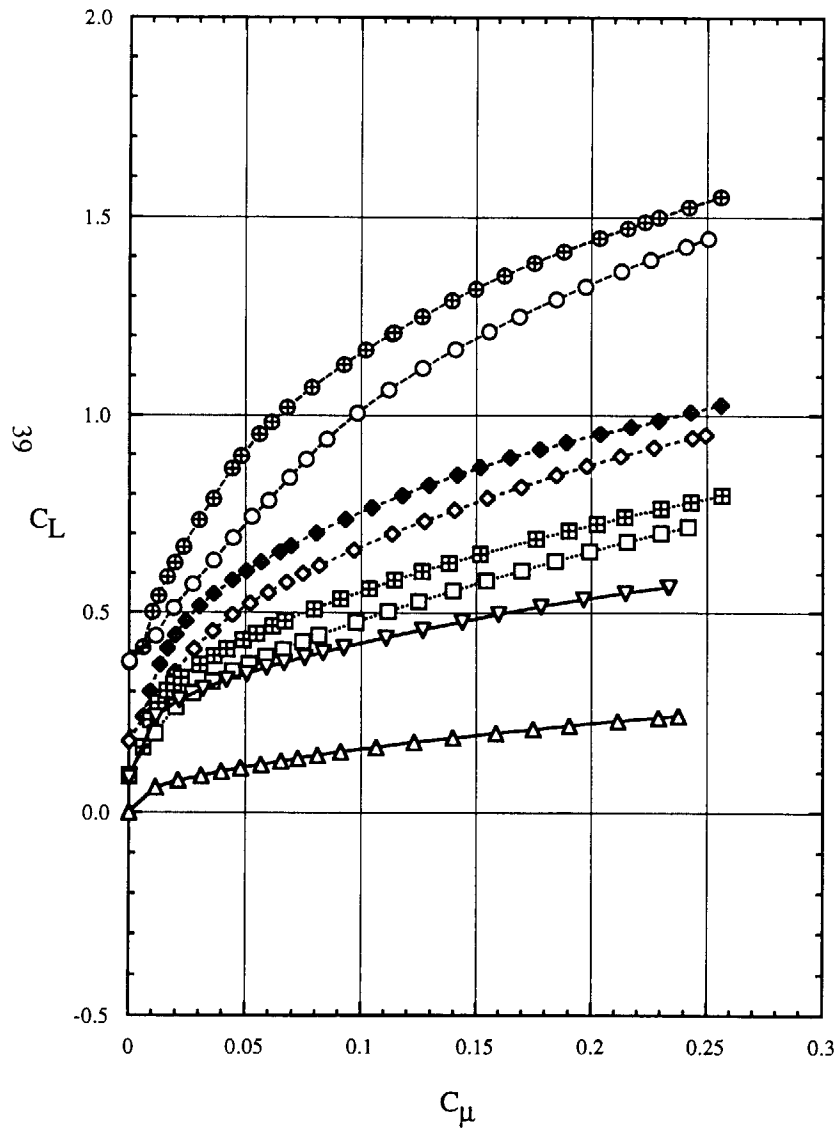


Figure 22 - Effect of varying CCW and plain flap deflection, slot height and blowing, $\alpha = 0^\circ$

a. Lift and Drag

MTF044 HSCT, Flap Effects, C_{M50} v. C_{μ} , L/D_{eq} v. C_{μ}

Tail Off, $\alpha = 0$

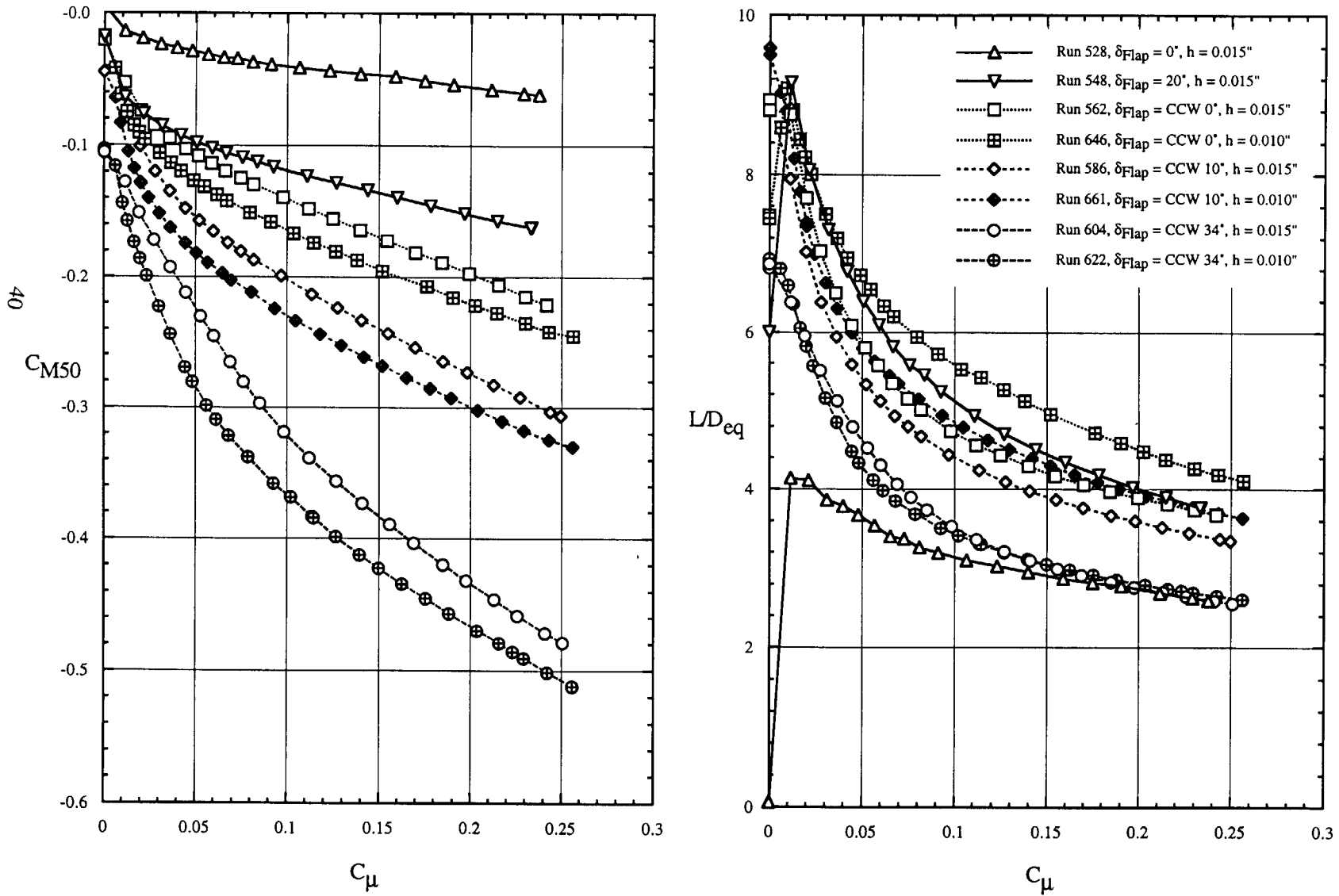


Figure 22 - Effect of varying CCW flap deflection, slot height and blowing, $\alpha = 0^\circ$

b. Pitch and Lift/Drag Ratio

MTF044 HSCT, Flap Effects, C_L v. C_D , C_L v. L/D_{eq}

Tail Off, $\alpha = 0$

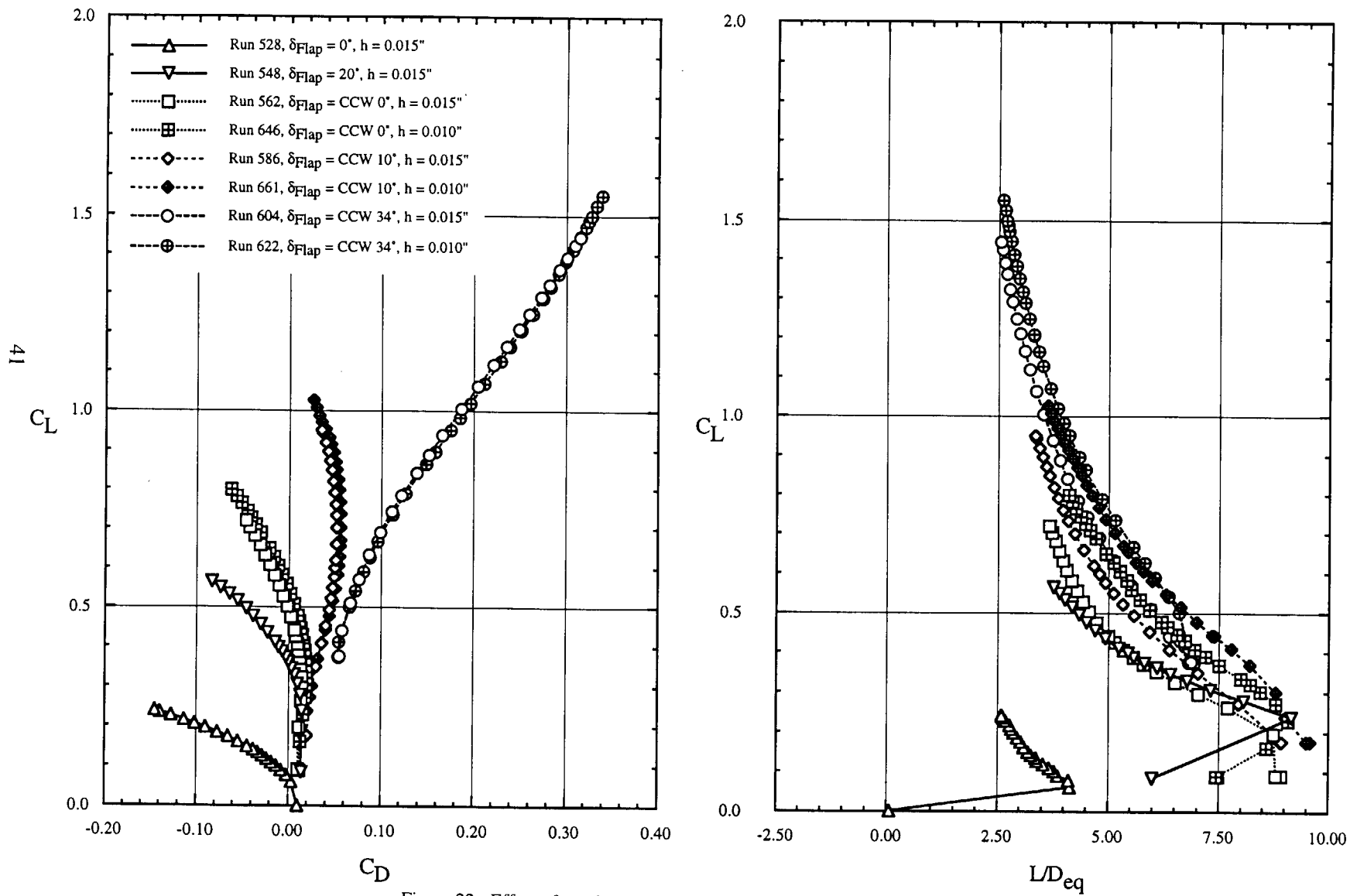


Figure 22 - Effect of varying CCW flap deflection, slot height and blowing, $\alpha = 0^\circ$

c. Drag Polars and Lift/Drag Ratio

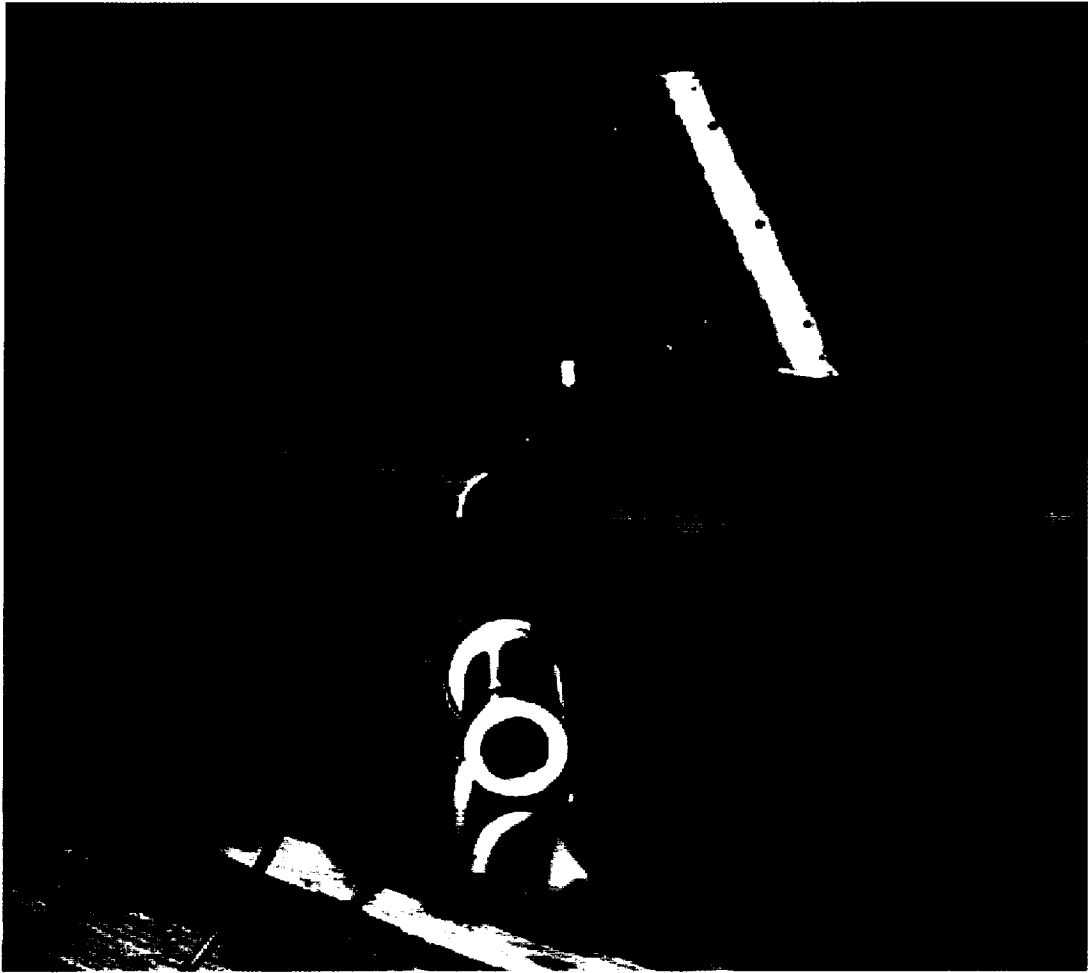


Figure 23- Blown Canard 1 and CC Cylindrical Canard



Figure 24 - Flow turning on aft-swept Canard 3 (inverted photo)



Figure 25- Flow turning on CC Cylindrical Canard (inverted photo)

a. Slot location at -20°



Figure 25- Flow turning on CC Cylindrical Canard (inverted photo)
b. Slot location at $+20^\circ$

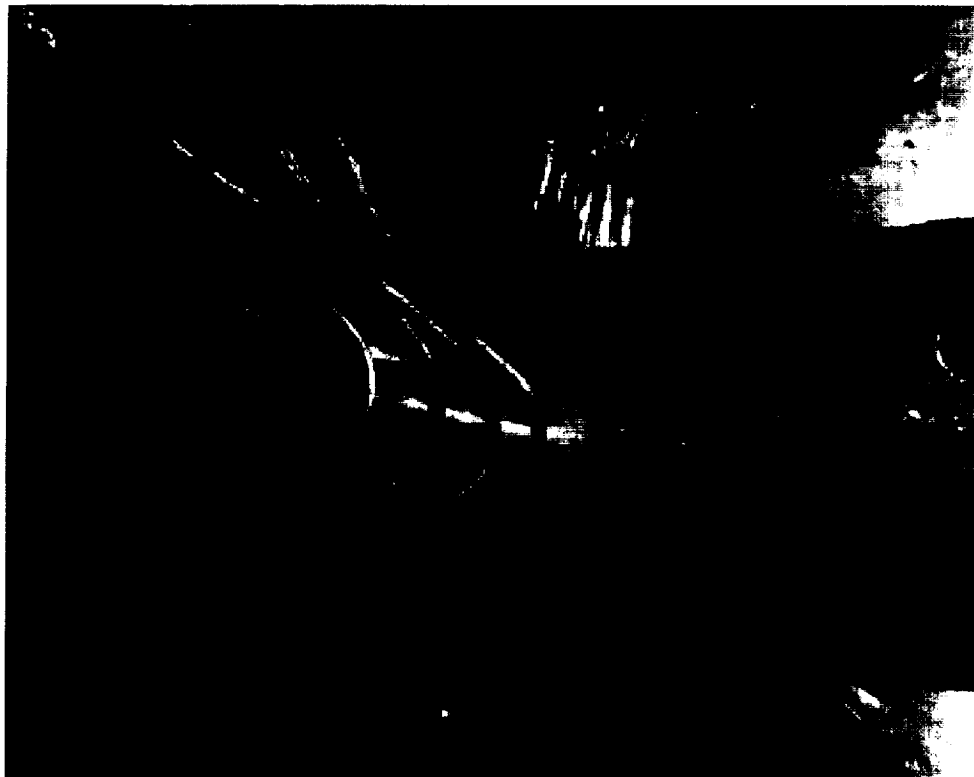


Figure 25- Flow turning on CC Cylindrical Canard (inverted photo)
c. Slot location at $+40^\circ$

MTF044 HSCT, CCW Blown Canard Effectiveness

C_L v. α , C_L v. C_D

$h_{ccw} = 0.010''$, $i_{tail} = 0^\circ$, $\delta_{Flap} = CCW 0^\circ$

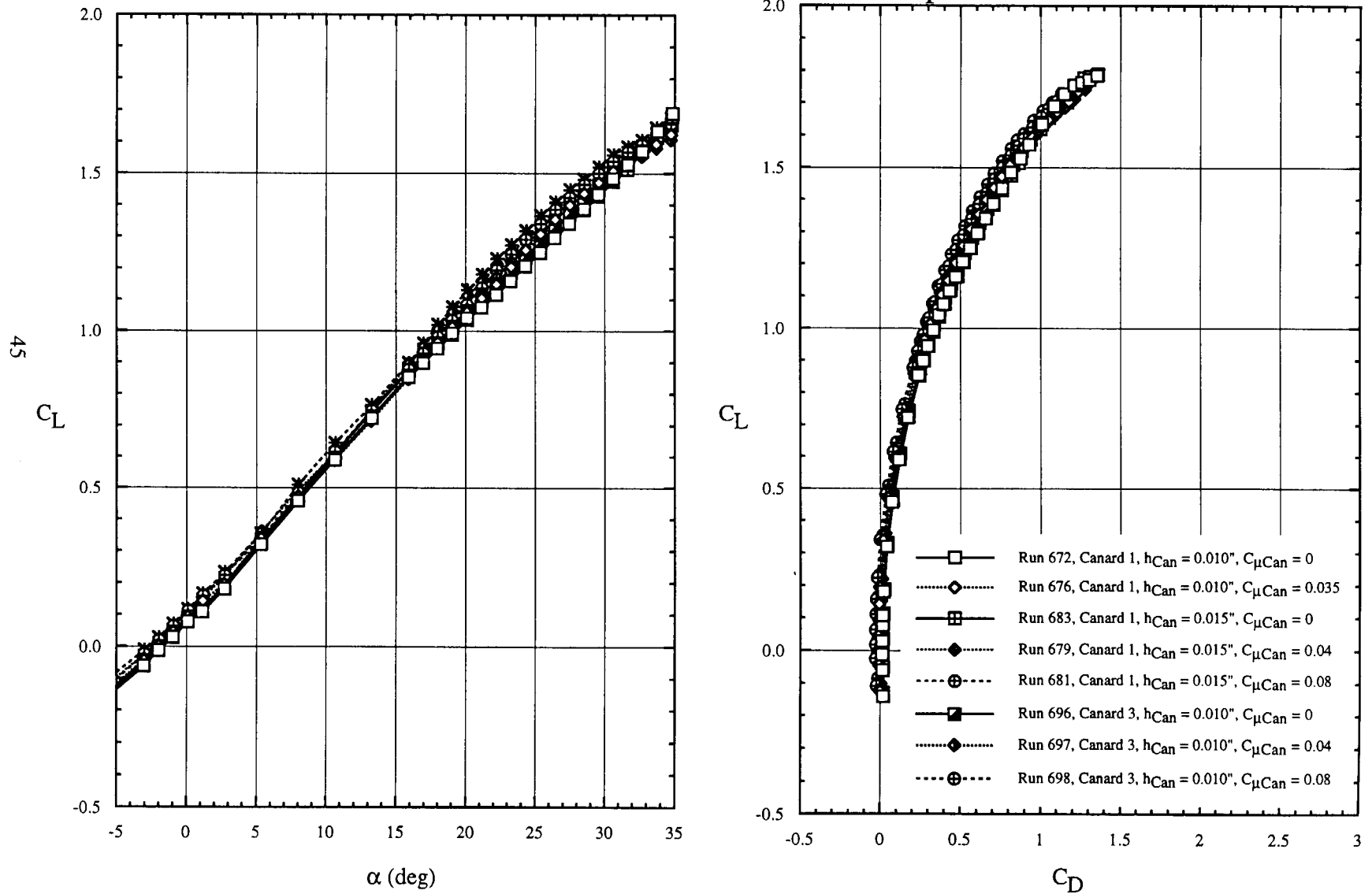
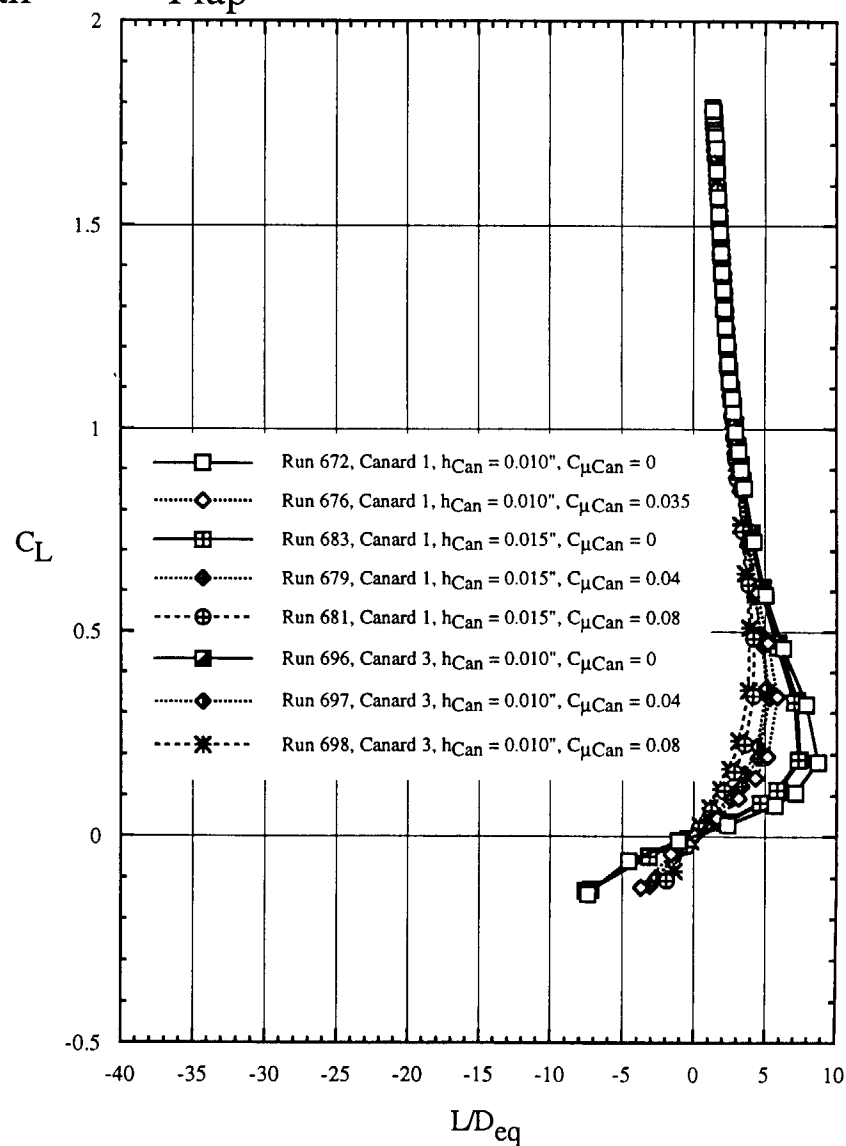
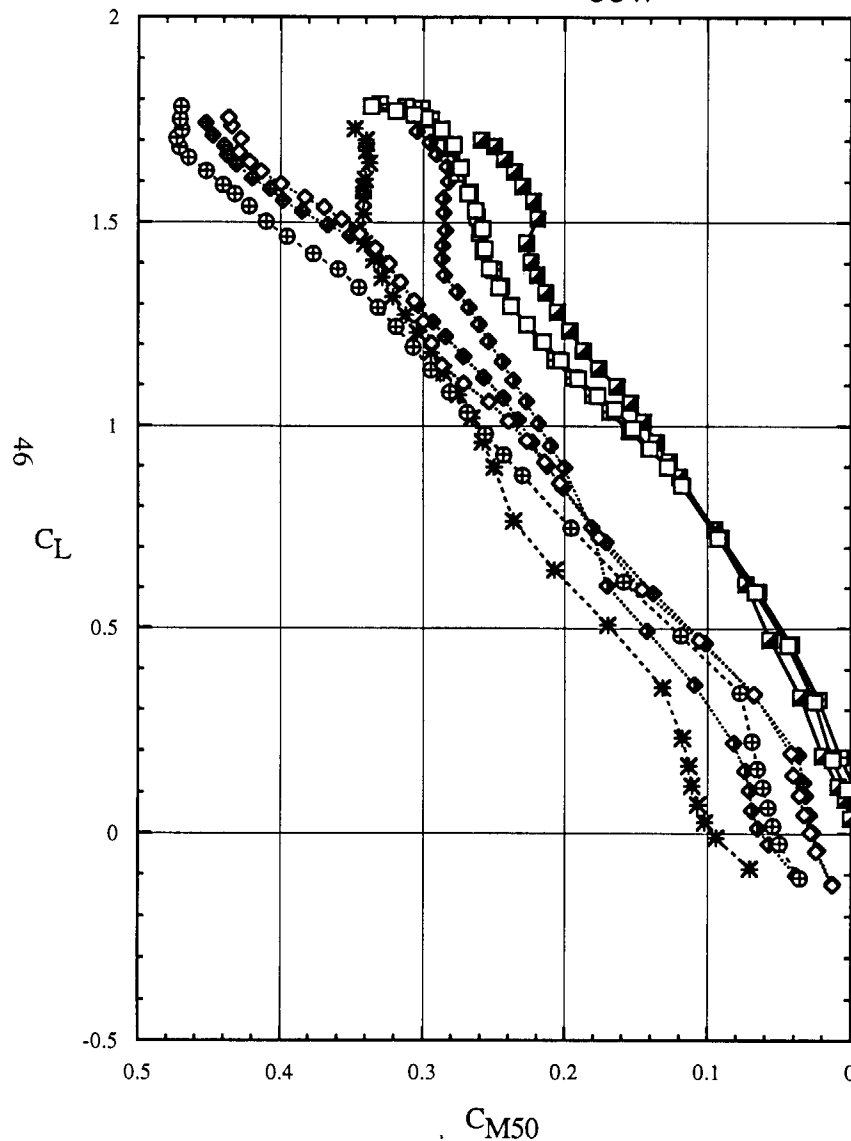


Figure 26 - Effect of Canard 1 and Canard 3 on CCW 0° flap, $C_{\mu CCW} = 0$
a. Lift and Drag Polars

MTF044 HSCT, CCW Blown Canard Effectiveness

C_L v. C_{M50} , C_L v. L/D_{eq}

$h_{ccw} = 0.010''$, $i_{tail} = 0^\circ$, $\delta_{Flap} = CCW 0^\circ$



- Run 672, Canard 1, $h_{Can} = 0.010''$, $C_{\mu Can} = 0$
- ⋯◇⋯ Run 676, Canard 1, $h_{Can} = 0.010''$, $C_{\mu Can} = 0.035$
- ▣— Run 683, Canard 1, $h_{Can} = 0.015''$, $C_{\mu Can} = 0$
- ⋯◆⋯ Run 679, Canard 1, $h_{Can} = 0.015''$, $C_{\mu Can} = 0.04$
- ⋯⊕⋯ Run 681, Canard 1, $h_{Can} = 0.015''$, $C_{\mu Can} = 0.08$
- Run 696, Canard 3, $h_{Can} = 0.010''$, $C_{\mu Can} = 0$
- ⋯◆⋯ Run 697, Canard 3, $h_{Can} = 0.010''$, $C_{\mu Can} = 0.04$
- ⋯*⋯ Run 698, Canard 3, $h_{Can} = 0.010''$, $C_{\mu Can} = 0.08$

Figure 26 - Effect of Canard 1 and Canard 3 on CCW 0° flap, $C_{\mu CCW} = 0.0$
 b. Pitch and Lift/Drag Ratio

MTF044 HSCT, CCW Blown Canard Effectiveness

C_L v. α , C_L v. C_D

$h_{ccw} = 0.010"$, $i_{tail} = 0^\circ$, $\delta_{Flap} = CCW 34^\circ$

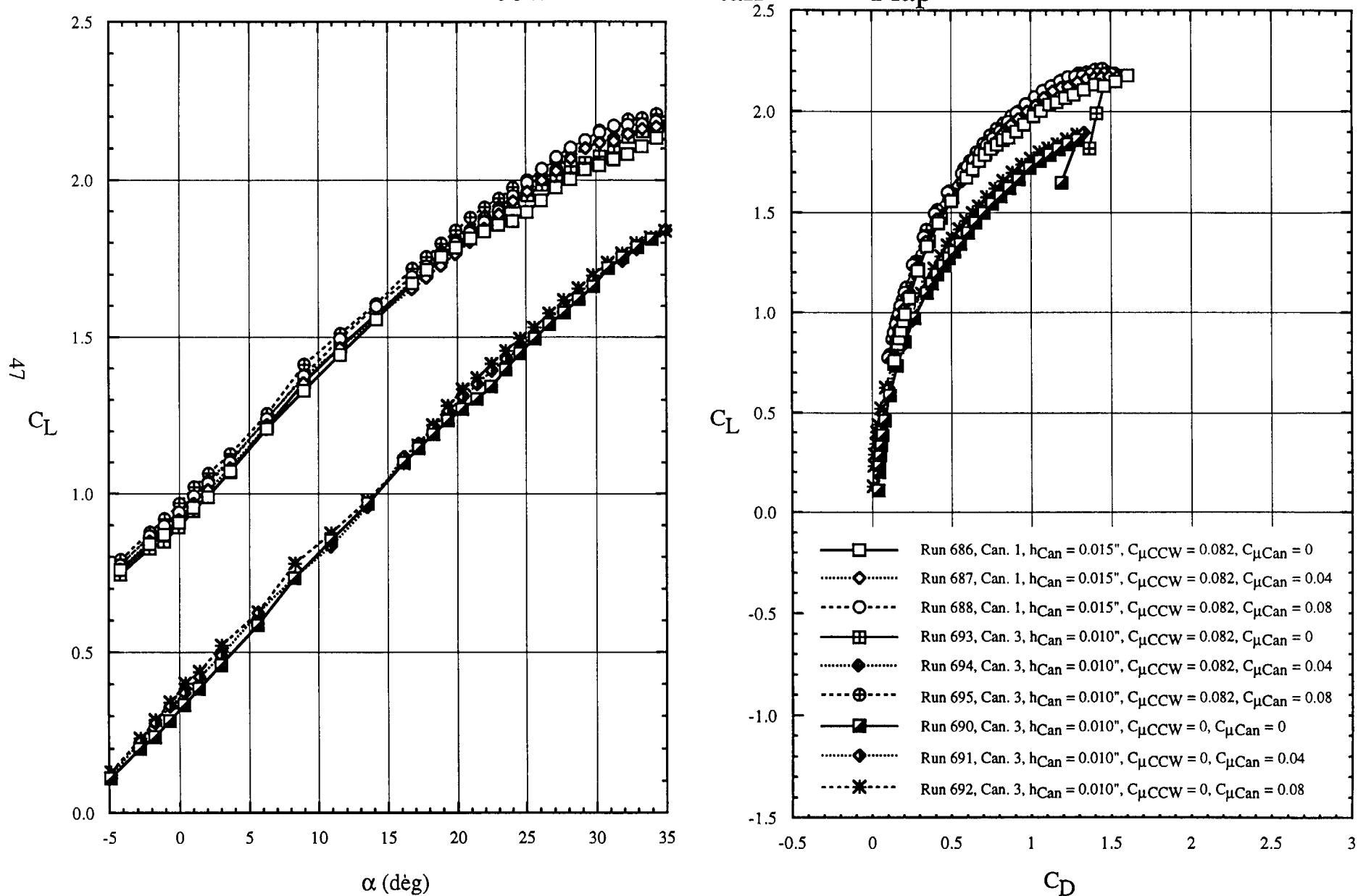


Figure 27 - Effect of Canard 1 and Canard 3 on CCW 34° flap
a. Lift and Drag Polars

MTF044 HSCT, CCW Blown Canard Effectiveness

C_L v. C_{M50} , C_L v. L/D_{eq}

$h_{ccw} = 0.010"$, $i_{tail} = 0^\circ$, $\delta_{Flap} = \text{CCW } 34^\circ$

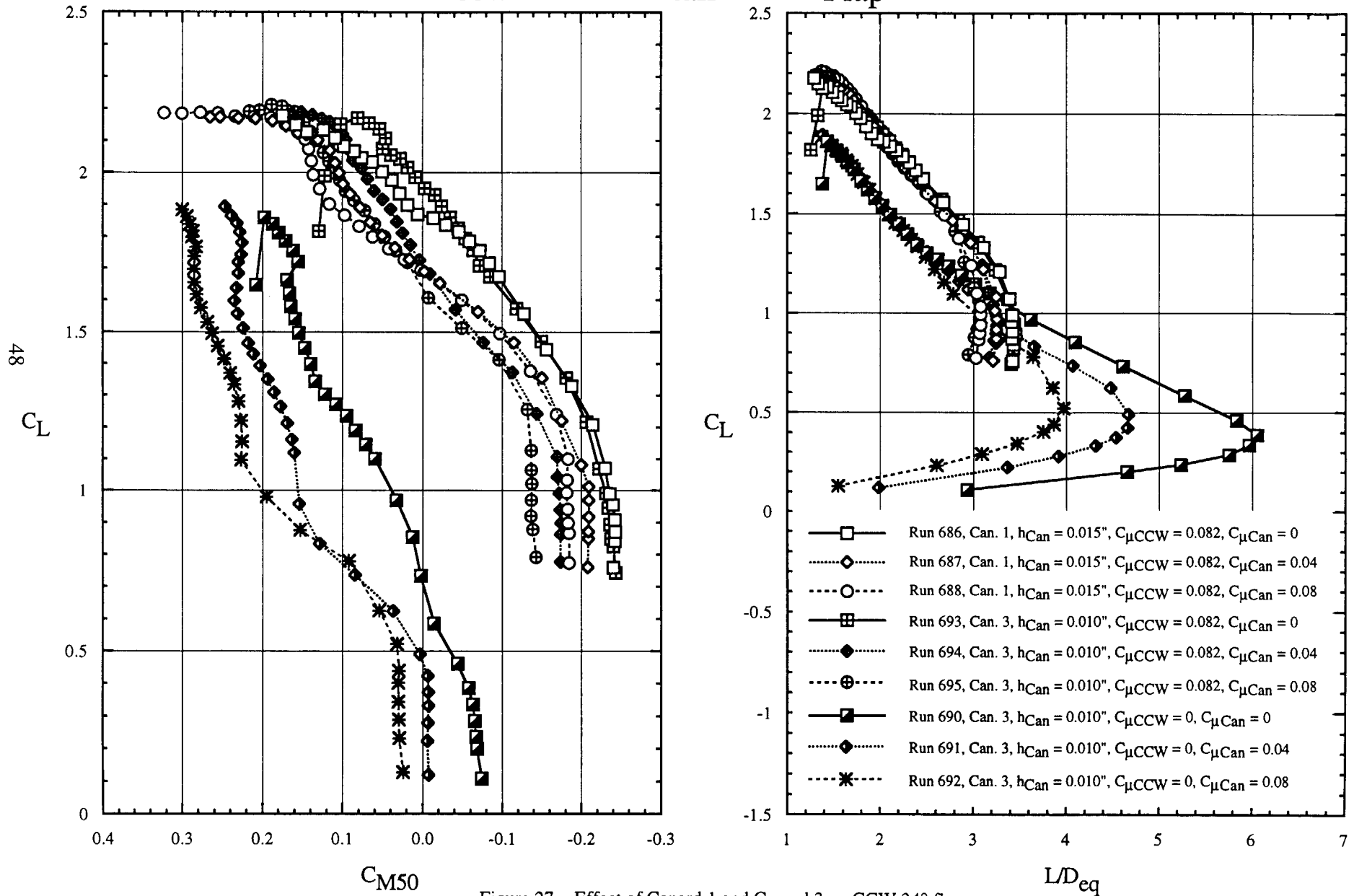


Figure 27 - Effect of Canard 1 and Canard 3 on CCW 34° flap
b. Pitch and Lift to Drag Ratio

MTF044 HSCT, Effects of CC Cylinder Canard Slot Location

C_L v. α , C_L v. C_D

$\theta_{\text{slot}} = -20^\circ$, $h_{\text{canard}} = 0.010''$, $h_{\text{CCW}} = 0.010''$, $i_{\text{tail}} = 0^\circ$, $\delta_{\text{Flap}} = \text{CCW } 0^\circ$

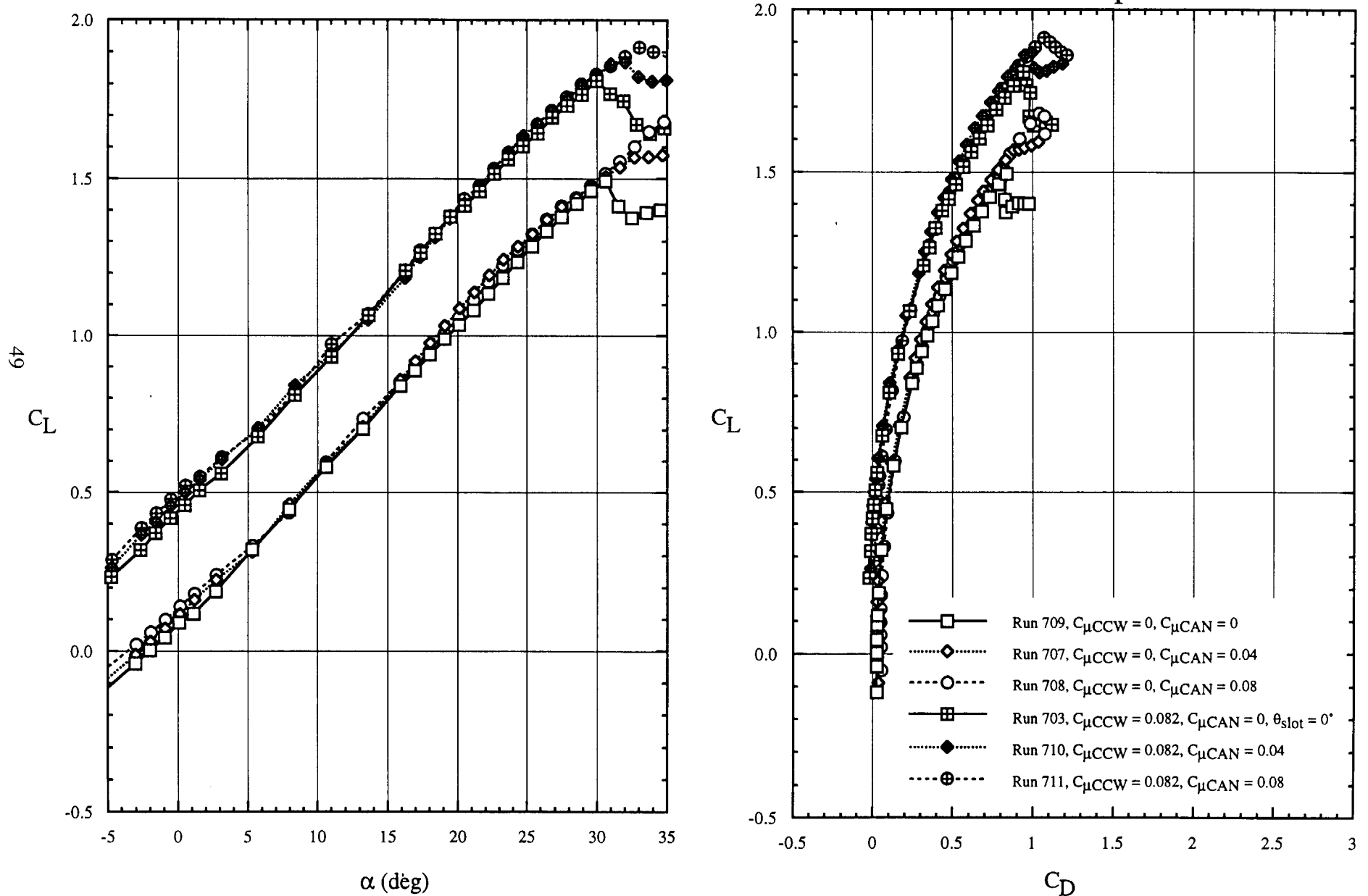


Figure 28 - Application of CC Cylinder Canard, slot location at -20° , to CCW 0° Flap Configuration

MTF044 HSCT, Effects of CC Cylinder Canard Slot Location

C_L v. C_{M50} , C_L v. L/D_{eq}

$\theta_{slot} = -20^\circ$, $h_{canard} = 0.010''$, $h_{ccw} = 0.010''$, $i_{tail} = 0^\circ$, $\delta_{Flap} = CCW 0^\circ$

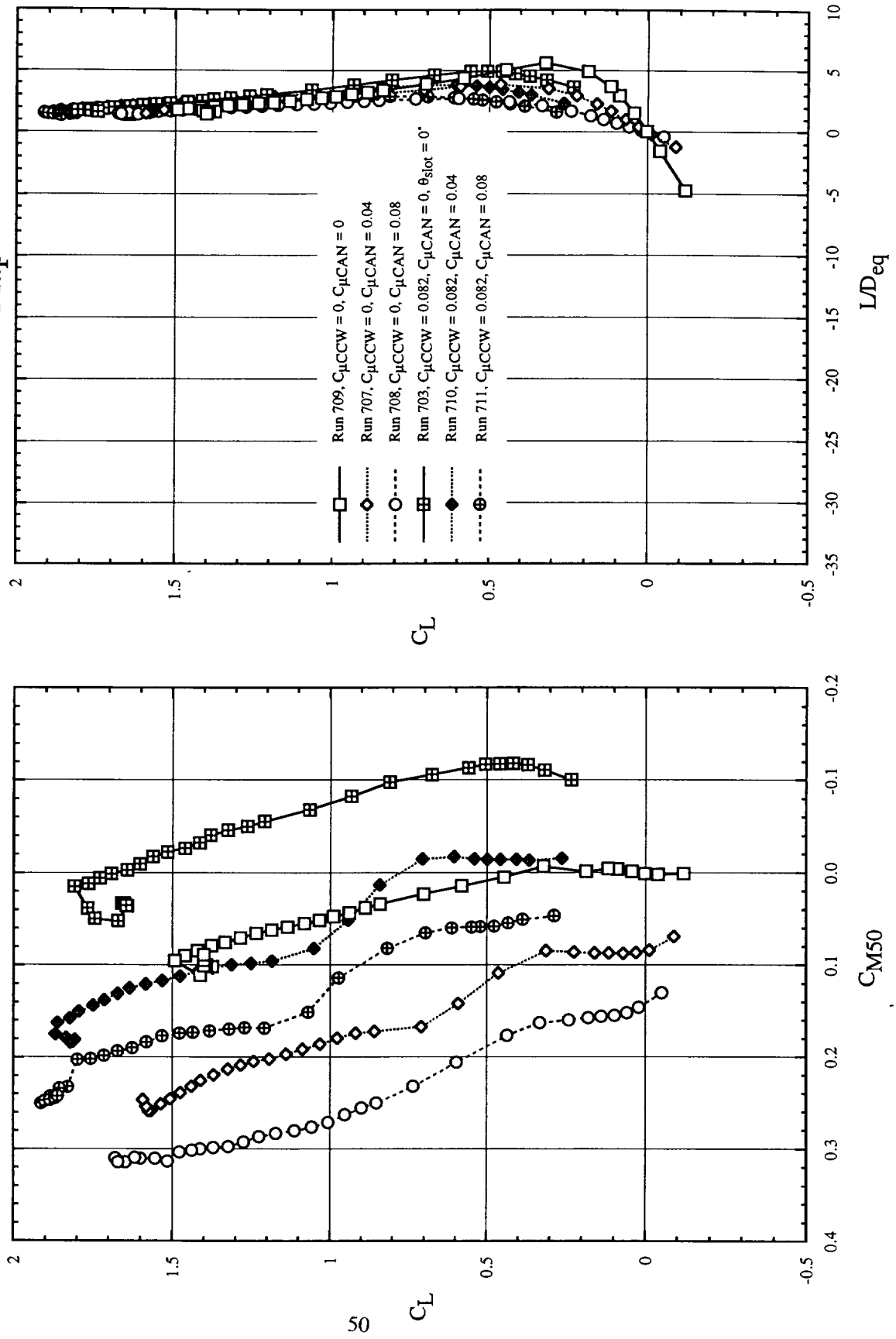


Figure 28 - Application of CC Cylinder Canard, slot location at -20° , to CCW 0° Flap Configuration
b. Pitching Moment and Lift/Drag Ratio

MTF044 HSCT, Effects of CC Cylinder Canard Slot Location

C_L v. α , C_L v. C_D

$\theta_{slot} = 0^\circ$, $h_{canard} = 0.010''$, $h_{ccw} = 0.010''$, $i_{tail} = 0^\circ$, $\delta_{Flap} = CCW 0^\circ$

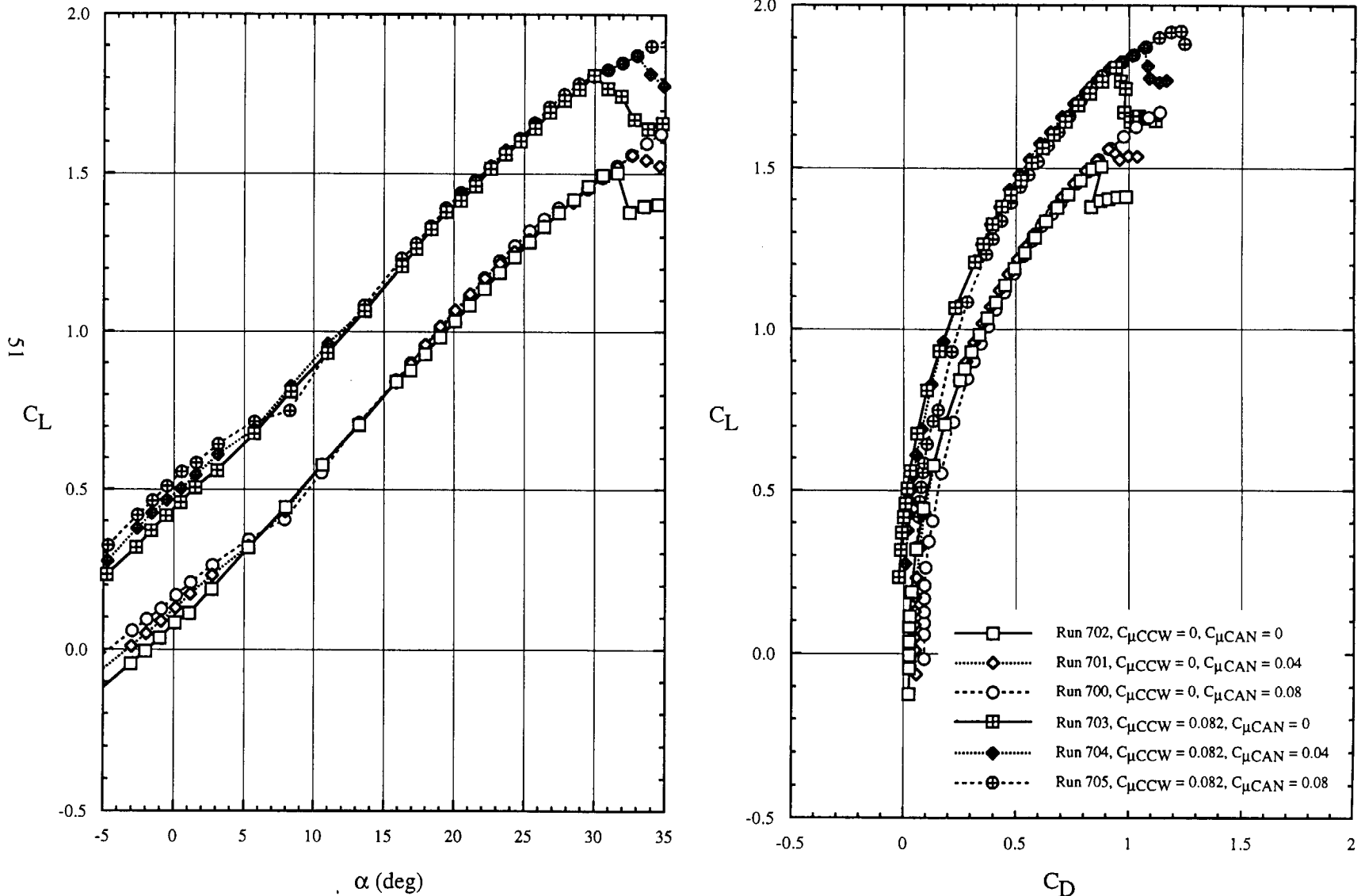


Figure 29 - Application of CC Cylinder Canard, slot location at 0° , to CCW 0° Flap Configuration
a. Lift and Drag

MTF044 HSCT, Effects of CC Cylinder Canard Slot Location

C_L v. C_{M50} , C_L v. L/D_{eq}

$\theta_{slot} = 0^\circ$, $h_{canard} = 0.010''$, $h_{ccw} = 0.010''$, $i_{tail} = 0^\circ$, $\delta_{Flap} = CCW 0^\circ$

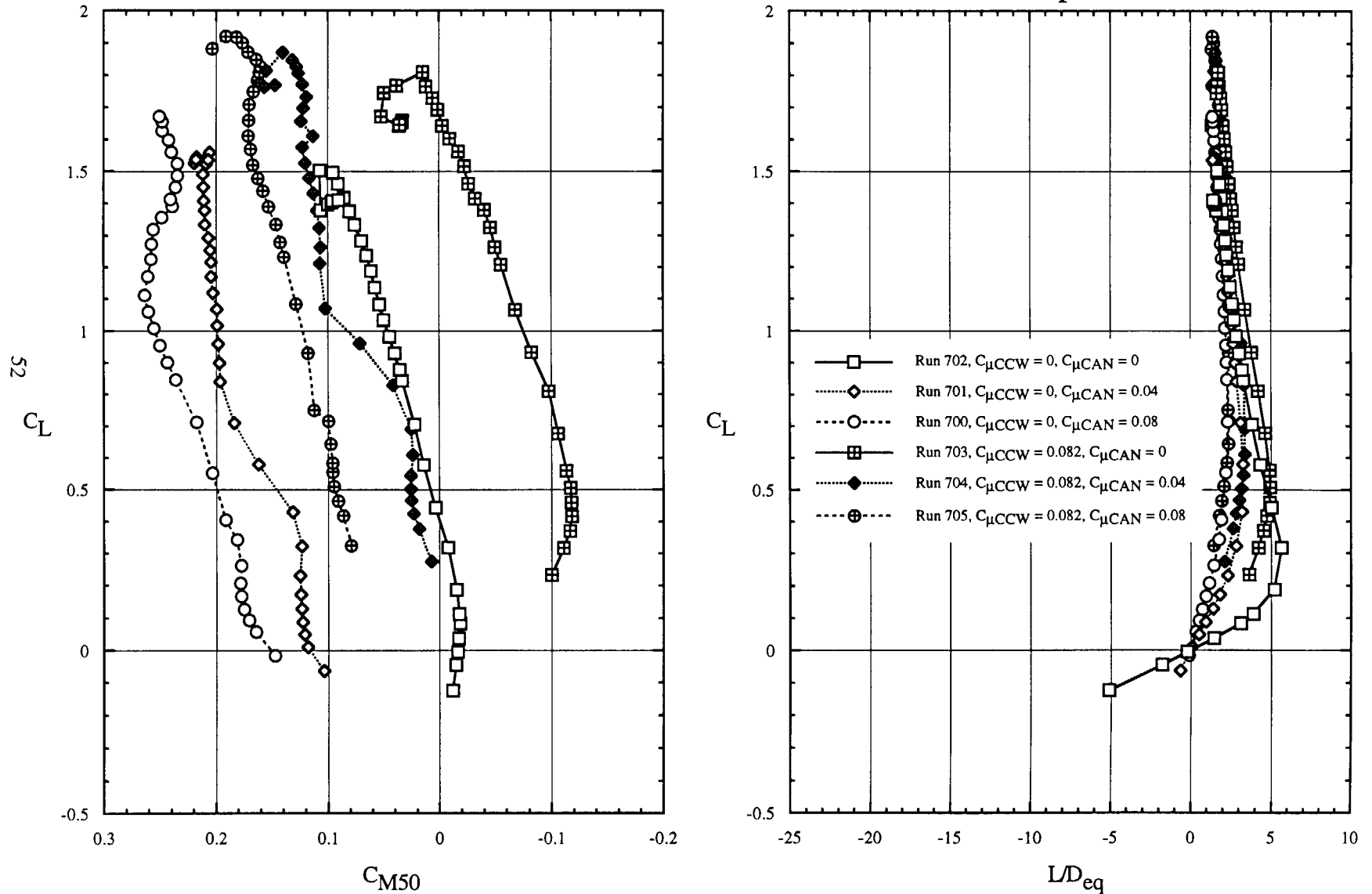
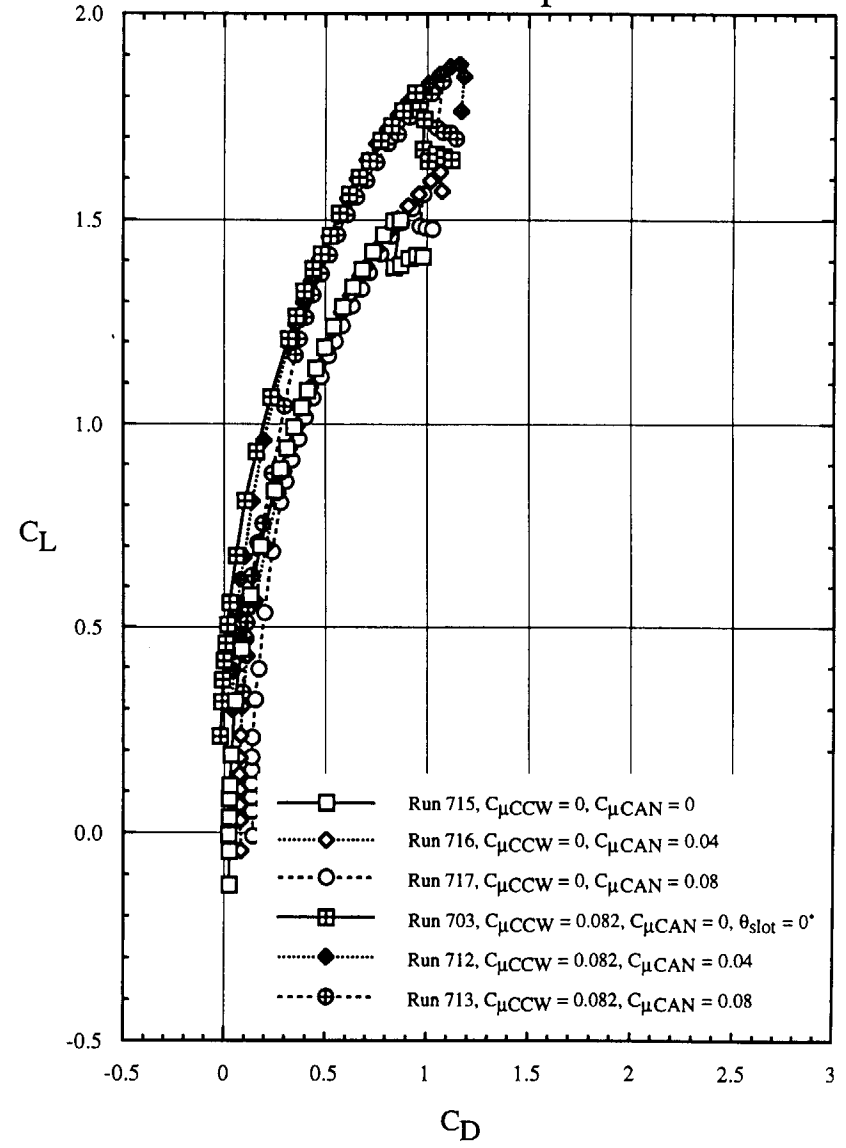
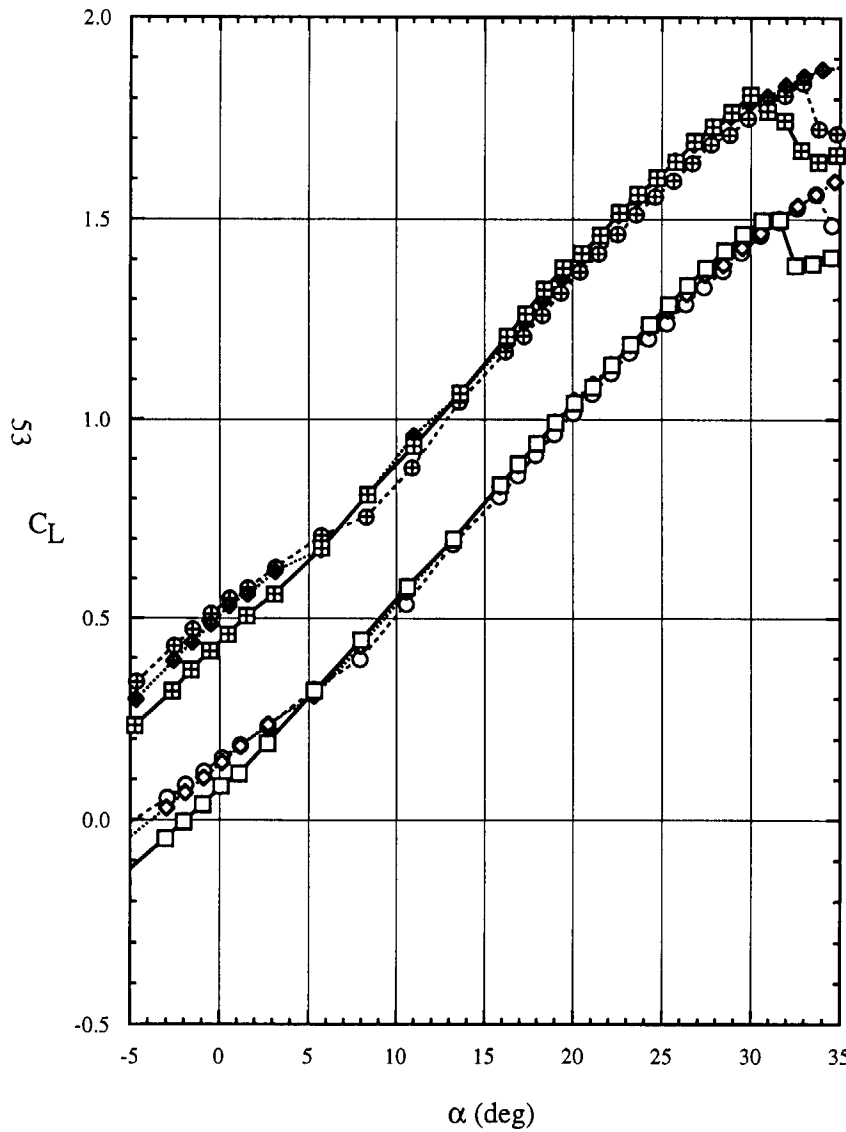


Figure 29 - Application of CC Cylinder Canard, slot location at 0° , to CCW 0° Flap Configuration
b. Pitching Moment and Lift/Drag Ratio

MTF044 HSCT, Effects of CC Cylinder Canard Slot Location

C_L v. α , C_L v. C_D

$\theta_{slot} = +20^\circ$, $h_{canard} = 0.010''$, $h_{ccw} = 0.010''$, $i_{tail} = 0^\circ$, $\delta_{Flap} = CCW 0^\circ$



- Run 715, $C_{\mu CCW} = 0$, $C_{\mu CAN} = 0$
- ◇ Run 716, $C_{\mu CCW} = 0$, $C_{\mu CAN} = 0.04$
- Run 717, $C_{\mu CCW} = 0$, $C_{\mu CAN} = 0.08$
- ▣ Run 703, $C_{\mu CCW} = 0.082$, $C_{\mu CAN} = 0$, $\theta_{slot} = 0^\circ$
- ◆ Run 712, $C_{\mu CCW} = 0.082$, $C_{\mu CAN} = 0.04$
- ⊕ Run 713, $C_{\mu CCW} = 0.082$, $C_{\mu CAN} = 0.08$

Figure 30 - Application of CC Cylinder Canard, slot location at $+20^\circ$, to CCW 0° Flap Configuration
a. Lift and Drag

MTF044 HSCT, Effects of CC Cylinder Canard Slot Location

C_L v. C_{M50} , C_L v. L/D_{eq}

$\theta_{slot} = +20^\circ$, $h_{canard} = 0.010''$, $h_{ccw} = 0.010''$, $i_{tail} = 0^\circ$, $\delta_{Flap} = CCW 0^\circ$

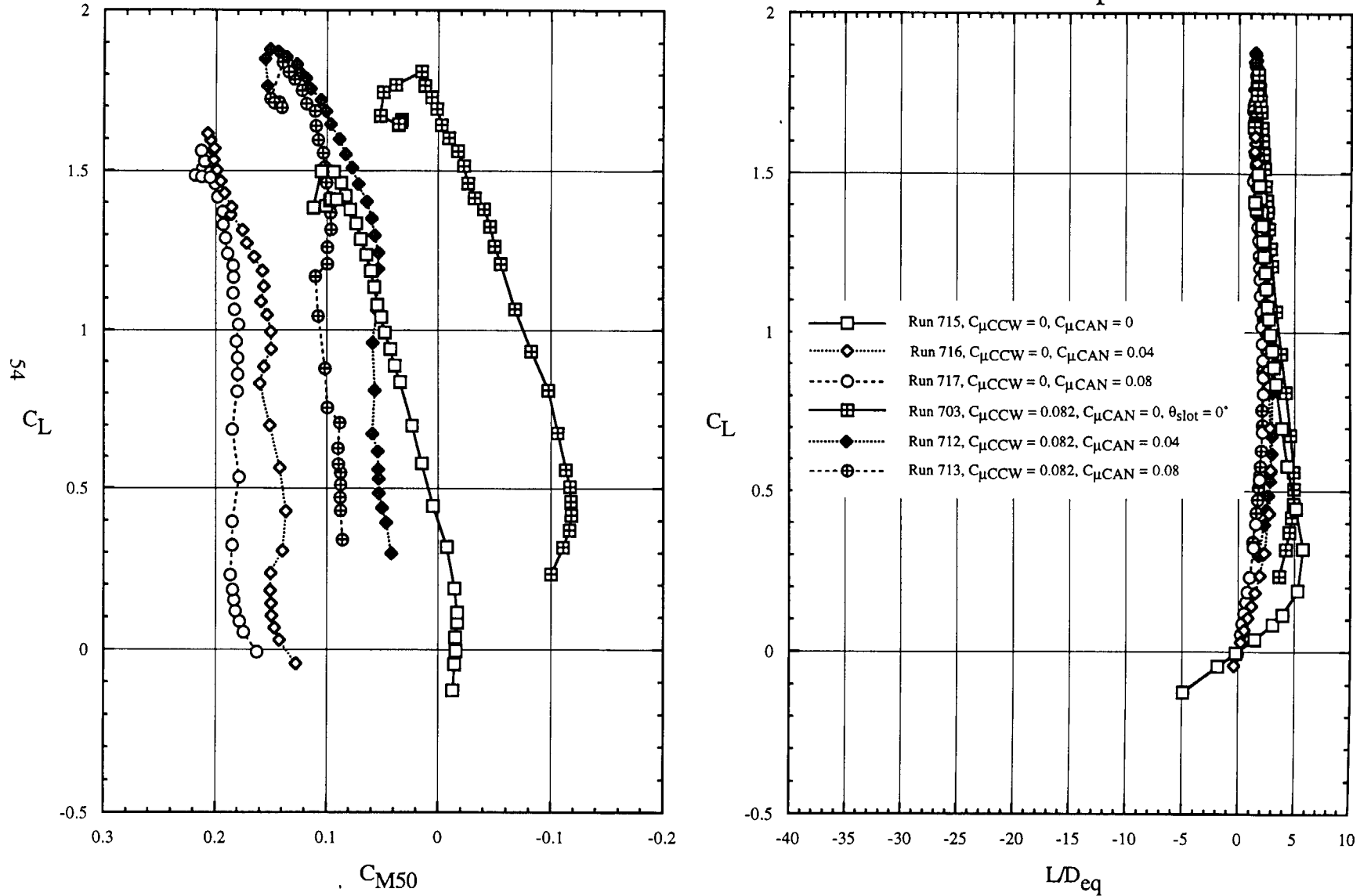


Figure 30- Application of CC Cylinder Canard, slot location at $+20^\circ$, to $CCW 0^\circ$ Flap Configuration
 b. Pitching Moment and Lift/Drag Ratio

MTF044, Effect of Canards on C_L and C_{M50} , CCW Flap=34°,
 $C_{\mu\text{CCW}}=0.0$, Tail=0°, $q=20$ psf

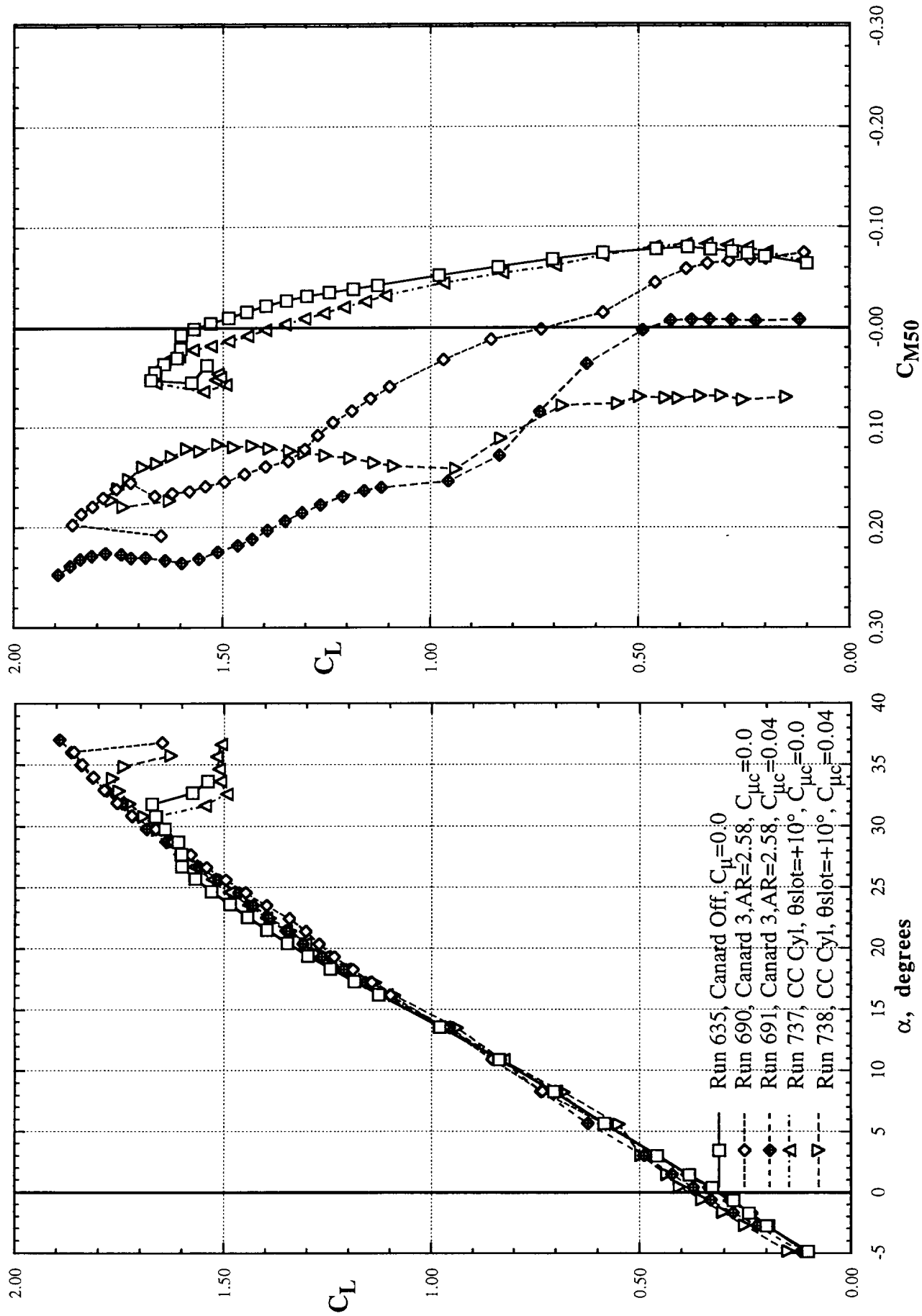


Figure 31 - Effect of three canards on CCW 34° Flap Configuration, $C_{\mu\text{CCW}} = 0.0$

MTF044, Effect of Canards on C_L and C_{M50} , CCW Flap=34°,
 $C_{\mu CCW}=0.082$, Tail=0°, $q=20$ psf

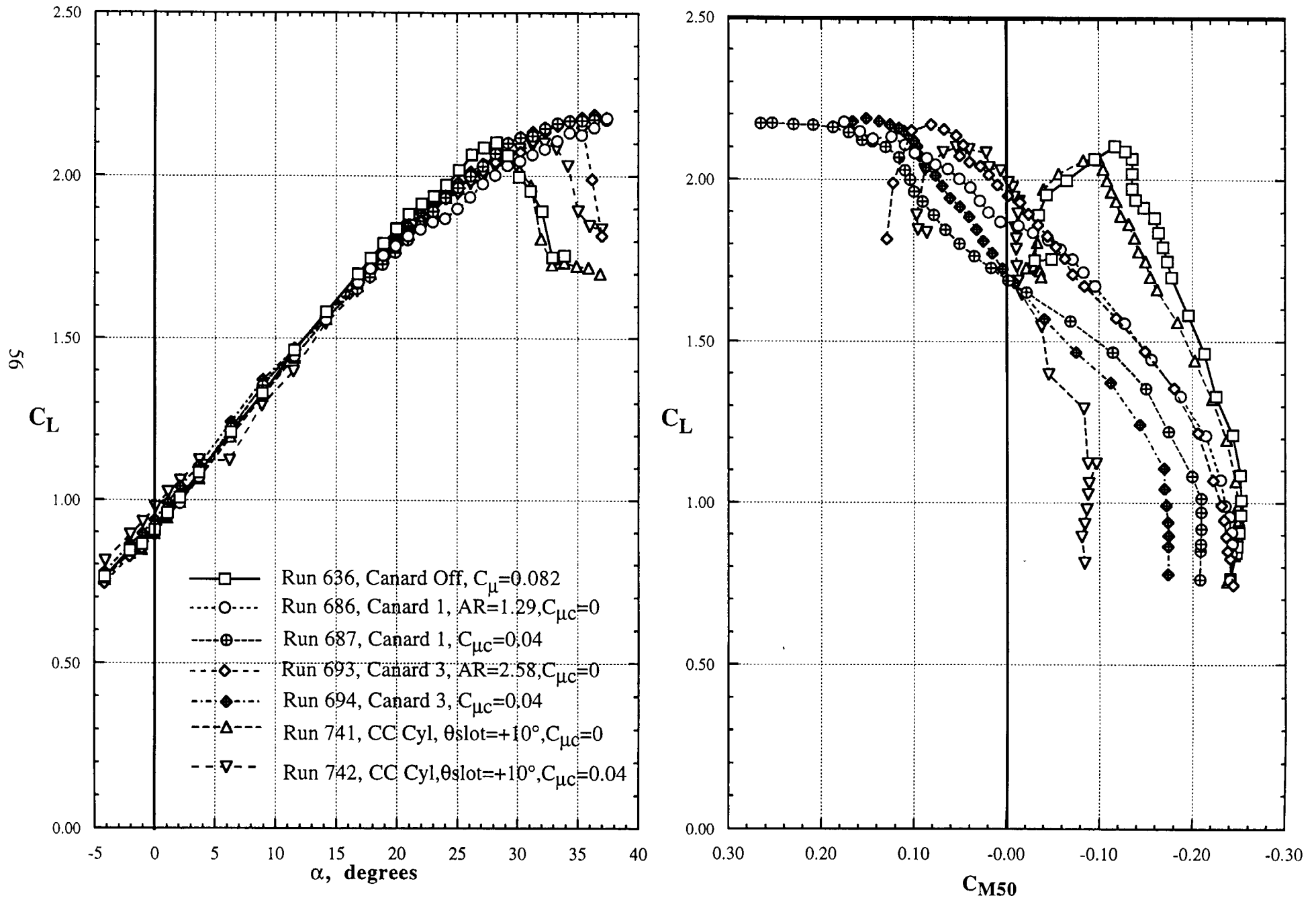


Figure 32 - Effect of three canards on CCW 34° Flap Configuration, $C_{\mu CCW} = 0.082$

MTF044CC Cylinder Canards, Effect of Slot Location on C_L and C_{M50} ,
 $C_{\mu CCW}=0.0$, CCW Flap= 34° , Tail= 0° , $\alpha=0^\circ$, $q=20$ psf

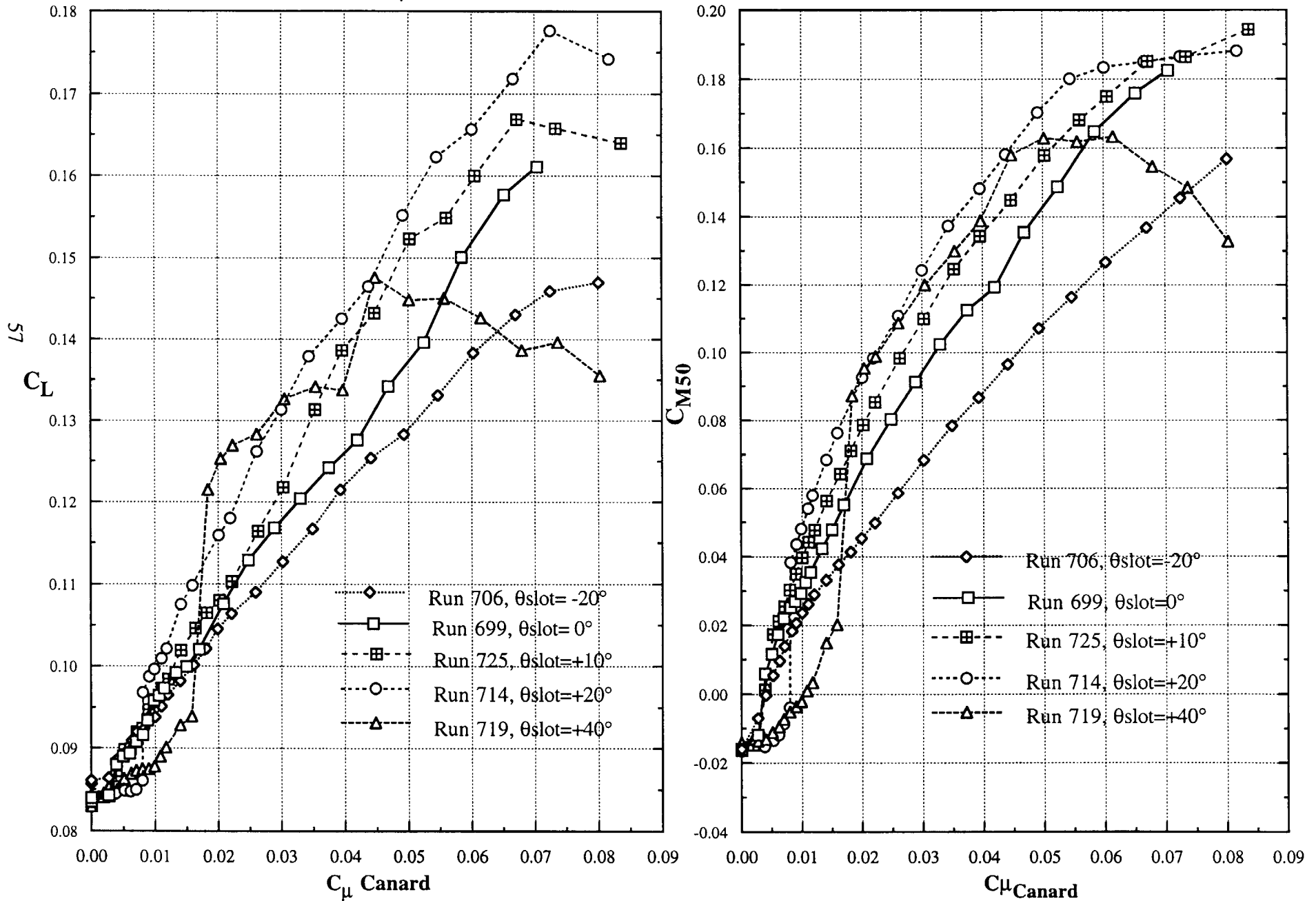


Figure 33- Effect of CC Cylinder Canard slot location on Lift and Pitch as a function of blowing

MTF044, CC Cylinder Canard Effect on C_L at High α
 $C_{\mu CCW}=0.0, \theta_{slot}=+10^\circ, Tail=0^\circ, \alpha=0^\circ, q=20 \text{ psf}, h=0.0/d$

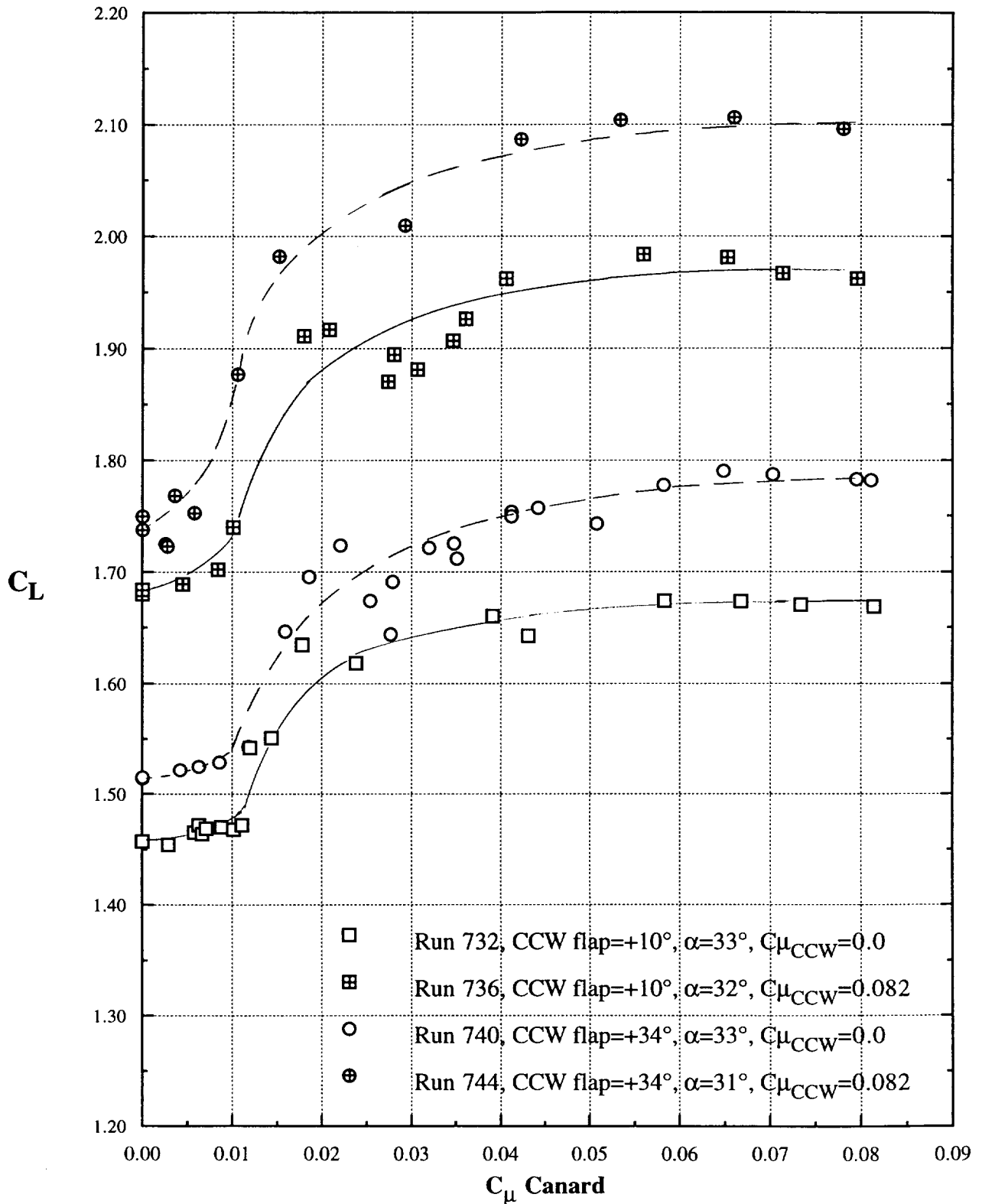


Figure 34 - Effect of Cylinder Canard blowing to increase stall angle

a. Lift as a function of $C_{\mu \text{ canard}}$

MTF044, CC Cylinder Canard Effect on C_{M50} at High α
 $C_{\mu CCW}=0.0, \theta_{slot}=+10^\circ, Tail=0^\circ, \alpha=0^\circ, q=20 \text{ psf}$

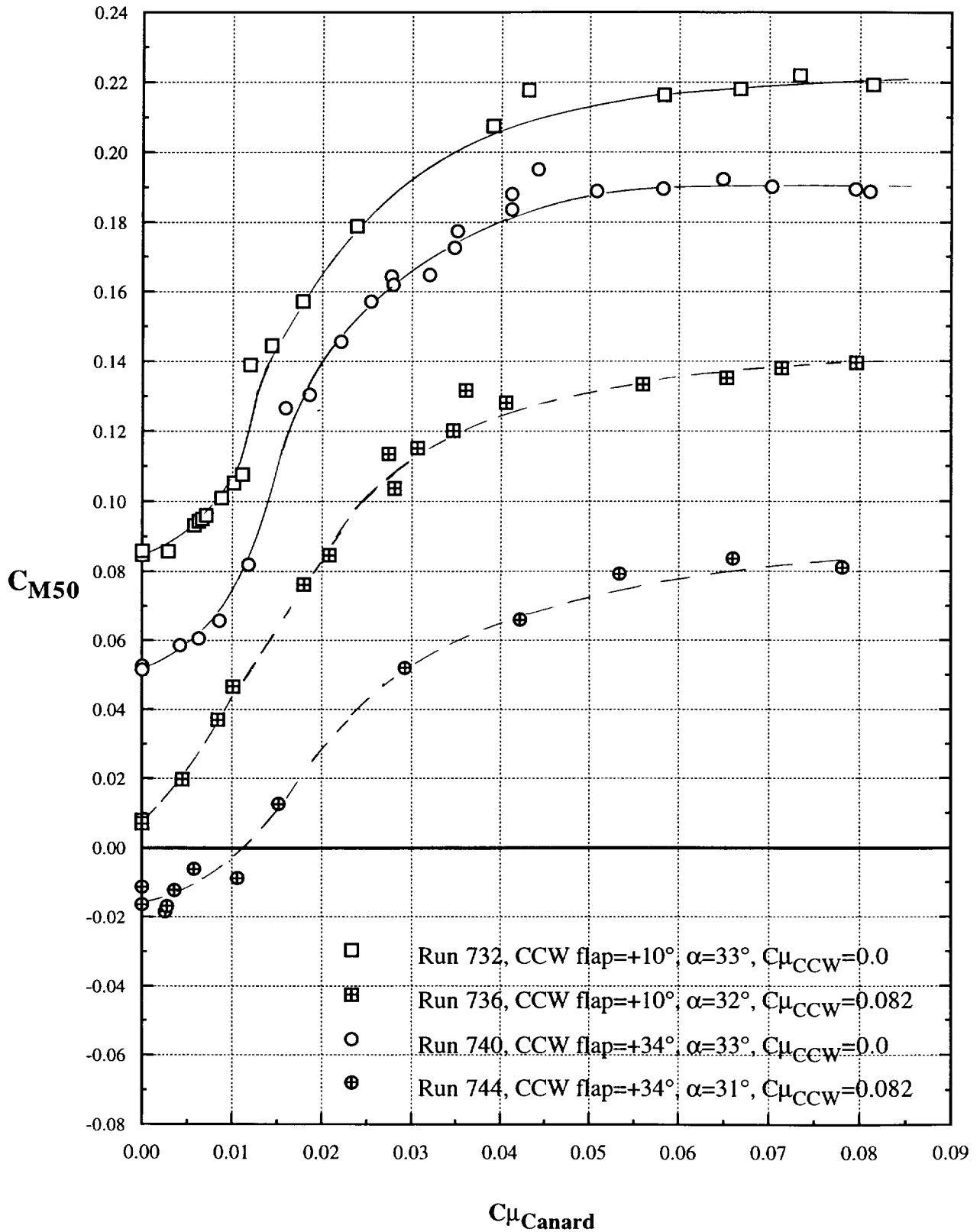


Figure 34 - Effect of Cylinder Canard blowing to increase stall angle

b. Pitching Moment as a function of $C_{\mu canard}$

MTF044, Pulsed Blowing, $q=20\text{psf}$, $\text{Alpha}=0^\circ$, $h=0.010''$

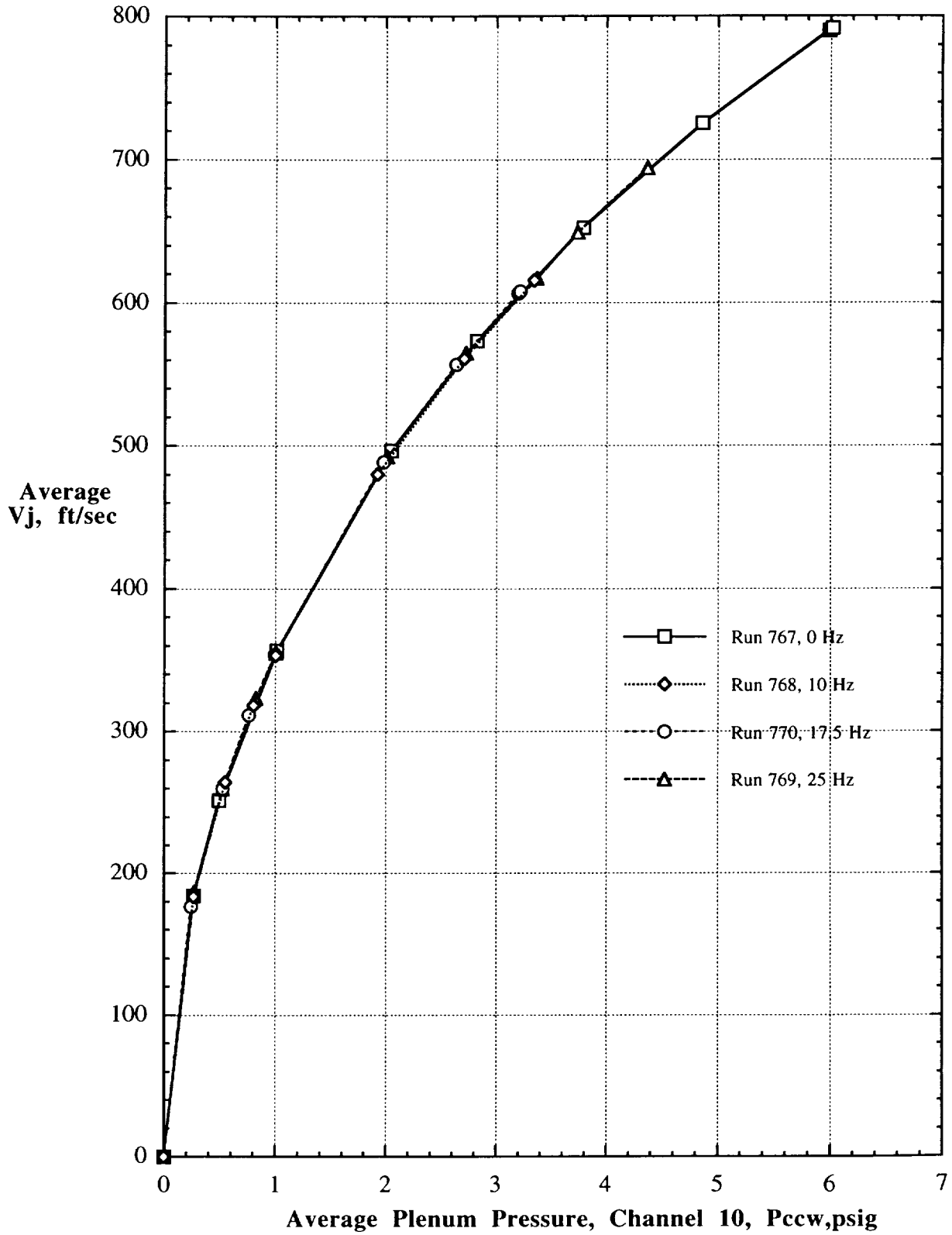


Figure 35 - Averaged jet velocity during pulsed blowing tests

MTF 044 Pulsed Blowing $q=20\text{psf}$, $\alpha=0^\circ$, $h=0.010''$

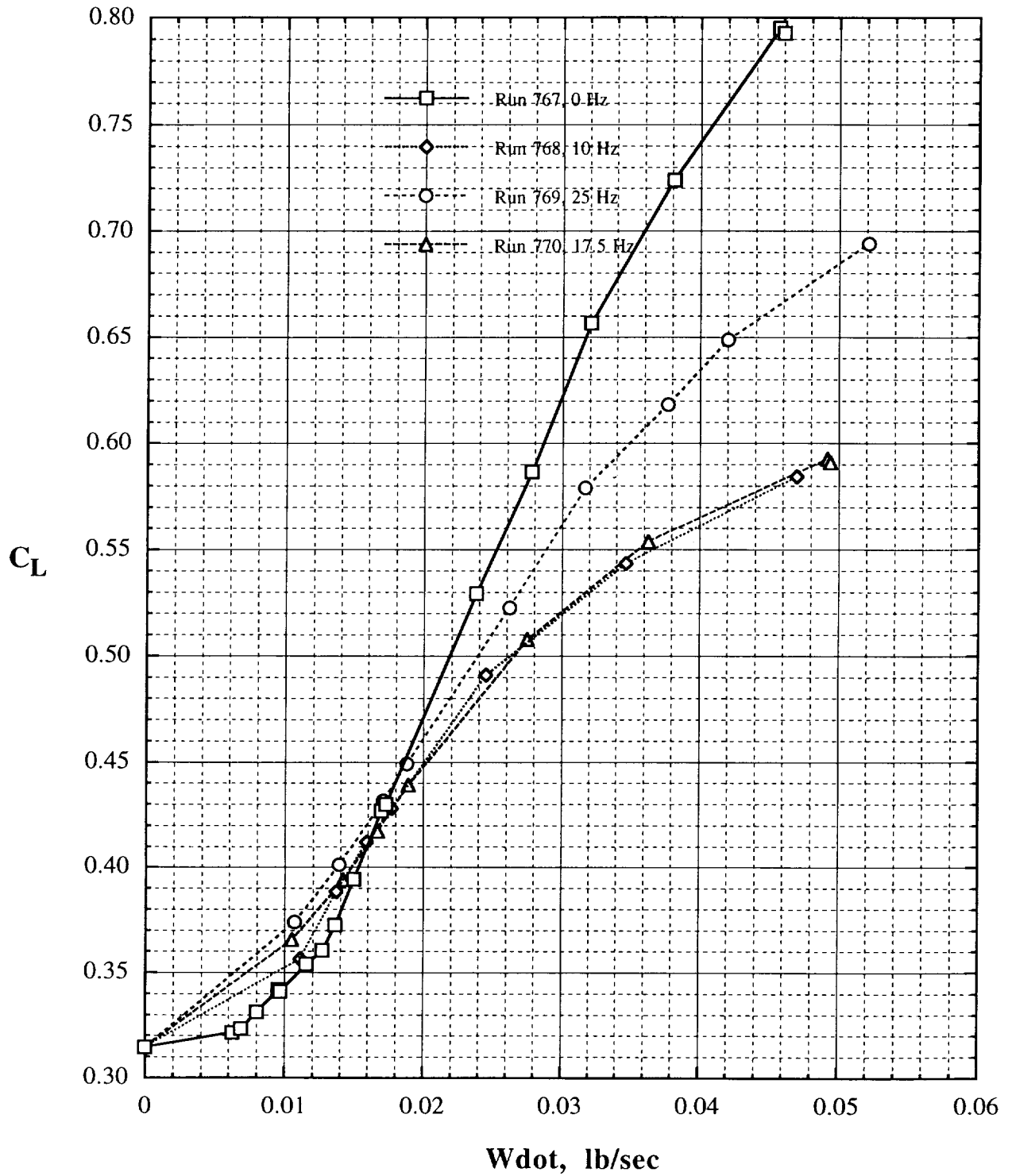


Figure 36 - Averaged lift and weight flow during pulsed blowing tests

MTF 044 Pulsed Blowing $q=20\text{psf}$, $\text{Alpha}=0^\circ$, $h=0.010''$

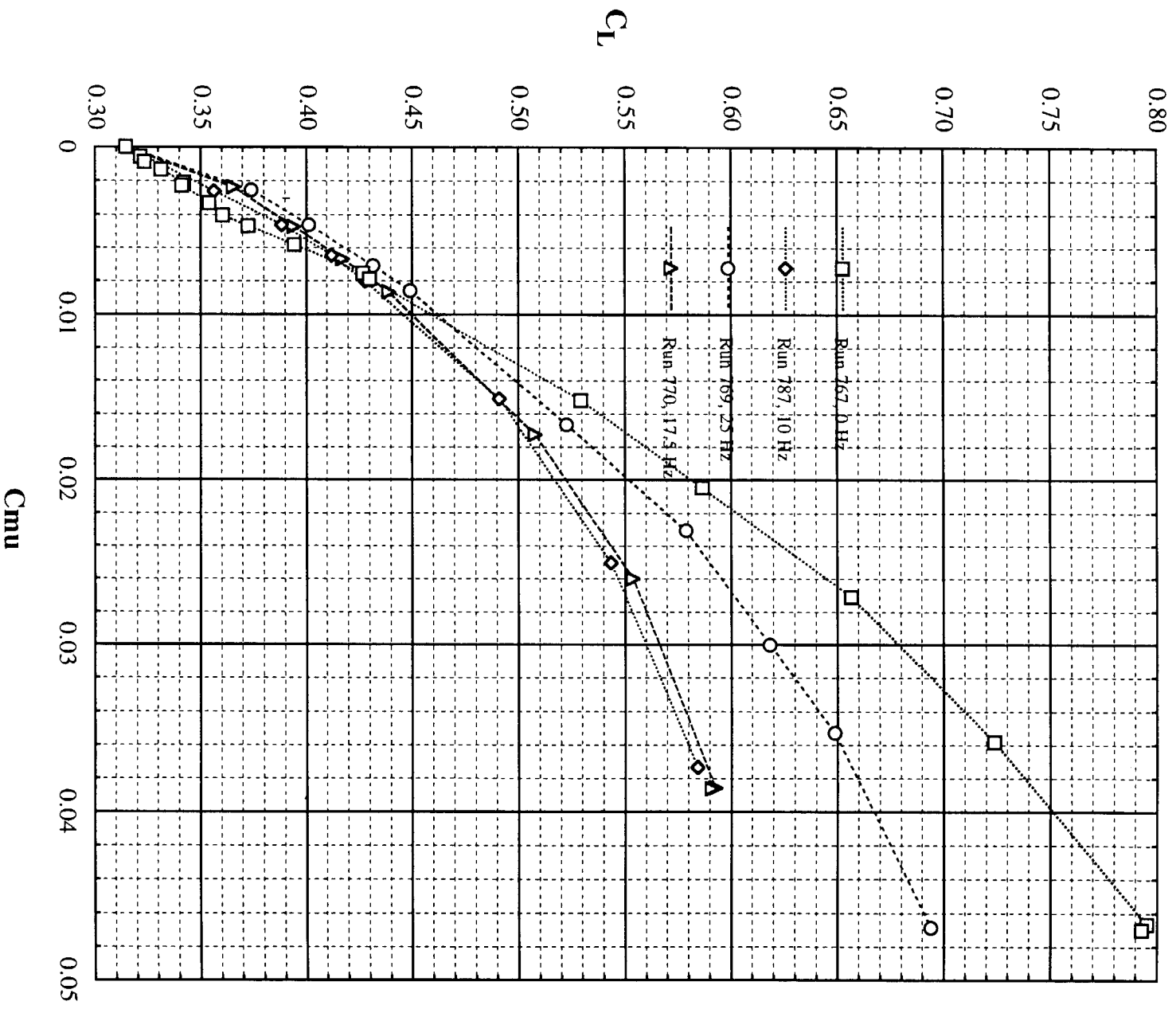


Figure 37 - Pulsed-blowing average lift as a function of C_{μ}

CONCLUSIONS

In the Task 1 portion of this NASA research grant, configuration development and experimental investigations have been conducted on a series of pneumatic high-lift and control surface devices applied to a generic HSCT model configuration to determine their potential for improved aerodynamic performance, as well as stability and control of higher performance transport aircraft. These investigations were intended to optimize pneumatic lift and drag performance; provide adequate control and longitudinal stability; reduce separated flowfields at high angle of attack; increase takeoff/climbout lift-to-drag ratios; and reduce system complexity and weight. Experimental aerodynamic evaluations were performed on a semi-span HSCT generic model with improved fuselage fineness ratio and with interchangeable plain flaps, blown flaps, pneumatic CCW high-lift configurations, plain and blown canards, a novel CC cylinder canard, and a clean wing for reference. Conventional tail power was also investigated for longitudinal trim capability.

Also evaluated was unsteady pulsed blowing of the wing high-lift system to determine if reduced pulsed mass flow rates and blowing requirements could be made to yield the same lift as that resulting from steady-state blowing. Depending on the pulsing frequency applied, reduced mass flow rates were indeed found able to provide lift augmentation at lesser blowing values than for the steady conditions.

Significant improvements in the pneumatic aerodynamic characteristics leading to improved performance and stability/control were verified, and the various components were compared to evaluate the pneumatic potential of each.

Specifically, the following results were shown:

- **Blown lift increases** at $\alpha = 0^\circ$ of greater than 15 times that of the unblown 20° plain flap and an 88% increase in $C_{L_{max}}$ due to blowing over the clean cruise configuration were demonstrated, plus blowing lift augmentations of **10-12 times the input jet momentum** (thrust) coefficient were measured at lower C_{μ} values. The CCW 34° configuration performed best in terms of higher lift and $C_{L_{max}}$ generated, followed in decreasing order by the CCW 10° , the CCW 0° , and the 20° and 0° plain blown flaps. All flaps were limited by jet turning produced by C_{μ} ; the plain blown flaps were generally limited by the flat upper surface angle of the flap trailing edge. The curved CCW surfaces produced much greater turning possibility. Overall $C_{L_{max}}$ achieved by the blown aircraft (without canards at this point) increased from 1.9 for the previous blown configurations (Appendix A) to 2.7 for this new one.
- **Drag reductions due to thrust recovery** were generated for the lesser-angle CCW and plain blown flaps, where up to 65-70% of the input blowing momentum could be recovered as negative C_D . Higher drag generated by the high-lift CCW configurations (CCW 34° and CCW 10°) could prove quite useful in slow-speed approaches with steep glide slopes.
- **Static thrust evaluations showed jet turning of up to 90°** for the pneumatic CCW configurations (base on the angle of the geometric trailing edge arc).
- **Equivalent lift/drag ratios**, including blowing penalties, were compared for the unblown and blown configurations. Maximum L/D_{eq} always occurred at lower C_L , with a value near 9 being recorded for the CCW flap at $C_L = 0.2$. At higher C_L values, much higher L/D_{eq}

values were achieved by the CCW flap configurations than by the plain flaps; in many cases, these values occurred at C_L values not even attainable by the blown or unblown plain flaps.

- **Nose-down pitching moment increased** with lift due to blowing. Unblown canards were able to provide trim, but their forward locations produced longitudinal instability in pitch as α increased; blown canards provided greater trim but with greater pitch instability.
- **A blown CC cylinder canard** produced jet turning angles as high as 135° , and adequate pitch trim as a result of the more-forward lift location. With blowing on, these produced near-neutral longitudinal stability because the cylinder was α -insensitive (showing no lift change as α increased)
- The CC cylinder canard provided greater lift capability and thus the potential for **smaller surface area** and the ability to be retracted, perhaps by telescoping. This also could produce reduction in canard weight and complexity.
- **Additional lift and pitch trim** provided by these pneumatic concepts offer the potential to achieve takeoff and climbout C_L and L/D_{eq} at zero or low angles of attack. This can eliminate the need to rotate the aircraft to high α , nose droop, synthetic vision, and aft fuselage upsweep.
- **The pulsed blowing experimental devices** used were not able to reach the frequencies and square-wave pressure traces desired, but did show that for low C_{μ} , steady state blown lift values could be achieved with required mass flows reduced by up to 45-50%.

In general, the potential of pneumatic devices as aerodynamic force and moment augmentors plus control surfaces, stability augmentors and aerodynamic efficiency improvement devices was confirmed for HSCT configurations, providing an alternative to conventional mechanical aerodynamic devices for performance improvement and controllability of advanced HSCT aircraft. The strengths of both the CCW-type high-lift and control-surface concepts were shown to exceed the capabilities demonstrated in the previous pneumatic HSCT tests. In addition, new simplified blown cylinder canards were verified, as was the potential of unsteady pulsed blowing to reduce the mass flow required for a given desired lift.

RECOMMENDATIONS

The experimental verification of these pneumatic lift and control devices has confirmed these concepts and offers the opportunity to continue their development for application to high-performance transport vehicles. Among possible follow-on efforts which could benefit from this research are:

- Further unsteady pulsed blowing subsonic evaluations to include improved pulse-generating devices with higher frequencies and better defined square-wave capability.
- Additional evaluations of the CC cylinder canard geometries to determine if they can be designed to create greater lift and moment and to increase pneumatic jet turning at smaller sizes yet

- Further evaluation of partial-span wing blowing slots and/or tailored spanwise slot geometry for more precise control of spanwise lift loadings and controllability, or movement of the blown flap segment further outboard on the wing for increased aerodynamic moment arm for low-speed roll and yaw generation
- Extension of pneumatic test configurations into a transonic evaluation of their capabilities, since that is where the moment and control capabilities could also prove quite beneficial

REFERENCES

1. NASA Langley Grant NAG-1-1517, "Continued Development and Application of Circulation Control Technology for Advanced Transport Aircraft," June 1993 - May 1997.
2. NASA Langley Contract NAS1-19061, "Research in Acoustics and Noise Control", Task Assignment 6, "Development and Application of Circulation Control Technology to Quiet Advanced Transport Aircraft," May 1991 - March 1992.
3. Englar, R. J. , M. J. Smith, S. M. Kelley, and R. C. Rover, "Development of Circulation Control Technology for Application to Advanced Subsonic Transport Aircraft", AIAA Paper 93-0644, presented at AIAA 31st Aerospace Sciences Meeting, Reno, NV January 11-14, 1993.
4. Englar, R. J. , M. J. Smith, S. M. Kelley, and R. C. Rover, "Application of Circulation Control Technology to Advanced Subsonic Transport Aircraft, Part II: Transport Application," *AIAA Journal of Aircraft*, Vol. 31, No. 5, Sept. - Oct., 1994, pp. 1169-1177.
5. Englar, R. J., C. S. Neibur and S. D. Gregory, "Pneumatic Lift and Control Surface Technology Applied to High Speed Civil Transport Configurations," AIAA Paper 97-0036, presented at the 35th AIAA Aerospace Sciences Meeting, January 6-10, 1997, Reno, NV.
6. Mavris, D. N., Bandte, O., and Brewer, J. T., "A Method for the Identification and Assessment of Critical Technologies Needed for an Economically Viable HSCT." AIAA Paper 95-3887, presented at the 1st AIAA Aircraft Engineering, Technology, and Operations Congress, Sept. 19-21, 1995, Los Angeles, CA.
7. Mavris, D. N., Bandte, O., and Schrage, D. P., "Economic Uncertainty Assessment of an HSCT Using a Combined Design of Experiments/Monte Carlo Simulation Approach." Paper presented at the 17th Annual Conference of the International Society of Parametric Analysis, May 1995, San Diego, CA.
8. Kirby, M. R., J.M. Lee, S. Qui, B. Roth and J. Tai, "Systems Analysis of Phneumatic Technology for HSCT Aircraft," Georgia Institue of Technology ASDL Final Report, Project A-5676, October 3, 1999.
9. Englar, R. J., and C. A. Applegate, "Circulation Control - A Bibliography of DTNSRDC Research and Selected Outside References (January 1969 through December 1983)," DTNSRDC-84/052, September, 1984.

10. Englar, Robert J., "Development of Pneumatic Test Techniques for Subsonic High-Lift and In-Ground-Effect Wind Tunnel Investigations," Paper #18, presented at the AGARD 73rd Fluid Dynamics Panel Meeting and Symposium, October 4-7, 1993, Brussels, Belgium.
11. Oyler, T. E., and W. E. Palmer, "Exploratory Investigation of Pulsed Blowing for Boundary Layer Control," North American Rockwell Report NR72H-12, January 15, 1972.
12. Williams, J. R., J. P. Ambrosiani, and W. E. Palmer, "Analysis of a Pulsing Wall Jet," North American Rockwell Report NR72H-325, Oct. 15, 1972.
13. Walters, R.E., D. P. Myer, and D. J. Holt, "Circulation Control by Steady and Pulsed Blowing for a Cambered Elliptical Airfoil," West Virginia University, Aerospace Engineering Report TR-32, July 1972.



AIAA 97-0036

**Pneumatic Lift and Control Surface
Technology Applied To High Speed Civil
Transport Configurations**

Robert J. Englar, Curt S. Niebur, and
Scott D. Gregory

Aerospace & Transportation Laboratory
Georgia Tech Research Institute
Georgia Institute of Technology
Atlanta, GA 30332-0844

**35th Aerospace Sciences
Meeting & Exhibit
January 6-10, 1997 / Reno, NV**

PNEUMATIC LIFT AND CONTROL SURFACE TECHNOLOGY APPLIED TO HIGH SPEED CIVIL TRANSPORT CONFIGURATIONS

Robert J. Englar*, Curt S. Niebur**, and Scott D. Gregory**
Aerospace & Transportation Laboratory
Georgia Tech Research Institute
Atlanta, GA 30332-0844

ABSTRACT

Experimental evaluations have been conducted of blown high-lift devices and control surfaces applied to improve the low-speed performance of generic High Speed Civil Transport aircraft. Plain blown flaps and advanced pneumatic high-lift devices have been integrated into highly-swept vortex-dominated wings. These produced large lift increases and significant drag reductions greater than full jet thrust recovery. Because conventional horizontal tails were found inadequate to trim these configurations, blown canards were employed. In addition to providing positive lift increments for trim, the canards were found to favorably influence the higher angle-of-attack vortex-lift characteristics of these wings. The downwash from these canards resulted in delay of wing vortex burst. The paper presents details of these investigations and test results which confirm the effectiveness of combined pneumatic high-lift devices and control surfaces on these HSCT aircraft.

INTRODUCTION

Various forms of blown aerodynamic devices have been evaluated in recent years to augment the low-speed, high-lift characteristics of modern-day aircraft. These aircraft, especially military configurations, usually have relatively high wing loadings and associated high takeoff and landing speeds with long ground rolls. Use of pneumatic devices, such as blown flaps or jet flaps, can augment the lift of mechanical flaps and reduce terminal-area speeds and

distances (ground roll as well as climb-out and approach flight paths). More recently, a concept known as Circulation Control (CC), which employs tangential blowing over highly rounded small trailing edges, has been shown to greatly augment lift and thus improve takeoff and landing capabilities¹⁻⁷. For the two-dimensional airfoils of subsonic aircraft using this technology^{2,4}, lift augmentation of nearly 80 times the input blowing momentum has been recorded, as has significant drag reduction due to jet thrust recovery and prevention of flow separation.

Recent interest in high-speed commercial aircraft such as the High Speed Civil Transport (HSCT) suggests that this pneumatic technology should greatly benefit these vehicles as well⁵. In addition to high wing loadings, these aircraft also frequently employ vortex lift on takeoffs and landings at high angles of attack. This has required such "features" as mechanical nose droop for visibility and highly-upswept aft fuselage contours for ground clearance upon rotation. Reduced wing sweep and increased wing planform area can improve low-speed flight, but may hinder high-speed cruise performance. A recent research program conducted at Georgia Tech Research Institute (GTRI) under the sponsorship of NASA Langley Research Center has evaluated the potential of blown aerodynamic devices for both lifting surface and control surface applications to high-speed commercial aircraft. Major goals of this program were to: (1) develop advanced pneumatic high-lift configurations for highly-swept wings; (2) evaluate blown canards for pitch trim, vortex control and lift augmentation; and (3) evaluate

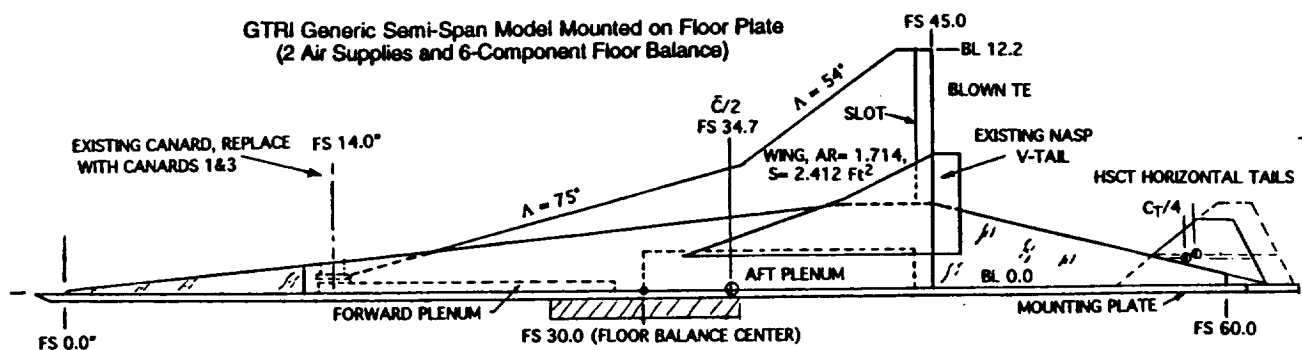


Figure 1 - Planform of the GTRI semi-span NASP/HSCT configuration

* Principal Research Engineer; Associate Fellow, AIAA
** Cooperative Education Student; Member AIAA

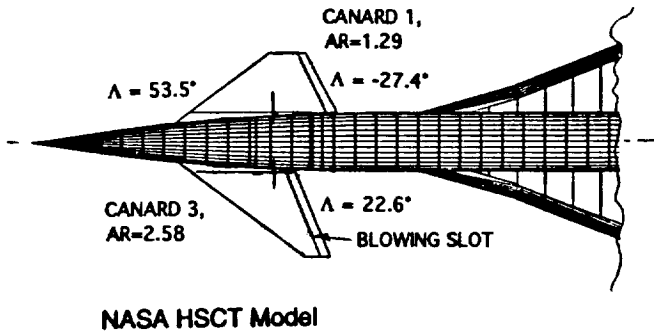


Figure 2 - NASA Generic HSCT configuration with Canards 1 and 3

conventional horizontal tails for trim and stability during vortex-dominated operation, both with and without wing blowing. The following sections will discuss the details of these blown lift and control devices, the experimental evaluations employed, the results of these parametric proof-of-concept investigations, and the potential applications.

EXPERIMENTAL APPARATUS, MODELS, AND TEST PROCEDURES

In this proof-of-concept evaluation, an existing half-span model at GTRI was deemed representative of a NASA generic HSCT configuration. These two configurations are shown in Figures 1 and 2. The half-span model employed here (Figure 1) was a generic National Aerospace Plane (NASP) model which had a wing planform and leading edge sweeps (75° and 54°) similar to certain current HSCT configurations. The sharply-beveled model wing leading edge (LE) was intended to generate strong LE vortex flows in the high-lift or high- α modes, and the remainder of the main wing airfoil was a flat plate up to the trailing edge slot (Figure 3). The wing had a trailing edge blowing plenum and a tangential slot exiting over the upper surface of a plain flap deflected 20°. A highly-curved CC trailing edge was fabricated to determine the effects of larger jet turning on lift augmentation. The CC "cruise configuration" (0° flap deflection) had a curved upper surface yielding 48° of jet turning when blown. A 34° deflection of the flat lower surface exposed an additional CC arc producing a total of 90° of jet turning. The unblown 20° plain flap is representative of conventional HSCT high-lift systems and thus serves as a baseline for comparison. The major objective here was to determine blown lift augmentation when operating in the rotational flowfields of the strong vortex from the wing's swept leading edge.

It was realized that HSCT configurations of this type might well benefit from a canard to trim with positive lift increment instead of tail download. Thus, two blown canards employing CC-type trailing edge curvature and

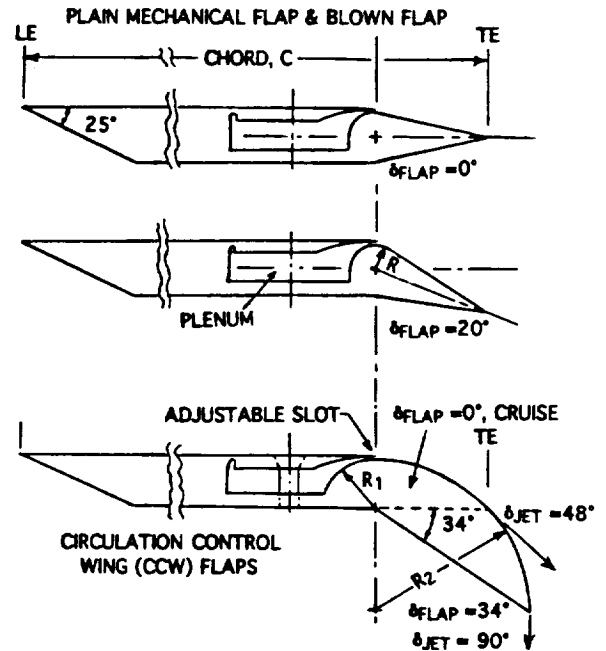


Figure 3 - Blown trailing-edge flap configurations

tangential blowing were manufactured and employed. Both had curved flap deflections very similar to the wing CC flaps of Figure 3. These canards, shown in planform in Figure 2, had similar areas and LE sweep (53.5°), but different aspect ratios and trailing edge sweep (For Canard 1, AR=1.29 with trailing edge forward sweep of -27.4°, while for Canard 3, AR=2.58 with TE aft sweep of 22.6°). They were tested at various vertical positions, as well as over a range of incidence, flap angle, and canard blowing coefficients, $C_{\mu c}$. They were located longitudinally 1.005 mean aerodynamic chord lengths ahead of the wing 0.50 MAC location. The blown plain flap and the CC flaps on the wing were tested at two flap deflections and over a range of wing blowing coefficient values, C_{μ} .

A series of investigations was conducted to evaluate pitch trim and stability characteristics of conventional horizontal tails. The existing NASP tail was removed (its short moment arm made it very ineffective) and two conventional horizontal tails were fabricated (see Figure 1). The first, an all-flying configuration without elevators, had a tail area 11.14% of the wing area, and a tail volume coefficient of 0.1312. Also tested was a similar tail geometry with an area increase of 50%, to 16.71% of the wing area, and a tail volume coefficient of 0.2059.

Experimental investigations were conducted in GTRI's Model Test Facility 30 x 43-inch subsonic research wind tunnel, which has been modified for evaluations of semi-span pneumatic models with two separate blowing air supplies. The half-span model was installed on a six-component floor-balance and separated from the tunnel wall boundary layer by a splitter plate, as shown in Figure 4. The floor balance was mounted below a turntable which allowed variation in angle of attack (α) up to 35 degrees. The wing and canard were supplied by independently -



Figure 4 - Semi-span generic HSCT model installed at high α in the GTRI Model Test Facility, including Canard 3

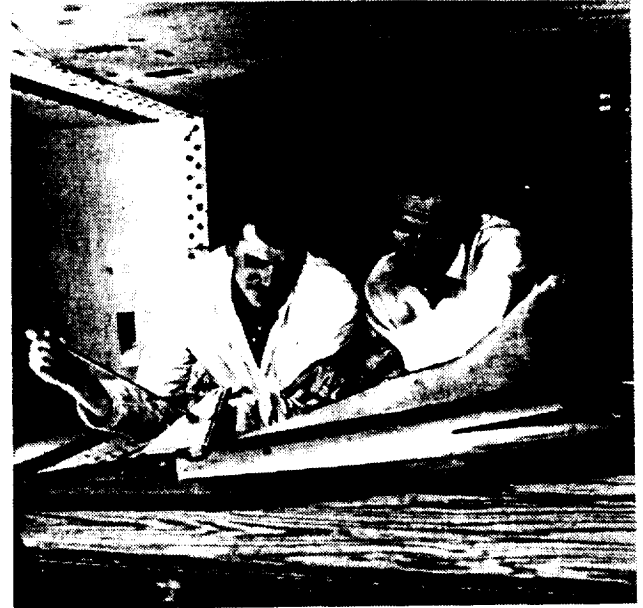


Figure 6 - Static flow visualization of blowing over Canard 3 aft-swept CC trailing edge

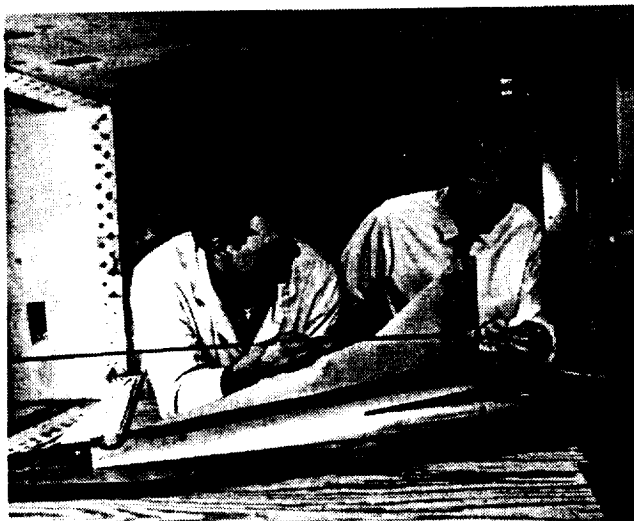


Figure 5 - Static flow visualization of blowing over 20-degree plain flap

controlled air supply lines passing through separate flow meters and through trapezes to minimize air pressure tares on the balance.

Static flow visualization (wind off) showed that the wing trailing-edge blowing jet sheet adhered to the plain flap surface and deflected 30-35° when the flap was mechanically deflected to 20° (Figure 5). In comparison, the highly curved CC trailing edge of the blown canard yielded jet turning of nearly 90° (Figure 6). Similar results were seen on the wing's CC flap configurations. Whereas this turning would prove effective in augmenting the canard's lift and providing pitch capability plus a positive lift increment to trim, the real payoff of the blown canard was expected to come from its ability to greatly reduce the upwash flowfield onto the swept wing leading edge.

TEST RESULTS

This generic blown HSCT model was tested subsonically over a large angle-of-attack range with each canard, with each tail, and for several flap configurations on the wing and canard trailing edges. The sketch in Figure 2 shows the canard locations relative to the wing leading edge. (Of course, on this half-span model, only one canard was tested at a time). Measured forces and moments at 0.50 MAC were corrected for small pressure tares and for the interference effects of the splitter plate. In these data, the blowing coefficients for either the wing or the canard are defined as:

$$C_{\mu} = \dot{m} V_j / (qS)$$

Here, \dot{m} is the measured slot mass flow, V_j is blowing jet velocity, q is freestream dynamic pressure and S is half-wing reference planform area. (For this semi-span model, a reference area for only one wing and aerodynamic forces and moments half those of a full-span configuration yield full-span 3-D coefficients).

Canard and Blowing Effects

Canards 1 and 3 (AR = 1.29 and 2.58, respectively) were evaluated at two vertical locations: high (fuselage centerline) and low (wing plane), but only with the 20° plain flap on the wing, not with the CC flap installed. Figures 7 and 8 present the tail-off lift curves and drag polars for the baseline unblown aircraft (cruise and 20° flap), and for the 20° blown flap, both with and without the canards. From the data taken, the lower aspect-ratio Canard 1 was found to be the more effective of the two, probably because its

forward-swept blowing slot aligned the jet sheet and downwash more effectively with the wing leading edge and its vortex. The lift and drag data shown in Figure 7 for Canard 1 are presented for both no wing blowing and for wing $C_{\mu} = 0.328$ (lesser C_{μ} values were evaluated and showed less total lift but greater lift augmentation per unit of blowing momentum). Canard blowing $C_{\mu c}$ of 0.0 and 0.10 are also shown. The unblown Canard 1 provided an increase of approximately 33% in lift and 27% in stall angle over the unblown clean cruise configuration due primarily to delay of wing vortex burst. Addition of blowing to the 20° wing flap (canard off) increased C_{Lmax} by 65% with little change in stall angle from the cruise configuration, whereas the unblown 20° flap by itself yielded only an 8% lift increase and a stall angle decrease compared to the clean aircraft. However, the real payoff occurred from combining the blown canard and the blown wing. Here, maximum C_L increased by 103% (to over 2.1) and the associated stall angle by 26% over the clean configuration. These are improvements achieved without canard deflection (incidence = 0°). The data are for the blown canard with no flap deflection beyond its initial cruise configuration (i.e., they're due primarily to blowing, not flap deflection). Figure 8 shows similar data for the AR=2.58 Canard 3, where, in general, the lift performance is somewhat less and drag reductions are similar to those with Canard 1. Tables I and II summarize maximum lift, drag, and stall angle changes due to blowing and the presence of each canard.

An additional advantage from these blown configurations is terminal area operation at much lower angle of attack and the ability to vary drag coefficient as needed. From Figure 7a, the maximum lift ($C_L=1.06$) of the clean configuration occurs at $\alpha=24^\circ$, while wing blowing of $C_{\mu}=0.328$ achieves that same C_L at $\alpha=8^\circ$.

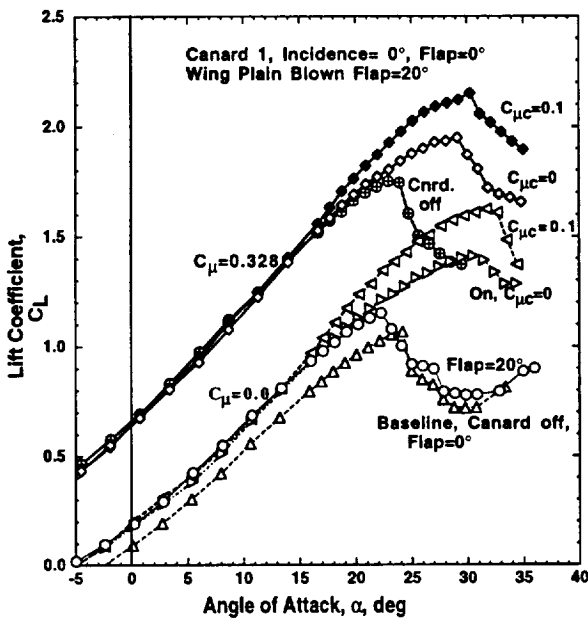


Figure 7 - Effectiveness of wing blowing and Canard 1 (AR=1.29) blowing, tail off: a. Lift curves

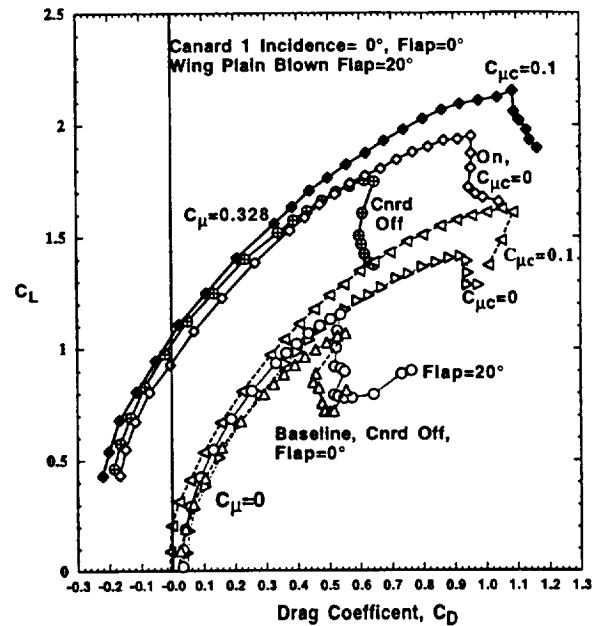


Figure 7 (Continued) : b. Drag polars

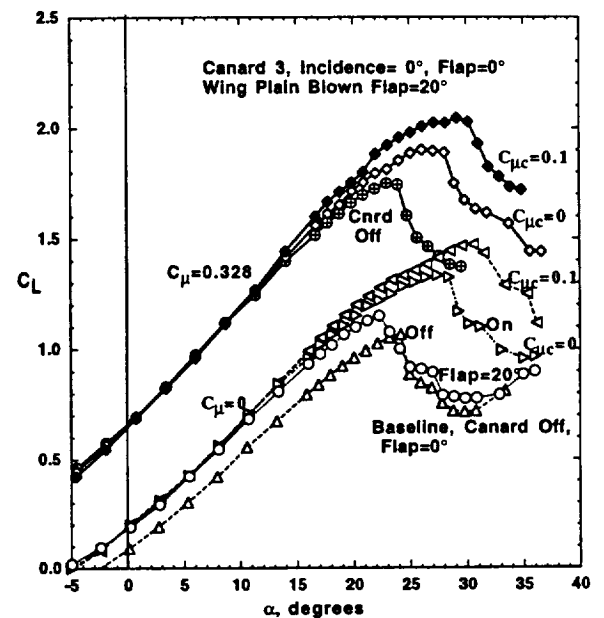


Figure 8 - Effectiveness of wing blowing and Canard 3 (AR=2.58) blowing, tail off: a. Lift curves

Significant drag reduction is also possible (Figure 7b). At the maximum lift value of the clean configuration, wing blowing alone ($C_{\mu} = 0.328$, no canard) reduces the drag from $C_D=0.56$ to 0.02. This is a combination of blowing thrust recovery and lower angle of attack on the wing and fuselage. At that same drag value for the clean configuration ($C_D = 0.56$ at C_{Lmax}), the lift can be increased from $C_L=1.06$ to 1.80 (67%) by use of wing and canard blowing. Adjustment of canard and wing blowing could optimize L/D values for both takeoff and landing flight paths.

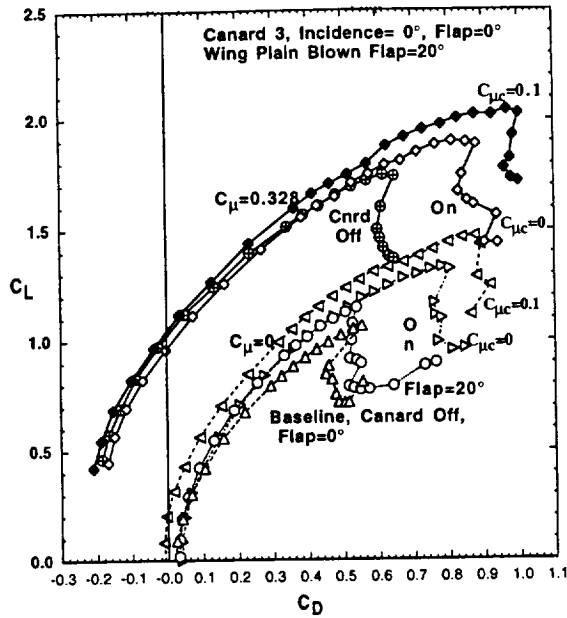


Figure 8 - Continued: b. Drag polars

C_{μ} , $dF=20^\circ$	Canard 1	Position	$C_{\mu c}$	ΔC_D at $C_L=1.0$	C_{LMAX} Increase	α_{max} Increase
0	Off		0	-17.4%	8.5%	-6.3%
"	On	HI	"	-9.1%	32.6%	26.7%
"	"	HI	0.1	-27.8%	52.8%	32.1%
"	On+Flap	HI	0	-6.5%	37.7%	32.9%
"	"	LO	"	-4.4%	31.1%	22.9%
"	"	HI	0.1	4.4%	50.9%	45.8%
"	"	LO	"	8.7%	32.1%	43.8%
0.328	Off		0	-103.3%	65.1%	-3.8%
"	On	HI	"	-93.5%	84.0%	21.3%
"	"	HI	0.1	-106.1%	102.8%	25.8%
"	On+Flap	HI	0	-87.4%	87.7%	25.0%
"	"	LO	"	-87.0%	84.9%	17.1%
"	"	HI	0.1	-87.4%	96.2%	34.2%
"	"	LO	"	-87.0%	79.3%	45.8%

Table I- Increments due to blown Canard 1 relative to Baseline Configuration (canard off, flap=0, $C_{\mu}=0$)

C_{μ} , $dF=20^\circ$	Canard 3	Position	$C_{\mu c}$	ΔC_D at $C_L=1.0$	C_{LMAX} Increase	α_{max} Increase
0	Off		0	-17.4%	9.5%	-7.5%
"	On	HI	"	-17.4%	24.5%	18.3%
"	"	LO	"	-9.1%	25.5%	-4.2%
"	"	HI	0.1	-28.3%	40.6%	28.6%
"	"	LO	"	-22.2%	40.6%	22.9%
"	On+Flap	HI	0	-8.7%	31.1%	22.4%
"	"	LO	"	-4.8%	26.4%	16.7%
"	"	HI	0.1	-13.0%	44.3%	28.6%
"	"	LO	"	-4.6%	34.9%	31.3%
0.328	Off		0	-103.3%	65.1%	-1.7%
"	On	HI	"	-95.9%	77.4%	16.2%
"	"	LO	"	-91.3%	82.1%	20.8%
"	"	HI	0.1	-104.4%	93.4%	20.3%
"	"	LO	"	-101.1%	91.5%	21.7%
"	On+Flap	HI	0	-91.3%	84.9%	20.3%
"	"	LO	"	-90.9%	83.0%	12.5%
"	"	HI	0.1	-91.3%	95.3%	20.3%
"	"	LO	"	-84.8%	93.4%	25.0%

Table II- Increments due to blown Canard 3 relative to Baseline Configuration (canard off, flap=0, $C_{\mu}=0$)



Figure 9 - Flow visualization showing vortex formation before and after canard blowing, $\alpha=29^\circ$
a. No canard blowing, vortex burst on wing



Figure 9 - (Continued)
b. Canard blowing, unburst vortex on wing

The main gain from the canard is confirmed by the vortex characteristics shown in Figure 9. This wind-on flow visualization showed that when canard blowing was applied, the strong downwash behind the canard greatly delayed or prevented vortex burst on the wing because of the reduced upwash over the swept leading edge. The first photo shows large vortex burst formation on much of the wing without canard blowing at $\alpha = 29^\circ$, which is beyond the stall angle. In the second photo, the unburst vortex is restored and the stall angle is extended by addition of the canard blowing. Figure 10 compares the lift performance of the blown canards (with flaps deflected) at different vertical locations .

One additional capability of the blown canard is

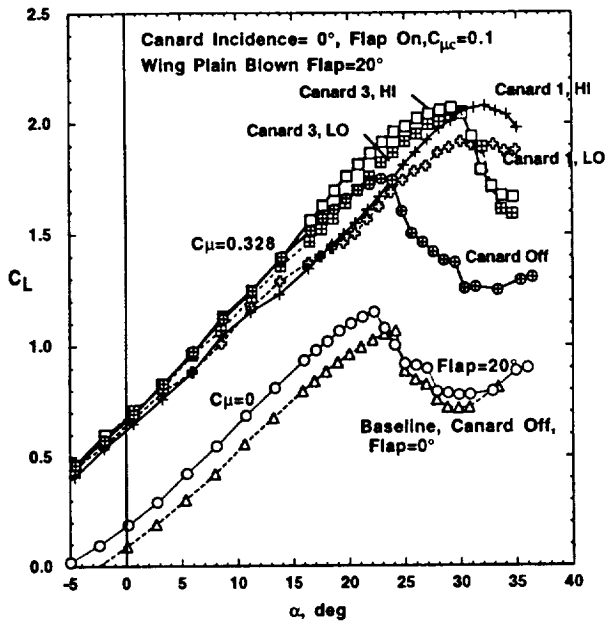


Figure 10 - Comparison of blown canards (with flaps) and baseline aircraft lift performance, tail off

longitudinal pitch trim. Whereas conventional tails usually yield download and lift loss to trim, a canard, especially when blown, generates nose-up pitch and a positive lift increment to trim. Figure 11 shows that for a moment center location of 0.50 MAC, the baseline flapped configuration (tail-off) is neutrally stable, but with a nose-down pitching moment. Addition of the canard provides nose-up pitch and trim capability, and blowing the canard further enhances this. With the wing flap blown, only the blown canard is able to trim the aircraft. As will be seen below, the conventional tail was inadequate for trim here.

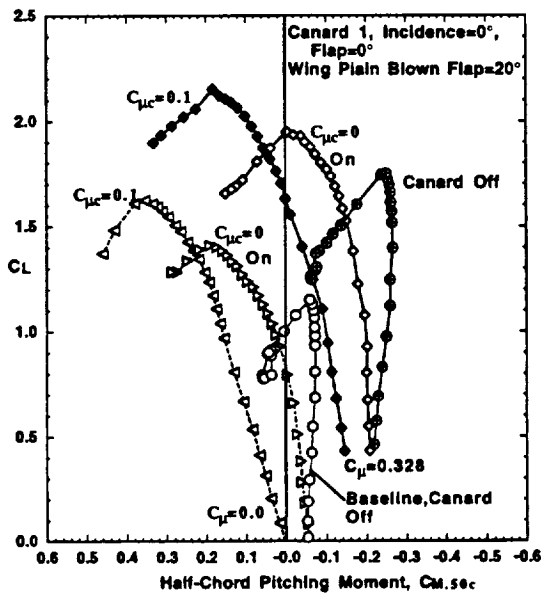


Figure 11 - Canard 1 pitch trim capability, 20° wing flap, tail off

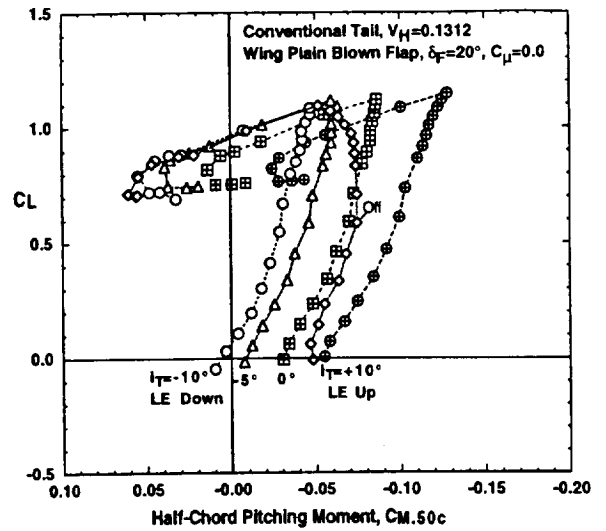


Figure 12 - Pitch provided by all-flying horizontal tail, $V_H=0.1312$

Tail Effectiveness

In a second phase of the present test, the ability of a conventional all-flying horizontal tail to trim this aircraft was evaluated. As seen in Figure 1, a tail with volume coefficient of 0.1312 and a larger one with a 50% increase in tail area (0.2059 tail volume coefficient) were evaluated. The baseline tail in Figure 12 restores longitudinal stability over the α range up to stall, but is inadequate when deflected to trim the aircraft. A 50% tail enlargement does trim the unblown aircraft (Figure 13), but not when wing blowing is applied. This tail also would require additional weight, structure and a cruise drag penalty. Figure 14a compares the conventional tail with the nose-up pitch capability of the canard, due either to canard incidence or to canard blowing. Adequate nose-up pitch trim is available, but the aircraft is longitudinally unstable at this center of gravity location. A

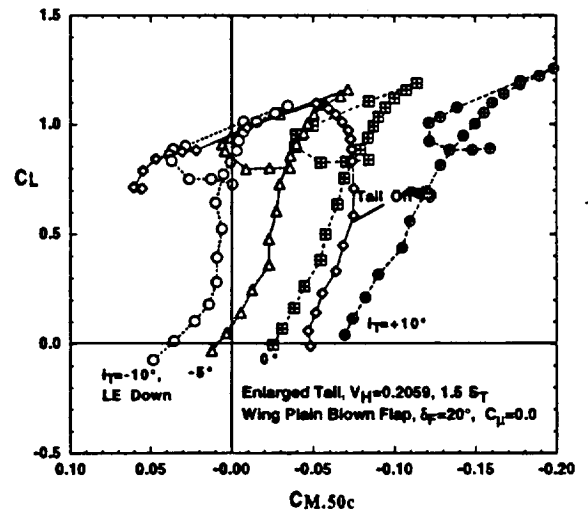


Figure 13 - Pitch provided by enlarged all-flying horizontal tail, $V_H=0.2059$

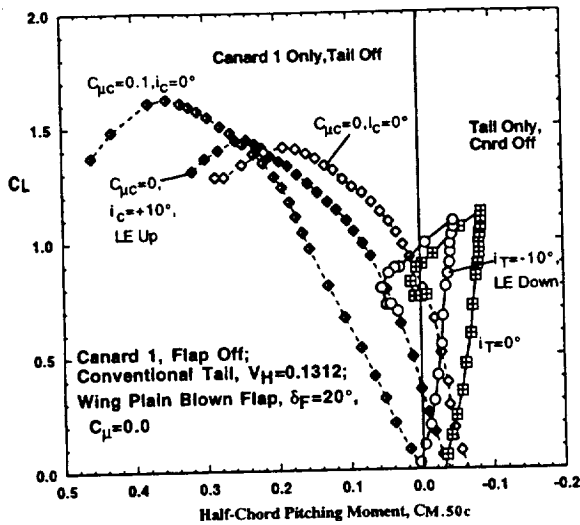


Figure 14 - Comparison of pitch trim and lift provided by horizontal tails and by blown Canard 1: a. Half-chord C_M

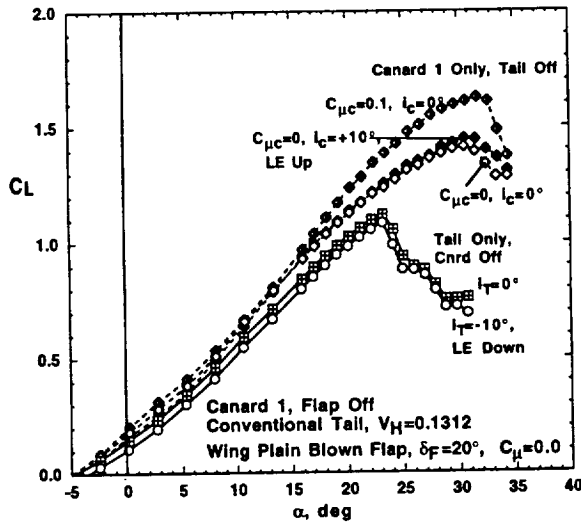


Figure 14 - (Continued) : b. Lift curves

combination of a smaller blown canard, a small horizontal tail, or further aft c.g. are suggested. Figure 14b shows the corresponding lift values.

Circulation Control Wing

Evaluation of an advanced blown wing was undertaken as a third phase of this test program. Based on the very high lift augmentation already confirmed for rounded trailing edge CCW configurations^{1,2,3,4,5} but designed to keep cruise drag low, the CCW flapped configuration of Figure 3 was applied to the HSCT model. In its cruise mode, the trailing-edge circular arc provided 48° of surface arc deflection; if that arc was extended by deflection of the lower surface by about 34°, (i.e., $\delta_{Flap} = 34^\circ$), then the jet turning angle would be 90°. This additional flap deflection is intended to provide much greater lift augmentation as well as drag generation for use on approach.

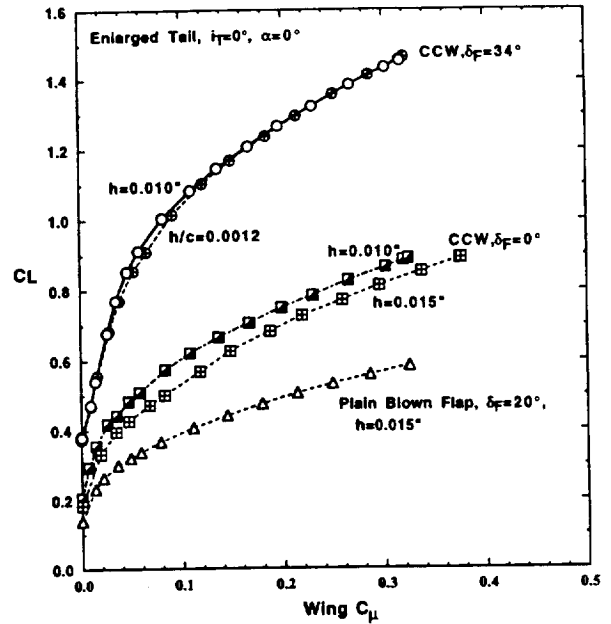


Figure 15 - Lift augmentation due to various blown TE flaps, $\alpha=0^\circ$, enlarged tail

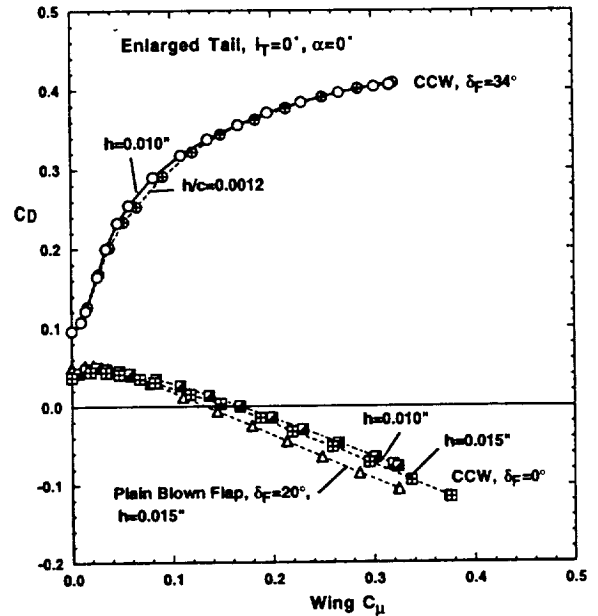


Figure 16 - Drag variation due to various blown TE flaps, $\alpha=0^\circ$, enlarged tail

Figure 15 shows how the additional jet turning of the three pneumatic flap configurations augments lift at $\alpha = 0^\circ$. The flapped CCW nearly doubles the lift of the undeflected CCW due to the additional jet turning, and nearly triples the lift of the plain blown flap. The effect of slot height variation is also seen here. Nose-down pitching moment was seen to increase with lift due to the increased aft loading produced by blowing. The ability of these three blown configurations to alter drag is shown in Figure 16, where the additional jet turning and lift also add to the induced drag. The cruise

CCW configuration and the 20° plain blown flap both reduce drag due to less jet deflection and more thrust recovery.

Figures 17 to 19 present variations in lift, drag, and pitching moment at constant wing C_{μ} values over a range of incidence for the two CCW configurations. Drag and pitch characteristics are similar to the comparisons made in previous figures when flap deflection was varied. Lift and stall angle show a new trend: for $\delta_{Flap} = 0^\circ$, the stall angle is relatively constant as C_{μ} increases, but for the greater flap deflection (34°), the stall angle is reduced as C_{μ} increases. Lift augmentation due to either α or C_{μ} appears to reach a

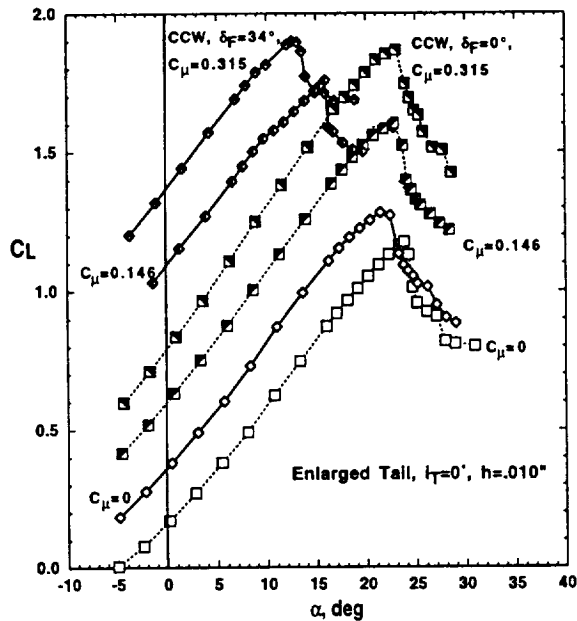


Figure 17 - Lift variation for two CCW flap deflections

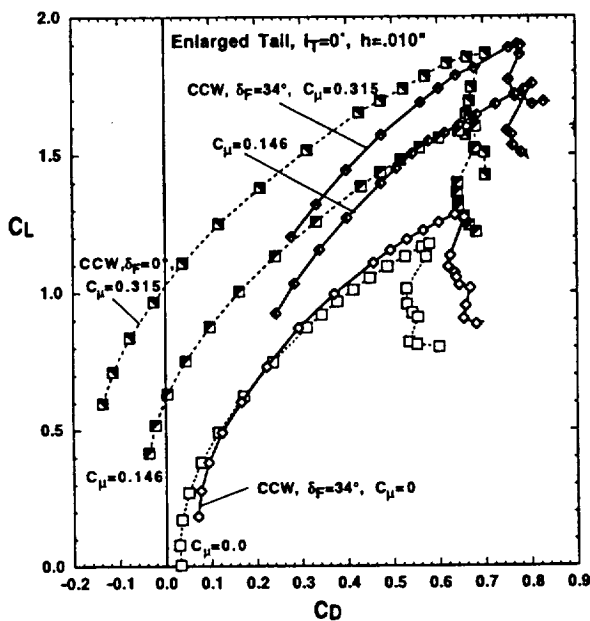


Figure 18 - Drag polars for two CCW flap deflections

limit for this wing near $C_L = 1.9$, which is probably related to increased vortex rollup due to circulation. Thus, even if the greater flap deflection yields much higher lift at lower incidence, overall wing circulation appears to be limited. This limitation appears to be independent of how that C_L is reached (by incidence, blowing or flap deflection). However, returning to Figures 7, 8, and 10 for example, higher lift can be achieved if the canard is used to carry part of the lift and to reduce the upwash angles at the swept leading edges, thus preventing the vortex breakdown. It would appear that control of vortex breakdown is an essential factor in generating higher lift on these highly-swept wings.

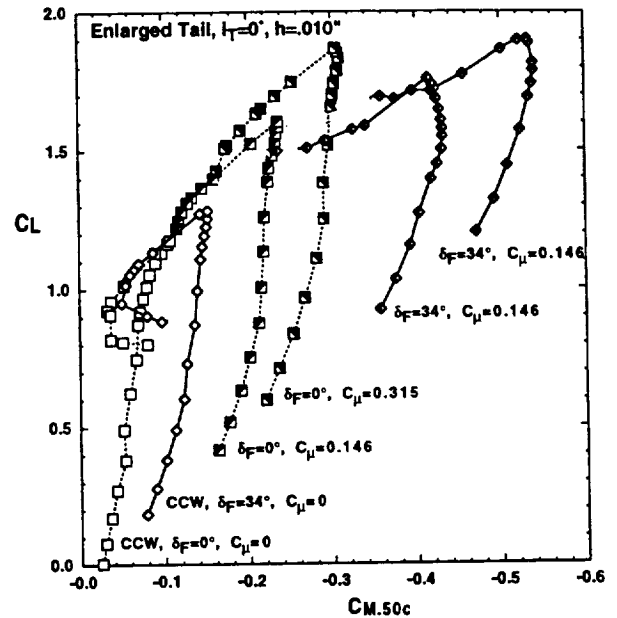


Figure 19 - Pitching moment variation for two CCW flap deflections

SUMMARY AND CONCLUSIONS

Subsonic evaluations of blown lift and control surfaces applied to highly-swept generic HSCT configurations have confirmed that blowing can significantly augment both force generation and control capability for these configurations. From these results, it is evident that the blown canard in combination with a blown vortex-generating wing can dramatically increase both lift and stall angle of HSCT-type aircraft by pneumatic force augmentation and by delay of swept-wing vortex burst. Dramatic drag reductions even greater than full thrust recovery are possible as well. Relative to the cruise baseline HSCT configuration, these blown devices have shown significant improvements, including the following:

- C_{Lmax} increases of more than 100% and stall angle increases of greater than 45%, resulting from a combination of blown canard and blown flap ability to augment circulation while delaying stall due to vortex burst. Lift augmentation values ($\Delta C_L/C_{\mu}$) measured

on these highly swept wings show a 1200% return on the blowing momentum input.

- Drag reductions greater than 100%, partly due to jet thrust recovery and partly due to operation at much lower body and wing incidence to achieve a desired lift
- Lift generation at much lower angle of attack, reducing the need for such typical HSCT characteristics as drooped nose and aft fuselage upsweep.
- Blown canards (or even unblown canards) appear able to trim the nose-down pitch of these configurations, as well as to limit the circulation-induced upwash and thus delay stall due to vortex bursting

Additional trends observed were:

- Neither the conventional nor the enlarged all-flying horizontal tails were able to trim this generic HSCT configuration in the high-lift modes tested. Unless canards were added, only the unblown 20° plain flap was trimmable by the tails. The canards alone provided the necessary trim capability, but were longitudinally unstable.
- Aerodynamic lift for the wing/tail combination appeared to reach a vortex-burst-induced limiting value for this aircraft, independent of how the wing circulation was achieved (incidence, blowing, flaps, etc.). Canards can help the configuration to exceed this limit by reducing upwash onto the wing and delaying vortex burst.

It thus appears that pneumatic high-lift devices and control surfaces can offer significant improvements in the low-speed characteristics of HSCT-type aircraft. However, vortex burst and stall need to be controlled, and some form of leading-edge device or canard should be considered. Conventional tail surfaces alone do not appear adequate to trim the high-lift devices evaluated, and thus a blown canard integrated with or replacing this tail looks quite promising.

REFERENCES

1. Englar, Robert J., Marilyn J. Smith, Sean M. Kelley and Richard C. Rover III, "Application of Circulation Control Technology to Advanced Subsonic Transport Aircraft, Part I: Airfoil Development," AIAA Paper No. 93-0644; *AIAA Journal of Aircraft*, Vol. 31, No. 5, Sept-Oct. 1994, pp. 1160-1168.
2. Englar, R. J. and C. G. Huson, "Development of Advanced Circulation Control Wing High-Lift Airfoils," AIAA Paper 83-1847, 13-15 July 1983; *AIAA Journal of Aircraft*, July 1984, pp.476-483.
3. Englar, R. J., et al, "Design of the Circulation Control Wing STOL Demonstrator Aircraft," AIAA Paper 79-1842, August 1979.
4. Englar, R. J. and C. A. Applegate, "Circulation Control - A Bibliography of DTNSRDC Research and Selected Outside References (January 1969 to December 1983)," DTNSRDC-84/052, September 1984.
5. Englar, Robert J., "Application of Pneumatic Lift and Control Surface Technology to Advanced Transport Aircraft," presented at *Transportation Beyond 2000: Engineering Design for the Future*, Conference at NASA Langley Research Center, Hampton, VA, September 26-28, 1995. Published in NASA Conference Proceedings, March 1996.
6. Englar, Robert J., Marilyn J. Smith, Sean M. Kelley and Richard C. Rover III, "Application of Circulation Control Technology to Advanced Subsonic Transport Aircraft, Part II: Transport Application," AIAA Paper No. 93-0644; *AIAA Journal of Aircraft*, Vol. 31, No. 5, Sept-Oct. 1994, pp. 1169-1177.
7. Pugliese, A.J. and R.J. Englar, "Flight Testing the Circulation Control Wing," AIAA Paper 79-1871, August 1979.

